Impact of Dissolved Ions in Manufacturing of Precipitated Calcium Carbonate (PCC)

Stefanie Scheinecker

In Fulfilment

of the Requirements for the Degree:

Master of Science

Institute for Applied Geosciences
Graz University of Technology

Thesis Supervisor: Univ.-Prof. Dipl.-Min. Dr.rer.nat. Martin Dietzel
Omya Intermediary: Michael Pohl

July 2014

Statutory Declaration

I herby declare that this thesis has been authored independently, that no other than the declared sources/resources have been used, and that all material which has been quoted either literally or by content from the used sources has been marked explicitly.

…… ……..

date signature

Acknowledgments

Firstly, I would like to express my very great appreciation to my thesis supervisor Prof. Dr. Martin Dietzel for supporting and advising me throughout my thesis. Furthermore, I would like to thank Mr. Michael Pohl from the company Omya for giving me the opportunity to write this thesis in cooperation with a globally recognised company. I am grateful for the assistance given by the staff of the laboratory of the Institute of Applied Geosciences at the Graz University of Technology and the staff of Omya.

In addition, I wish to thank my family and close friends for their support, motivation and encouragement throughout my work.

Last but by no means least I would love to and I am thanking “Hopfen und Malz, Gott erhalt’s”.

Abstract

The present precipitated calcium carbonate (PCC) process is based on the addition of CO_2 - containing gas into a suspension of calcium hydroxide ($Ca(OH)_2$) particles (milk of lime). The milk of lime itself is produced by wet slaking of burned lime (CaO) under suitable process conditions. The mass balance and the rate of the processing and the end product's quality are essentially controlled by parameters such as temperature, aqueous solution chemistry, lime composition and rate of CO_2 gas addition.

In the first step of the thesis industrial process waters used for slaking of quicklime from 16 worldwide subsidiaries of the company Omya GmbH were analysed for their chemical composition in terms of dissolved ions in order to create cataloguing of typical water qualities of industrial slaking waters and furthermore to identify possibly critical components. The investigated slaking waters derived from different sources in the industrial manufacturing process comprising process waters, wastewaters, cleaning waters, waters from the compressor, flue gas condensate and filtrates from the dewatering centrifuges. The pH ranged from 2.4 to 12.7. The calcium and sulphate concentrations showed wide variations, with values from 1.1 to 817 mg/L for calcium and 1.56 mg/L as a minimum and 1550 mg/L as a maximum for sulphate.

After considering the elemental composition, components of the industrial waters and their potential impact on the product quality the components for the subsequent laboratory experiments were chosen. In total, fourteen carbonation experiments were conducted where 0.5 or 50 mM of divalent Mg, Sr, Zn, Mn and Fe (as chlorides; and SO_4 as sodium salt) were added to the slurry of slaked lime prior to carbonation. They resembled an industrial-scale experiment in respect to reactor design, temperature, CO_2/air influx and sodium citrate addition.

In general, all conducted experiments resulted in scalenoedric shaped calcite crystals (S-PCC) except for initial 50 mM of Sr. The larger Sr ions are preferably incorporated into aragonite type structures, as present in the end member mineral strontianite ($SrCO_3$). This behaviour was suggested to cause aragonite to be precipitated besides calcite despite the addition of sodium citrate as an inhibitor for aragonite formation. In case of the Sr addition smaller $CaCO_3$ aggregates ranging from 1 to 2 µm in size with thin individual aragonite needles up to a length of 1.5 to 2 µm compared to the PCC without additive (2 - 2.5 µm) were visualised by scanning

electron microscopy. In all other experiments calcite was formed, but, with individual crystal size and shape strongly depending on the distinct additives and their concentration level. For instance at 50 mM of Zn the crystals had a size of 2 µm with comparatively short individual needles (0.5 -1 µm). The same was valid for the experiment with 50 mM SO_4, only that the aggregates were larger (< 5 µm) and the individual needles appeared to be packed together more tightly. These variations can have a great effect on the application range of the final PCC product.

Concerning the mass balance the present study showed that the used lime was rich in magnesium. Therefore some solutions' high magnesium values derived from the lime itself. However, it is noteworthy that the magnesium was not incorporated into the final solid products but stayed in the solutions after the carbonation process.

With regards to brightness, all samples apart from the manganese chloride experiments stayed within an acceptable range between 90.7 and 97.3 % according to R457. The values for the manganese samples were between 27 % (50 mM Mn) and 93 % (0.05 mM Mn).

The monitored PCC processing of each trial was modelled using the computer code PhreeqC by considering thermodynamic equilibrium for simplification. The following reaction stages are valid for all experiments (except for 50 mM of SO_4): (i) a nearly constant pH period at about 12.5 during $CaCO_3$ precipitation throughout the addition of a CO_2 containing gas, (ii) steep pH decrease caused by consumption of the provided $Ca(OH)_2$ amount from the slurry with a short-term pH buffering period induced by the dissolution of in stage (i) formed Mg hydroxide phases where neutralisation reaction low is reached at pH 7 – 7.5 reflecting the given CO_2 partial pressure of CO_2 supply, and (iii) a slight re-increase of pH through dissolution of encapsulated $Ca(OH)_2$ relicts (only valid for one experiment). In the case of 50 mM sulphate gypsum already precipitated during the slaking process. Gypsum did not precipitate during the carbonation process.

The consistence of the data recorded during the precipitation experiments and the developed modelling approach showed that modelling may be used as a promising tool for testing prospective PCC processing.

Kurzfassung

Der vorliegende PCC Prozess (Herstellung künstlichen Kalziumkarbonates) basiert auf der Einleitung von CO_2-haltigem Gas in eine Suspension aus Kalziumhydroxid ($Ca(OH)_2$) Partikel (Kalkmilch). Die Kalkmilch selbst wird durch Nasslöschen von Branntkalk (CaO) unter geeigneten Prozessbedingungen hergestellt. Der Umsatz und die Geschwindigkeit dieses Prozesses als auch die Qualität des Endprodukts sind wesentlich bestimmt von Parametern wie Temperatur, Zusammensetzung der Lösung und des Brandkalkes und Zugaberate an gasförmigen CO_2.

In der ersten Phase der Arbeit wurden industrielle PCC Prozesswässer aus 16 weltweiten Produktanlagen, welche für das Löschen von Branntkalk verwendet werden, bezüglich ihrer beinhaltenden gelösten Ionen analysiert, um eine Katalogisierung typischer Wasserqualitäten als Komponenten industrieller Löschwässer als auch eine Identifizierung möglicher kritischer Inhaltsstoffe zu ermöglichen. Die untersuchten Löschwässer stammten aus unterschiedlichen Quellen und beinhalteten Prozesswässer, Abfallwässer, Wässer aus Zentrifugen, Wässer aus Kompressoren, Abgaskondensate und Filtrate der Abwasserzentrifugen. Der pH der analysierten industriellen Wässer umfasste Werte von 2,4 bis 12,7. Nicht nur der pH Wert zeigte eine enorme Variabilität sondern auch z.B. die Kalziumkonzentration mit Werten zwischen 1,1 und 817 mg/L oder Sulfat mit 1,6 mg/L als Minimum und 1550 mg/L als Maximum.

Es wurden 14 Karbonatisierungs-Experimente im Labor unter analogen Konditionen zum industriellen Prozess durchgeführt (z.B.: Reaktordesign, Temperatur, CO_2/Luftzufluss), bei denen 0,5 bzw. 50 mM der zweiwertigen Additive Mg, Sr, Zn, Mn, Fe (als Chloride; und SO_4 als Natriumsalz) der CaO-Suspension vor der Karbonatisierung zugegeben wurde. Des Weiteren wurde 0,1 % Natriumcitrat beigemengt, um die Ausfällung von Aragonit zu hemmen.

Für alle durchgeführten Experimente mit Ausnahme des Versuchs mit 50 mM Sr, wurden im Endprodukt die gewünschten skalenoedrischen Kalzit-Kristalle (S-PCC) identifiziert. Anders das Ergebnis für Strontium. Die großen Sr Ionen werden bevorzugt in die Aragonit-Struktur eingebaut. Dies bewirkte trotz der Zugabe von Natriumcitrat die Co-Präzipitation von Aragonit mit Kalzit. Die Rasterelektronenbilder zeigten in diesem Fall kleinere Aggregate mit einer Größe von 1 - 2 µm mit feineren

Nädelchen mit einer Länge von 1,5 – 2 µm als die der Referenzfällung ohne Additive (2 - 2,5 µm).

In allen anderen Experimenten wurde Kalzit gebildet. Ferner hängt die Größe und Art der gebildeten Kalzit-Kristalle deutlich vom jeweiligen Additiv und dessen Konzentration ab. Zum Beispiel im Experiment mit initial 50 mM Zn. Hier haben die Aggregate eine Größe von 2 µm mit kurzen einzelnen Nadeln (0,5 – 1 µm). Das Experiment mit initial 50 mM SO_4 zeigte ein ähnliches Bild. Hier wiesen die Aggregate jedoch eine Größe von bis zu 5 µm auf und die Nadelaggregate traten kompakter auf. All diese Variationen können einen großen Einfluss auf die Qualität des Endprodukts in Hinblick auf mögliche Verwendungen haben.

Die Massenbilanz ergab, dass der verwendete Kalk sehr reich an Magnesium war. Dies erklärt die teils sehr hohen Magnesiumkonzentrationen einiger experimenteller Lösungen. Jedoch ist es wichtig anzumerken, dass das Magnesium nach dem Karbonatisierungsprozess nicht in das Endprodukt eingebaut wurde sondern zum Großteil in Lösung blieb.

Der Weißheitsgrad der Produkte liegt mit Ausnahme der Experimente mit der Zugabe an Manganchloride in einem Bereich von 90,7 – 97,3 % nach R457. Die Werte des Weißheitsgrades für die Manganexperimente lagen für das Endprodukt zwischen 27 % (50 mM Mn) und 93 % (0,05 mM Mn).

In einem hydrogeochemischen Modellierungsansatz wurde die Entwicklung des Pauschalumsatzes der Fällungsreaktion der einzelnen Versuche simuliert (PhreeqC). Für alle Experimente, ausgenommen der Versuch mit initial 50 mM SO_4, können die folgenden Reaktionsstufen modelliert werden: (i) pH Konstanz während der $CaCO_3$ Fällungsphase bei 12,5 während der Zugabe von CO_2 haltigem Gas (ii) rasche pH Abnahme auf Grund des Verbrauchs von $Ca(OH)_2$ mit kurzfristiger pH Pufferung durch die Auflösung von in Stufe (i) mitgefälltem Mg-Hydroxid Phasen und letztendlich die Neutralisationsreaktion bei pH zwischen 7 und 7,5 gemäß dem voreingestellten CO_2 Partialdruck (Versuchsabbruch) und (iii) Wiederanstieg des pH Wertes über die Auflösung von gekapselten $Ca(OH)_2$ Relikten (nur über einen Versuch ersichtlich). Im Falle von initial 50 mM Sulfat bildete sich bereits während des Löschvorgangs Gips. Dies hatte zur Folge dass sich während der Karbonatfällung kein Gips mehr bildete.

Die gute Übereinstimmung der während der Fällungsprozesse aufgezeichneten Daten mit jenen der Modellierung zeigt das Potential zukünftige Fällungsbedingungen vorab mittels Simulationen zu testen.

Table of Contents

1. Introduction

During the last couple of years much attention has been paid to precipitated calcium carbonate (PCC) due to its wide ranging industrial applications such as for paper coatings, fillers, paints, rubbers, plastics, adhesives production and numerous others (Ukrainczyk et al., 2008; Matsumoto et al., 2010).

Those high quality products require specific physical and chemical properties, e.g. morphology, surface characteristics and size distribution (Kosma and Beltsios, 2012). Morphology, for instance, is significantly affected by temperature, mixing procedure of solutions, pH, supersaturation in respect to calcium carbonate polymorphs, addition of additives and the type of operating system. Therefore, recent research has been focused on receiving replicable results on how and whereby those parameters are being influenced (Isopescu et al. 2009; Jung et al., 2010). This process is mainly based on the carbonation of an alkaline slurry containing slaked lime by adding CO_2 (Kadota et al. 2013).

This thesis aims to determine the effect of the solution chemistry on the final PCC product for a given production process. Thus, the main focus is on how added dissolved ions at different concentrations are being incorporated into the calcium carbonate ($CaCO_3$) structure or precipitated at separate solids during the PCC process and their impact on the product's properties mainly concerning crystal structure shape and size by using X-ray Diffraction, Scanning Electron Microscopy, Attenuated Total Reflectance Infrared Spectroscopy and X-ray Fluorescence besides monitoring the overall reaction progress by pH, specific conductivity and temperature.

For the selection of relevant additives, which subsequently were used for the precipitation experiments, 39 process waters used for slaking of quicklimes from different subsidiaries of the Omya GmbH at different process stages were analysed for their chemical composition using ion chromatography and inductively coupled plasma optical emission spectroscopy with regard to their elemental composition. The ions which were present at high concentration levels, were chosen for the carbonation experiments to decipher their potential influence on the end product's quality.

2. Basic Concepts

2.1. pH

The pH denotes the negative logarithm of the activity of $H_3O^+_{(aq)}$ ions (also written as H^+) in aqueous solutions. The pH of "pure" aqueous solutions is given by the dissociation constant of water K_W:

$$K_W = (H_3O^+) \cdot (OH^-) \quad (1)$$

($K_W = 10^{-14}\ mol^2/L^2$ at 25°C). In pure water the amount of H^+ ions equals that of OH^- ions:

$$(H_3O^+) = (OH^-) \quad (2)$$

(considering for simplification: activity = concentration). Combining equations (1) and (2) gives the relations:

$$(H_3O^+)^2 = (OH^-)^2 = 10^{-14}\ mol^2/L^2 \quad (3)$$

$$(H_3O^+) = (OH^-) = 10^{-7}\ mol/L \quad (4)$$

In order to avoid the use of potencies pH is given as the negative logarithm at the base of 10 of (H_3O^+) or (OH^-) resulting in pH = pOH = 7 for a pure aqueous solution.

2.2. Alkalinity

Alkalinity gives a solution's ability to neutralise acids. In a solution various anion complexes can be used as a buffer. Therefore, the total alkalinity (A_T) is being measured. In most aqueous solutions the bicarbonate (HCO_3^-) is of great importance for the alkalinity. Considering the high pH of the experiments in this study (pH ≈ 12) the A_T was shifted towards carbonate and hydroxide ions.

$$A_T\ (meq/L) = [HCO_3^-] + 2[CO_3^{2-}] + [OH^-] \quad (5)$$

2.3. Specific conductivity

The specific conductivity (SpC) gives the potential of a matter to conduct an electric current. It is measured in the SI unit S m^{-1} (Siemens per metre). The electrical conductivity of a matter is the reciprocal of the electrical resistivity (Ω).

$$SpC = \Omega^{-1} \tag{6}$$

In contrast to the specific conductivity, the electrical resistivity measures the strength of a matter opposing the flow of an electric current:

$$\Omega = \rho \cdot \frac{l}{q} \tag{7}$$

l: length of conductor
q: cross-sectional area of the specimen
ρ: electric current

The SpC of aqueous solutions varies strongly depending on temperature and dissolved ions. Hence, to pre-empt temperature effects the conductivity is measured at 25°C.

2.4. Ion charge balance

An ion charge balance gives the difference of charge produced by anions and cations in aqueous solutions in percentage (Knights and Stenner, 1999). Anions are negatively charged ions (e.g. Cl^-). Cations, in contrast, are positively charged ions such as Ca^{2+}. In an aqueous solution the sum of charges induced by dissolved anions and cations should always be balanced, which means that the solution is electrically neutral.

$$\Sigma[cations]\ (meq/L) = \Sigma[anions]\ (meq/L) \tag{8}$$

The amount of ions is given in milliequivalents/litre [meq/L] for the calculation of the ion balance. The resulting calculation of the difference of the ion charge balance in percentage is:

$$\% \text{ difference} \frac{(\Sigma[\text{cations}]-\Sigma[\text{anions}])}{\Sigma[cations]+\Sigma[anions]} = *100 \quad (9)$$

2.5. $CaCO_3$ modifications

Carbonate minerals are salts of the acidic carbon group H_2CO_3. They are characterised by their anion complex CO_3^{2-}. Three anhydrous modifications of calcium carbonates occur in natural systems: calcite is the thermodynamically stable modification at standard conditions (25°C, 1 atm), whereas aragonite and vaterite are metastable (Morse and Mackenzie, 1990). $CaCO_3$ polymorphs can show a great variety of different crystal shapes (Niedermayr et al., 2013).

In both the calcite-type ([6] – fold coordination) and the aragonite-type ([9] coordination) the Ca ion can be replaced by other divalent ions of varying radii. According to the size of the substituting ion it is either preferentially incorporated into the calcite-type or the aragonite-type. Ions with a radius larger than Ca (>1.06 Å) such as divalent Sr, Ba or Pb crystallize rhombic and, thus, are preferably incorporated in the orthorhombic aragonite structure. On the other hand, ions with a radius Å < 1.06 such as divalent Mg, Mn, Zn or Fe crystallise rhombohedral and are usually incorporated into the [6]–fold coordinated calcite-type (Böttcher and Dietzel, 2010).

2.6. Dissolution of inorganic carbon species

The general dissolution reaction for calcium carbonate polymorphs is given by the reaction

$$CaCO_3 = Ca^{2+} + CO_3^{2-} \qquad \boldsymbol{K_s} \quad (10)$$

As gaseous CO_2 ($CO_{2(g)}$) dissolves in water the following dissolved inorganic carbons (DIC) are formed: aqueous carbon dioxide ($CO_{2(aq)}$), carbonic acid (H_2CO_3), bicarbonate ions (HCO_3^-) and carbonate ions (CO_3^{2-}) (Appelo and Postma, 2009). At 25°C $CO_{2(aq)}$ is about 600 times more abundant than H_2CO_3. Therefore, for simplification the latter species are combined to H_2CO_3*. In the equation below [ ] indicates molar concentrations.

$$[H_2CO_3^*] = [CO_{2(aq)}] + [H_2CO_3] \quad (11)$$

The gaseous carbon dioxide ($CO_{2(aq)}$) reacts to carbonic acid ($H_2CO_{3(aq)}$) according to the hydration reaction

$$CO_{2(g)} + H_2O = H_2CO_3^* \qquad K_0 \tag{12}$$

The carbonic acid dissociates firstly to bicarbonate (HCO_3^-) according to the dissociation reaction

$$H_2CO_3^* = H^+ + HCO_3^- \qquad K_1 \tag{13}$$

via the release of H^+ ions and subsequently to the carbonate ion following the dissociation reaction

$$HCO_3^- = H^+ + CO_3^{2-} \qquad K_2 \tag{14}$$

where dissociation level depends on pH (Stumm and Morgan, 1996)

The equilibrium constants (K) at 25°C are determined according to the expressions

$$K_H = \frac{(H_2CO_3^*)}{P_{CO_2}(H_2O)} = 10^{-1.46} \tag{15}$$

$$K_1 = \frac{(H^+)(HCO_3^-)}{(H_2CO_3^*)} = 10^{-6.35} \tag{16}$$

$$K_2 = \frac{(H^+)(CO_3^{2-})}{(HCO_3^-)} = 10^{-10.33} \tag{17}$$

(for 25°C; Schwartz and Zhang, 2003). From the above equations the distribution of the different DIC species as a function of pH can be calculated (Fig.1). At pH < 6.3, 6.3 < pH < 10.3, pH > 10.3 the $H_2CO_3^*$, HCO_3^- and CO_3^{2-}, respectively, is the dominant DIC species.

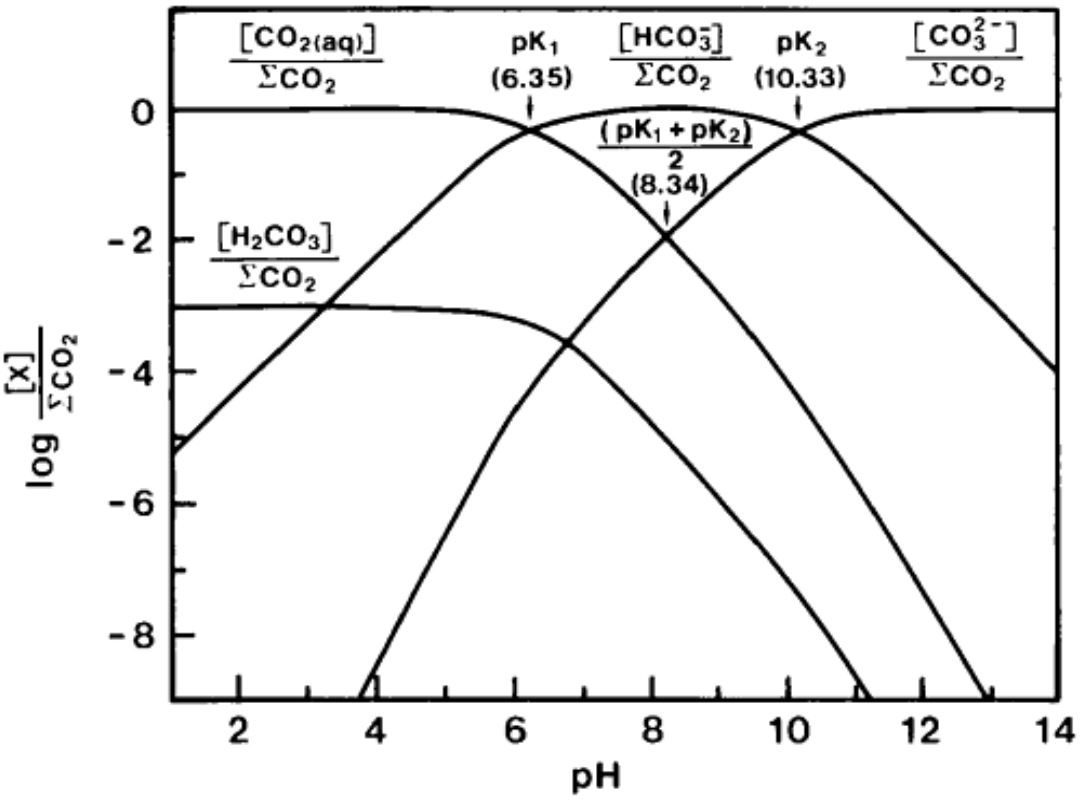

Figure 1: A Bjerrum diagram for the relative proportions of chemical species in respect to dissolved inorganic carbon as a function of pH, for the case where all activity coefficients are equal to 1. pK's are values at 25°C. (Morse and Mackenzie, 1990)

2.7. Carbonate solubility

The solubility of calcium carbonates is given by their individual solubility products (Ks) according to the equation

$$Ks = (Ca^{2+}) \cdot (CO_3^{2-}) \tag{18}$$

at thermodynamic equilibrium conditions and at a given temperature of 25°C (see equation (10)). The solubility product of calcite is $10^{-8.48}$, and hence, is lower than that of aragonite with $10^{-8.34}$ (at 25°C; Dietzel, 2011). Therefore, calcite is the stable $CaCO_3$ polymorph at 25°C. However, with increasing temperature the solubility of calcium carbonates decreases. Increasing pressure leads to an increase of the solubility.

The saturation degree Ω with respect to calcite is obtained by the expression

$$\Omega_{Calcite} = (Ca^{2+})\ (CO_3^{2-}) / K_{calcite} = (IAP) / K_{calcite} \quad (19)$$

(Ca^{2+}) and (CO_3^{2-}) are the carbonate activities and $K_{calcite}$ is the solubility product for calcite. The saturation index (SI) can be calculated by the equation

$$SI = log\ (\Omega) \quad (20)$$

$\Omega = 1$ solution and solid are in thermodynamic equilibrium
$\Omega < 1$ solution is undersaturated, mineral can dissolve
$\Omega > 1$ solution is supersaturated, mineral can precipitate

Therefore, the SI (or Ω) indicates whether a mineral may either dissolve or precipitate or is in equilibrium by equating the measured ion activity product (IAP) of a solution with the solubility product of the mineral.

2.8. CO_2 exchange and precipitation of $CaCO_3$

Two mechanisms may occur when water gets into contact with the Earth's atmosphere. Depending on the P_{CO2} (CO_2 partial pressure in atm) water can either degas or absorb CO_2. Degassing occurs when the P_{CO2} of the Earth's atmosphere ($P_{CO2} = 10^{-3.5}$ atm) is lower than the solution's internal one. CO_2 degasses from the solution until it reaches a P_{CO2} of $10^{-3.5}$ atm. Consequently, the solution's pH increases. The relative percentage of CO_3^{2-} in respect to the DIC increases and the solution may reach supersaturation with respect to $CaCO_3$.

CO_2 absorption, on the contrary, occurs when the P_{CO2} of the Earth's atmosphere is higher than that of the solution. Therefore, the solution is usually undersaturated with respect to CO_2 and hence is able to take up carbon dioxide from the atmosphere. Due to a high pH CO_2 is mainly converted into carbonate ions. This, however, may lead to an elevated supersaturation in respect to calcite.

2.9. Isomorphic replacement

As mentioned in section 2.5 divalent ions such as Mg or Sr can substitute the Ca ions in the crystal lattice of calcium carbonate minerals. Depending on their ionic radius they are either preferably incorporated into the trigonal calcite structure or the orthorhombic structure of aragonite (see Tab.1).

However, the incorporation of different ions into carbonate minerals depends on various factors such as temperature, solution composition, precipitation rate, etc. (Böttcher and Dietzel, 2012). The incorporation of foreign ions into calcium carbonate is expressed by the following general equation

$$xCa^{2+} + (1 - x)Me^{2+} + CO_3^{2-} = Ca_xMe_{(1-x)}CO_3 \quad (21)$$

(Böttcher and Dietzel (2010). Furthermore, for divalent metal ions the incorporation into calcite can be expressed by the distribution law according to the expression

$$\left(\frac{[Me]}{[Ca]}\right) calcite = D_{Me}\left(\frac{[Me]}{[Ca]}\right) aq \quad (22)$$

The concentrations are given in brackets and D_{Me} represents the partition coefficient.

Table 1: Carbonate minerals and their solubility values at 25°C and 1 bar (from Morse and Mackenzie, 1990)

Mineral	**Formula**	**-log K_s**
Calcite	$CaCO_3$	8.30
Aragonite	$CaCO_3$	8.12
Vaterite	$CaCO_3$	7.73
Monohydrocalcite	$CaCO_3 \cdot H_2O$	7.54
Ikaite	$CaCO_3 \cdot 6H_2O$	
Magnesite	*$MgCO_3$*	*8.20*
Nesquehonite	$MgCO_3 \cdot 3H_2O$	5.19
Huntit	$CaMg_3(CO_3)_4$	30.46
Hydromagnesite	$Mg_4(CO_3)_3(OH)_2 \cdot 3H_2O$	36.47
Dolomite	*$CaMg(CO_3)_2$*	*17.09*
Strontianite	$SrCO_3$	8.81
Witherite	$BaCO_3$	7.63
Barytocalcite	$CaBa(CO_3)_2$	17.68

2.9.1. Mg incorporation

Magnesium ions generally show an affinity for the calcite crystal type (Morse et al., 2007). The Mg/Ca ratio in the solution can significantly affect $CaCO_3$ supersaturation of the solution and precipitation behaviour (Zhang and Dawe, 2000). Zhang and Dawe further state that magnesium gets incorporated in calcite seed surfaces, which can change the morphology of the crystal. Factors, which may influence the incorporation, are the local solution chemistry, precipitation rate and temperature. Moreover the experiment conducted by Saulnier et al. (2012) exhibited that the Mg fractionation did not show any correlation with either pH or temperature. Yet, an increase in D_{Mg} was observed from the core to the rim of the calcite crystal grains. Other related and common Mg precipitates are e.g. nesquehonite ($MgCO_3 \cdot 3H_2O$) or brucite ($Mg(OH)_2$).

2.9.2. Sr incorporation

The divalent Sr ion is much more likely to be incorporated into the orthorhombic structure of aragonite than in the trigonal structure of calcite (Morse et al, 2007). Tang et al (2008) showed that the calcite precipitation rate was severely affected by the composition of the solution and the solution's pH, respectively. The incorporation of Sr into $CaCO_3$ is controlled by the distribution coefficient (D_{Sr}). Using the surface entrapment model D_{Sr} can be calculated at any specific temperature and precipitation rate (Böttcher and Dietzel, 2010). According to the equation

$$D_{Sr} = \frac{([Sr]/[Ca])s}{[(Sr]/[Ca])aq} \tag{23}$$

by Tang et al. (2008) D_{Sr} is defined as the molar ratio of [Sr] and [Ca] in the solids (s) to the molar ratio of [Sr] and [Ca] in the aqueous solution (aq). The distribution coefficient is temperature dependent and therefore can be used to determine precipitation rates at a constant temperature (Tang et al., 2008, and Nehrke et al., 2007). Böttcher and Dietzel (2010) stated that the incorporation of strontium into calcite is controlled by temperature, precipitation rate, the concentrations of additional foreign ions (substitution) and the solution's chemical composition. The precipitation rate itself is dependent on the calcium concentration, CO_2 partial pressure and pH (Tang et al., 2008). There is a positive correlation

between D_{Sr} and the growth rate of calcite. Nehrke et al. (2007) suggested that at a constant pH and a given supersaturation the growth kinetics of calcite depend on the solution's stoichiometry in the case of Ca/CO_3 ratio. Hence, the Sr/Ca ratio reflects the effects of supersaturation and stoichiometry of the aqueous phase on the crystal growth kinetics.

2.9.3. Zn incorporation

Nehrke et al. (2007) claimed that by adding zinc ions to a solution the nucleation time (time before crystallisation starts) increases. Already at a concentration of 10^{-5} mM (at a pH above 7) Zn inhibits the interaction between reagents and the calcite through formation of surface precipitation, such as hydrozincite ($Zn_5(OH)_6(CO_3)_2$) and zinc hydroxide ($Zn(OH)_2$) coating the calcite surface (Zhang et al, 2012).

2.9.4. Mn(II) incorporation

Mn is strongly absorbed on the calcite surface also at concentrations below rhodochrosite ($MnCO_3$) solubility (Morse et al, 2007). According to Franklin and Morse (1983) Mg availability via dissolution of Mg calcite is influential on the interaction of Mn with calcite. Furthermore, in dilute solutions an uptake of the divalent manganese ion may lead to the nucleation of $MnCO_3$ (rhodochrosite) and subsequent growth.

The distribution coefficient D_{Mn} (in respect to calcite) is affected by growth kinetics and temperature. The D_{Mn} is value decreasing when the growth rate is decreasing or the temperature is increasing (Walter and Dromgoogle, 1989). Pingitore et al. (1988) stated that the partition coefficient of Mn into calcite is inversely related to the precipitation rate.

2.9.5. SO_4^{2-} incorporation

Fernandéz-Díaz et al. (2010) suggested that depending on the ratio between $[SO_4^{2-}]$ and $[CO_3^{2-}]$ and the nucleation time either calcite, aragonite or vaterite are being formed. This study also showed that concerning calcite and vaterite, SO_4 incorporation is positively and linear related to the SO_4^{2-}:CO_3^{2-} ratio of the solution. A higher sulphate content in the solution is suggested to decrease the solubility of calcite. Additionally, SO_4 may influence the form of the calcite. Fernandéz-Diaz et al (2010) investigated that with increasing SO_4 the calcite became blockier. Finally, the

experiments of Morse et al. (2007) showed that the incorporation of sulphate into the calcite lattice increases with the precipitation rate.

2.9.6. Fe(II) incorporation

As mentioned by Böttcher and Dietzel (2010) the Fe/Ca ratio during the precipitation of calcite is higher in the precipitate than in the aqueous solutions. The distribution coefficient D_{Mn} is slightly larger than D_{Fe}. Furthermore, Böttcher and Dietzel (2010) pointed out that the incorporation of Fe(II) ions in calcite is limited at a low temperature but is, however, easily promoted by the presence of Mn. During the incorporation of Fe(II) in carbonate minerals the iron can oxidise to Fe(III). Subsequently, oxides and hydroxides and respective aquocomplexes can be formed (Böttcher and Dietzel, 2010).

3. Methodology

3.1 Analytical methods

3.1.1. Solution Analyses

The water samples from several international branches of the company Omya were received for analysis (Table A-1). Experimental solutions were taken at different stages during the experiment ((i) initial solution, (ii) after slaking, (iii) after carbonation) for analyses.

Analyses comprised the determination of the solutions pH, conductivity (µS/cm), temperature (°C), suspended solids (mg/L), alkalinity (EN ISO 996-1, 1995) and element content by ion chromatography (IC; Dionex ICS-3000) and inductively coupled plasma optical emission spectrometry (ICP-OES; Perkin Elmer Optima 4300 DV). The former IC analysis has an analytical error of ≤ 3%. For latter ICP-OES analyses the analytical error is ≤ 5%.

The samples were filtered through 0.45 µm membranes and either diluted with Milli-Q water (Millipore Integral 3: 18.2 $M\Omega cm^{-1}$) for IC or acidified with 2% bidistilled HNO_3 for analysis with ICP-OES in order to characterise their ion content.

Subsequently, the alkalinity was determined by hand via titration with 0.05 M HCl solution using Methyl orange, according to EN ISO 996-1 (1995). Furthermore, the hardness of the waters in °dH (German degrees) and the DIC (dissolved inorganic carbon) were calculated.

3.1.2. Solid phase characterisation

The filter cakes from the filtration of the industrial solutions were dried at room temperature for 24 hours and subsequently at 105°C. After each drying step the weights of the cakes were recorded. The solid content in mg/L was calculated from the samples' weight at 105°C. The filter cakes from the precipitation experiments were only dried at 105°C for several hours.

The dried filter cakes at the end of the experiments were analysed for their mineralogical composition using XRD (X-ray diffractometer, Bruker D8) at Omya. The equipment used was a position sensitive device (PSD) LynxEye detector system. The program DiffracPlus-EVA and the mineral database ICDD were used for peak identification. Using the program TOPAS Rietveld refinement calculations of the

analysed XRD patters were taken to determine the modal mineral composition, applying the fundamental parameter approach. A variable 6.00 mm divergence slit width (40 kV) at a 2θ angle ranging from 4° to 70°, a step size of 0.008° and a time/step of 0.2 seconds was applied, which gave a total of 30 minutes of measuring time for each sample. Powdered samples were used for the analyses. To verify the caliumcarbonate polymorphs the peak areas (A_I) of the XRD patterns were employed for the quantification of the $CaCO_3$ polymorphs according to the equations (the distribution of the $CaCO_3$ polymorphs was measured or calculated via Rietveld as well as with the underneath equation)

$$X_{Cc} = \frac{1}{1 + 6.4\,\frac{A_{Ar221}}{A_{Cc104}} + 5.7\,\frac{A_{Va110}}{A_{Cc104}}} \tag{24}$$

$$X_{Ar} = 6.4\,\frac{A_{Ar221}}{A_{Cc104}}\,X_{Cc} \tag{25}$$

(adapted from Kotoyannis and Vagenas, 2000). The values 6.4 and 5.7 were taken from Niedermayer et al. (2013) and are proportionality constants. The peaks at d_{104} (3.035 Å) for calcite and d_{110} (1.973 Å) for aragonite were adopted for evaluation.

The solid phases were further characterised using ATR-FTIR Perkin Elmer Spektrum 100 (Attenuated Total Reflectance – FT-Infrared Spectroscopy) within a range from 450 to 4000 cm^{-1}. For the chemical analyses XRF (X-ray Fluorescence, Bruker S4 Pioneer) analyses were carried out using a wavelength dispersive XRF system with a 4kW rhodium tube and an excitation voltage of up to 60 kV. The examinations were executed with the program AXS34 (FQuant). The total graspable wavelength area was scanned in the StepScan Mode.

Finally, the bulk solid phases' crystal shape and size was ascertained with a SEM (Scanning Electron Microscope, ZEISS DSM 982 Gemini using 5kV and gold coated samples).

3.2. Industrial solutions

39 samples or industrial solutions were used for chemical characterisation. The water samples were provided from different plants of the company Omya from all over of the world. A list of their Sample ID, origin and the type of water is given in Tab. A-1, sorted by plant location.

The occurring water types were:

- WW...waste water
- CFW…centrifuge water
- CDW…condensate water
- PW…process water
- CLW…cleaning water
- COW…compressor water

3.3. PCC experiments

3.3.1 Materials

For the slaking and precipitation process bidistilled water was mixed with different additives: magnesium chloride hexahydrate ($MgCl_2 \cdot 6H_2O$; Roth), strontium chloride hexahydrate ($SrCl_2 \cdot 6H_2O$; Roth), zinc chloride ($ZnCl_2$; Emsure), manganese (II) chloride ($MnCl_2 \cdot H_2O$; Sigma Aldrich), sodium sulphate (Na_2SO_4; Roth) and iron (II) chloride hydrate ($FeCl_2 \cdot H_2O$; Riedel-de Haen). A list of the conducted experiments is given in Table A-2. Additionally, sodium citrate ($Na_3C_6H_5O_7$) by Brenntag CEE GmbH was added to each solution before the slaking process in order to inhibit the formation of aragonite and trigger the calcite precipitation.

Furthermore, the lime (mostly CaO from burned limestone) used for the slaking process was obtained by calcination of a natural limestone. It was called “Tagger “ and was provided by Omya.

3.3.2 Experimental setup

A series of fourteen experiments were conducted. The methodology was consistent throughout all the experiments. The two variables were the amount and kind of additive (see section 3.3.1 and Tab. A-2). A schematic outline of the single steps of the conducted experiments is given in Fig.2.

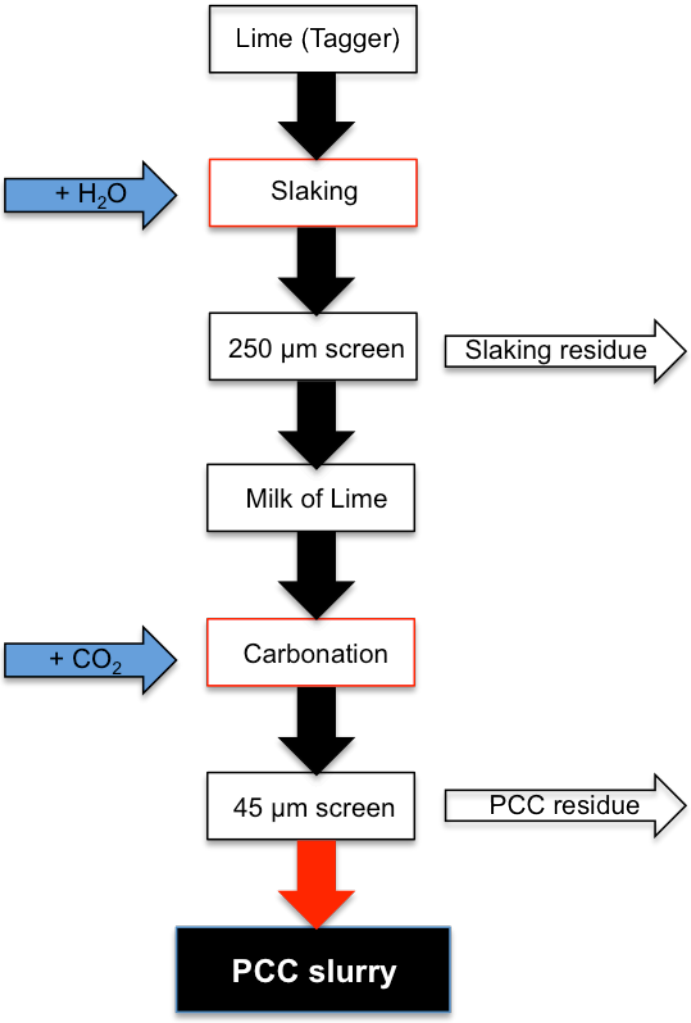

Figure 2: Schematic depiction of the experiments' different steps

For the slaking process 5 litres of distilled water containing 0.1% sodium citrate were mixed in a large container (with or without salt addition). The solution was heated, while being continually stirred, until a temperature of 40°C was reached. Subsequently, a sample of this initial solution was taken to analyse the concentration of the composition of the dissolved components.

Subsequently, 1000 g of lime (Tagger) were added to the 5 litres of the above sodium citrate solution. In order to achieve a homogenous suspension, the suspension was stirred continuously for a reaction time of 25 minutes. The temperature was monitored throughout the slaking-process at 2, 5, 10, 20 and 25 minutes. After the given reaction time of 25 minutes 4 L of the prepared suspension at a temperature of 40°C were added to yield an experimental volume solution of 9 litres in total (this one litre of water was added later in case the temperature would have risen above 90°C during the slaking process to bring the temperature back down). The solution was mixed for 5 min with a stirrer. Subsequently, solids > 200 µm in size were separated from the suspension with a sieve. The sieved solution is called milk of lime (MoL). 8 litres of the MoL were then being used for the carbonation. The separated solid was washed with water and then placed into the oven for drying at a temperature of 105°C.

After the slaking process eight litres of the MoL were placed into a specially designed precipitation reactor (Figs. 3 and A-1). According to the requirements for the precipitation tests, the process parameters for all the trials were a starting temperature of 50°C, a CO_2/air flux of 15 l/min with 20% of CO_2 (P_{CO_2} = 0.2 atm).

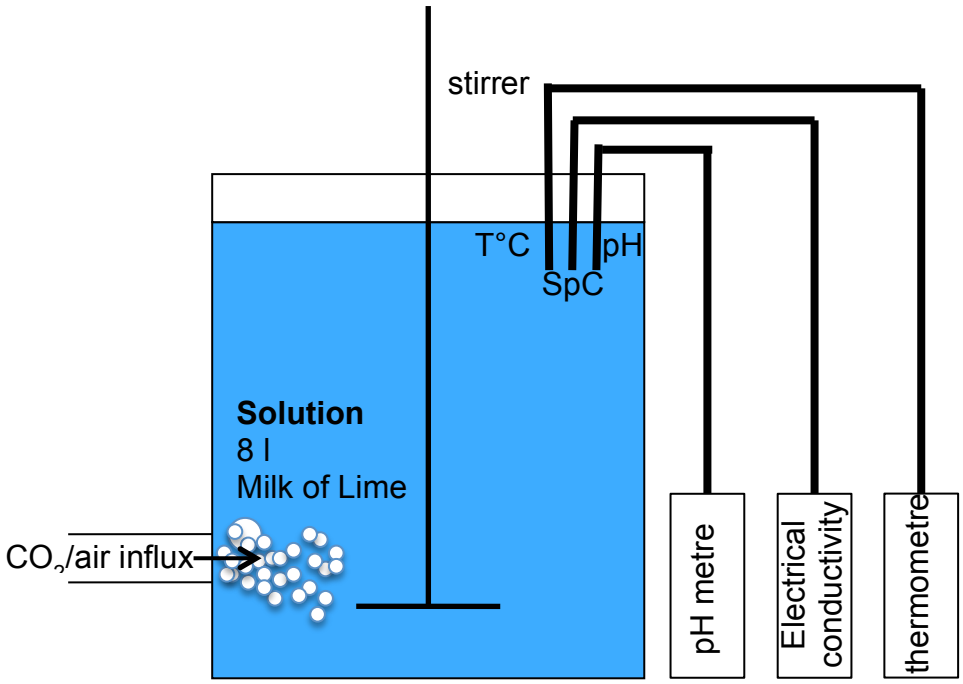

Figure 3: Experimental setup for the $CaCO_3$ precipitation

Furthermore, pH and conductivity were automatically measured in the suspension (slurry) throughout the whole experiment. The stirrer of the reactor was operated at a speed of 1450 rpm once the starting temperature of 50°C was obtained. The CO_2 gas inflow was stopped five minutes after the conductivity dropped to its minimum. With a time delay of about three minutes, the pH reached its lowest value as well.

After the experimental run the suspension was sieved through a 45 µm sieve to separate the solids from the fluid. The screenings were washed and dried in the oven at 105°C. The finally obtained slurry was analysed with various techniques, which are described in more detail in section *4.2.2.*

After the precipitation process the remaining suspension was filtered (0.45 µm) in order to create a filter cake. This filter cake was washed with ethanol. The resulting filter cake equals the final product in the large-scale process.

Accordingly, two different filter cakes per experiment were obtained by filtering the milk of lime (> 200 µm) as well as the solution after precipitation (> 0.45 µm). Its solid content in percentage was measured twice. Once after filtering, when the cake was still wet, and once after drying the cake overnight in the oven at a temperature of 105°C. The measured solid content is given in percentage.

Following the drying process the acquired filter cake of the sieved carbonated product (0.45 µm) was used for determination of the specific surface area, brightness, SEM and XRD.

As mentioned above, the analogous experiments were conducted for the experiments 2 to 14 (see Table A-2). However, different additives at varying amounts were added to the initial solution. The aim was to observe their influence on the slaking as well as on the carbonation process.

3.4. Experimental background

As stated in section 2.8 there are two different general directions concerning the CO_2 exchange between gas phases and aqueous solutions. Obviously, for the conducted experiments the absorption of CO_2 was valid. The suspension (slaked lime and finally milk of lime) was characterised by a pH of about 12.5. Due to this high pH and the on-going supply of CO_2 during the carbonation process the carbon dioxide was rapidly absorbed by the solution, which finally led to the precipitation of solid calcium carbonate.

The dominant reactions, which led to the precipitation of $CaCO_3$ under the prevailing laboratory conditions, are

$$CO_2 + OH^- = HCO_3^- \quad (26)$$

$$HCO_3^- = CO_3^{2-} + H^+ \quad (27)$$

$$Ca^{2+} + CO_3^{2-} = CaCO_3 \quad (28)$$

$$CO_2 + OH^- + Ca^{2+} = CaCO_3 \quad (29)$$

3.5. Modelling approach

The ion balance and hydrochemical parameters were determined using the programs AquaChem and PhreeqC (database miteq.v4.dat; database was modified concerning the citrate related according to Gautier (2012)).

PhreeqC was also used to re-enact the precipitation processes throughout the carbonation experiments. The results were compared to the values monitored in the laboratory reactor, to verify the concurrence between the recorded and modelled reaction. The PhreeqC program code is based on: (i) a defined solution chemistry including the starting amount of sodium citrate and additives, (ii) a stated amount of portlandite and of MgO for maximum dissolution to reach equilibrium (values are given from chemical analyses of used lime and the addition of lime), (iii) equilibrium with calcite and portlandite. The given values were changed according to the various additives, where the calculation basis was the weighed proportions in mg/L (Tab. A-6c). Finally, the CO_2 was introduced into the system in 100 steps until neutralisation was reached. This modelling approach allows for identification of hydrochemical parameters such as pH for any given time.

4. Results

4.1. Industrial solutions

The results concerning the measured values for the various industrial solutions can be found in Table A-1 (Appendix). The ion composition of the samples varied significantly depending on the origin of the water. Thus, the waters originating from the same production state (e.g. waste water) were looked at separately. Figure 4 depicts the composition of the waters regarding their main components ordered by water type. However, those states also vary from subsidiary to subsidiary.

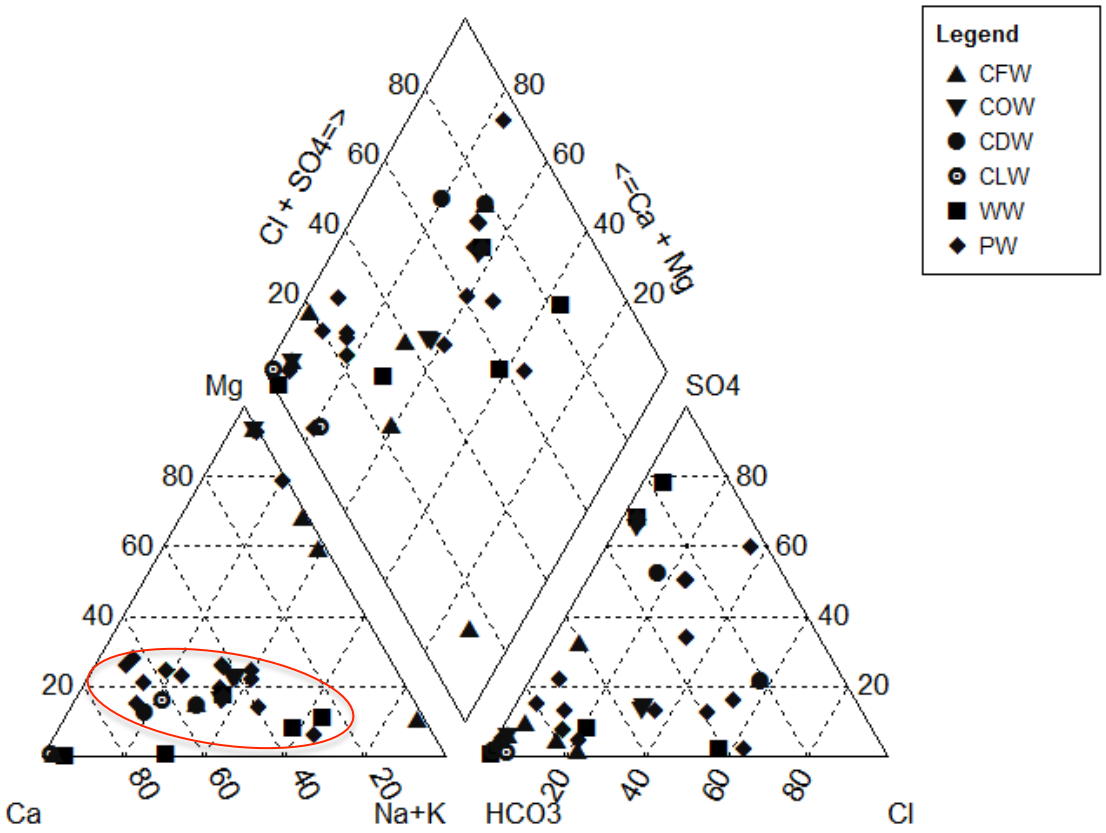

Figure 4: Piper plot of the industrial solutions in mol/L. CFW…Centrifuge Water, COW...Compressor Water, CDW...Condensate Water, CLW...Cleaning Water, WW...Waste Water, PW...Process Water

Most solutions had a pH between 6 and 9 and a calcium concentration up to ≈ 80 mg/L (Fig.5). The process waters' (PW) pH ranged from 6 to 9 and the Ca values ranged from 4 to 72 mg/L. In the wastewater samples (WW) the pH was distinctly higher with values between 7.5 and 12.5. Their calcium concentrations were widely spread starting at 7 mg/L up to 724 mg/L. The waters from the centrifuge (CFW) had the lowest Ca concentrations with 5.5 ± 2 mg/L with the exception for one sample, which had 469 mg/L.

In addition, they displayed an average pH of 8.6. The waters from the compressors (COW) exhibited the lowest pH values with a minimum of 2.4 and a maximum of 7.2. Their measured calcium concentration lay between 3.5 and 34.5 mg/L. The two samples of cleaning waters (CLW) did show very different behaviours concerning pH and Ca concentration. The former were 7.3 and 12.4 and for latter the values were 134.8 and 817.3 mg/L. The last water type, the water from the condensers (CDW), had an average pH of 7.4 and a calcium concentration of 15.3 and 74.7 mg/L, respectively.

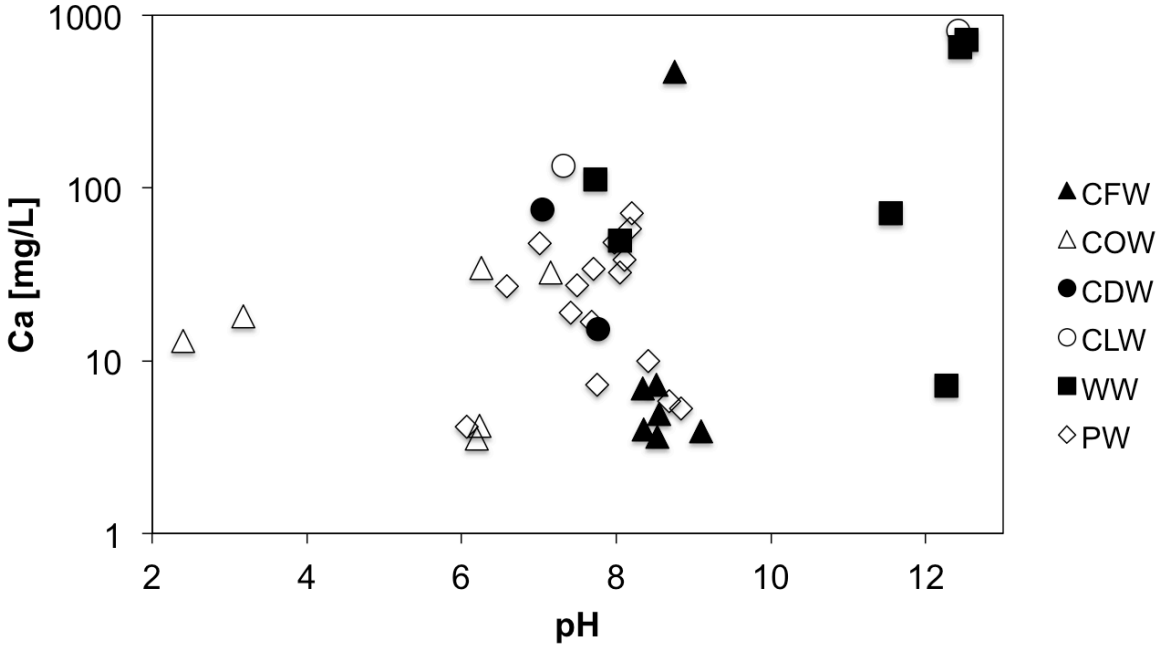

Figure 5: The calcium concentrations plotted against the pH of all industrial solutions. CFW…Centrifuge Water, COW...Compressor Water, CDW...Condensate Water, CLW...Cleaning Water, WW...Waste Water, PW...Process Water

The Mg to Ca concentration showed a positive relation as can be seen in Fig. 6. This could result from the Mg:Ca ratio of the slurries used for the precipitation processes. The consumption of Ca and Mg during the precipitation resulted in an increasingly alkaline solution (Na+K). The mean value for Mg was 5.7 mg/L and 26.9 mg/L for Ca. The CFWs presented a different correlation between calcium and magnesium content than all other samples. Their Mg concentrations were significantly higher.

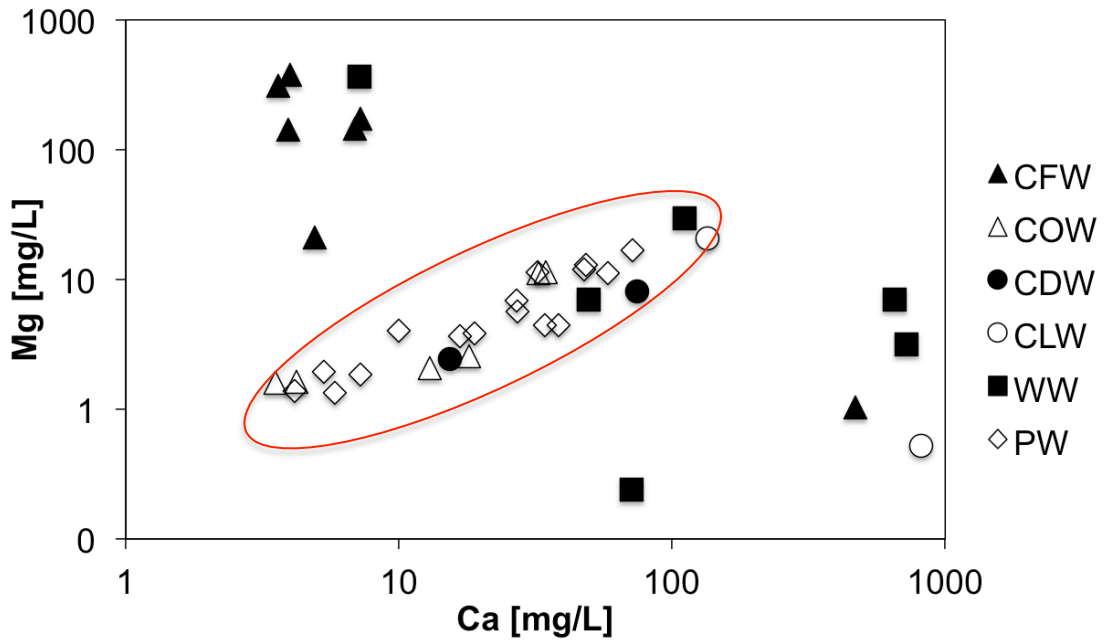

Figure 6: The magnesium concentrations plotted against the calcium concentrations in mg/L for all industrial solutions. CFW…Centrifuge Water, COW...Compressor Water, CDW...Condensate Water, CLW...Cleaning Water, WW...Waste Water, PW...Process Water

Figure 7 compares the calcium concentration in mg/L with the saturation index of calcite of all samples. The solution was saturated with respect to calcite for CLW. For COW and CDW the aqueous solution was undersaturated with respect to calcite. The water types for which both saturation stages were recorded was PW, WW and CFW. In that case of PW the saturation index for calcite ($SI_{calcite}$) lay between -2.1 and 0.9, for WW between -1.1 and 2.9 and for CFW between -1.5 and 2.7.

The industrial solutions' pH was plotted against the $SI_{calcite}$ in Fig. 8. The process waters showed an increasing saturation index with increasing pH. The process waters occurred undersaturated as well as supersaturated with respect to calcite. For those samples the $SI_{calcite}$ was between -2.1 and 0.9 with a pH ranging from 6.6 to 8.8. In this case the pH and SI seemed to correlate. With increasing pH the saturation state increased as well. The wastewaters were with the exception of one solution supersaturated with respect to calcite. The pH values were between 7.7 and 12.4 and the $SI_{calcite}$ between -1.1 and 2.9. A low pH and a mean $SI_{calcite}$ of -0.8 defined the waters from the compressors. The CDWs showed a very similar behaviour with average pH and SI values of 7.4 and -0.9, respectively. The waters from the centrifuge had a mean pH of 8.5. Concerning the saturation state, all samples except for one were supersaturated. Their mean value was 0.5. Finally, the

two cleaning waters showed very different results concerning pH and $SI_{calcite}$. The values for former were 9.9 and 12.4 and for latter 0.65 and 3.19.

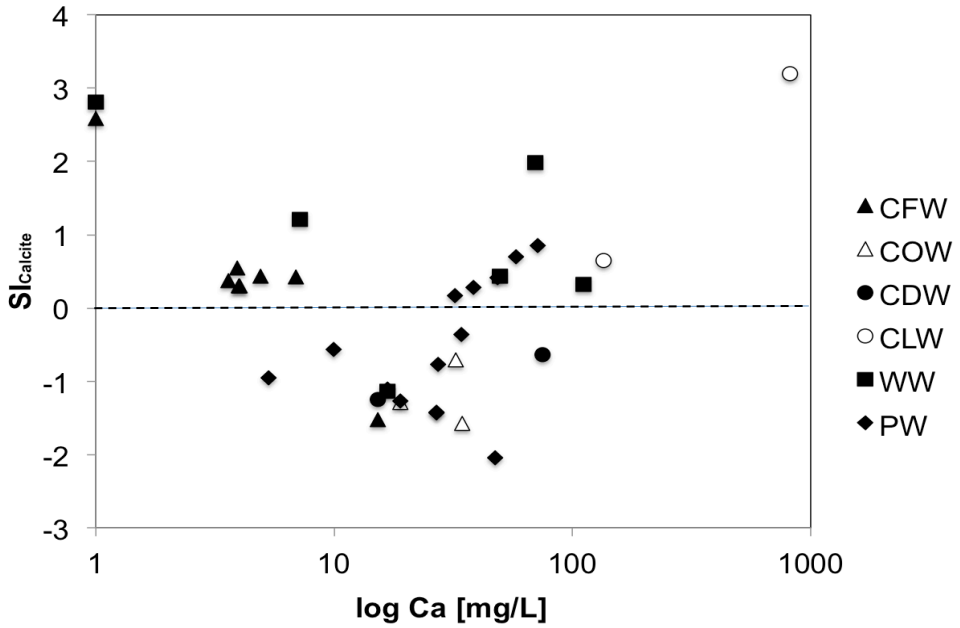

Figure 7: The SI of calcite plotted against the calcium concentrations of the industrial waters ordered by water type. CFW…Centrifuge Water, COW...Compressor Water, CDW...Condensate Water, CLW...Cleaning Water, WW...Waste Water, PW...Process Water

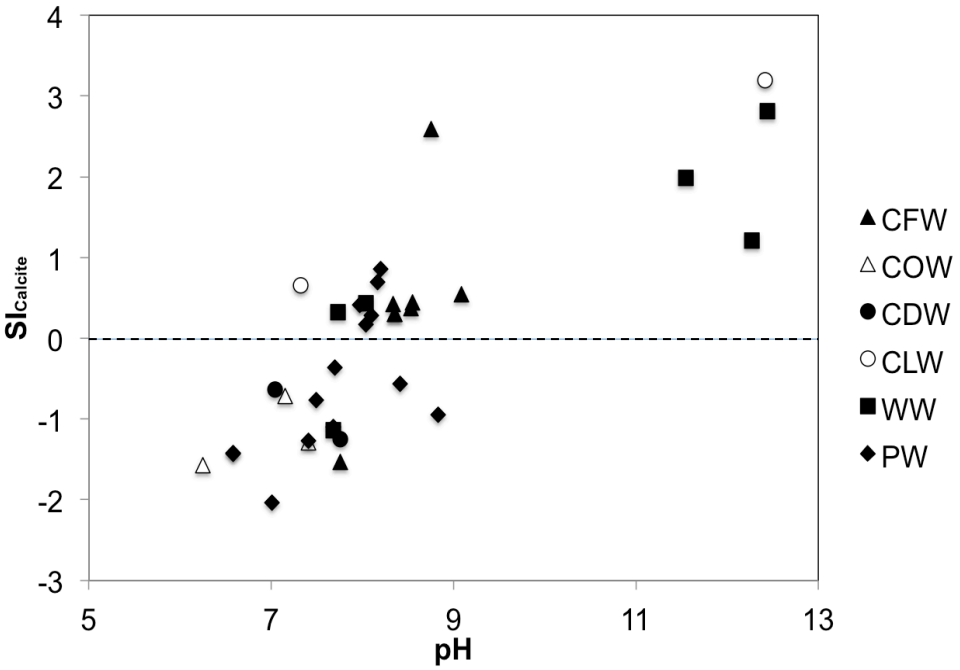

Figure 8: The SI of calcite plotted against the pH of the industrial waters ordered by water type. CFW…Centrifuge Water, COW...Compressor Water, CDW...Condensate Water, CLW...Cleaning Water, WW...Waste Water, PW...Process Water

The aluminium concentrations compared to the silica concentrations depicted in Fig. 9 did not show an obvious correlation. The mean values for Al and Si were 100 µg/L and 7.7 mg/L, respectively.

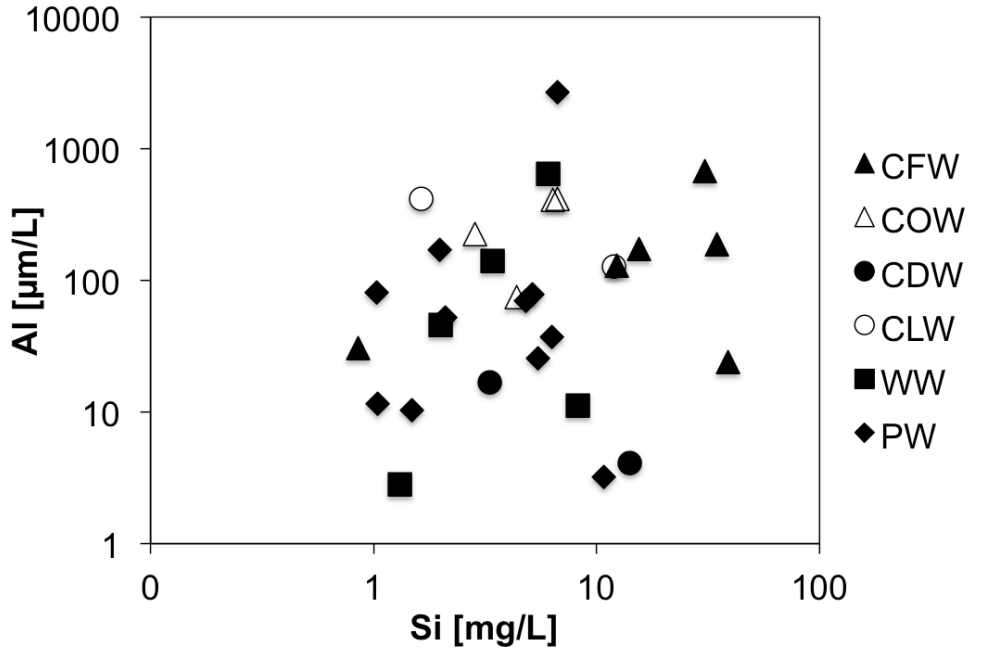

Figure 9: The aluminium concentrations plotted against the silica concentrations for all industrial solutions. CFW…Centrifuge Water, COW...Compressor Water, CDW...Condensate Water, CLW...Cleaning Water, WW...Waste Water, PW...Process Water

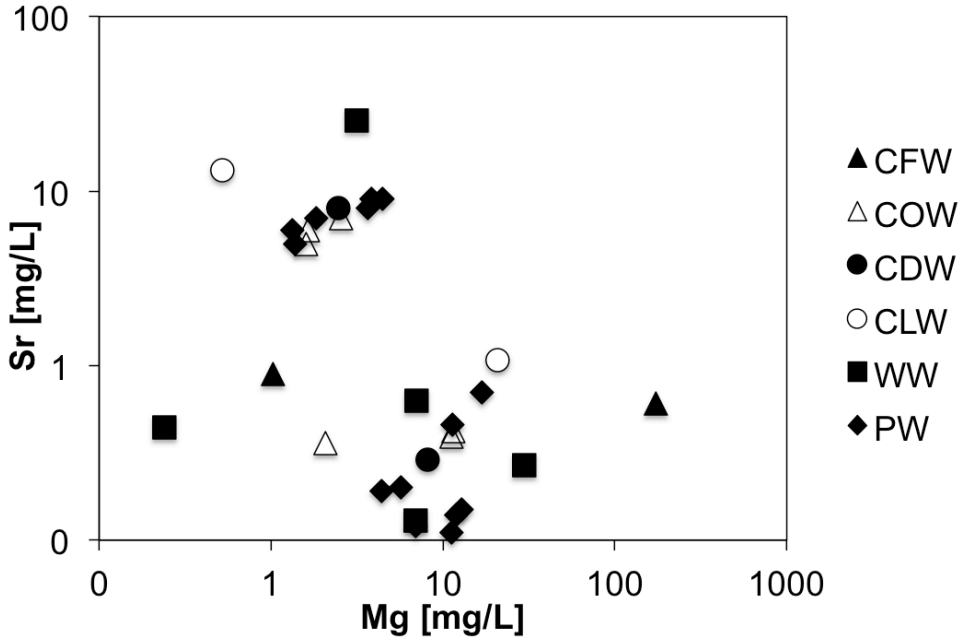

Figure 10: Strontium concentrations plotted against magnesium concentrations in mg/L. CFW…Centrifuge Water, COW...Compressor Water, CDW...Condensate Water, CLW...Cleaning Water, WW...Waste Water, PW...Process Water

Looking at the strontium and magnesium concentrations of all the industrial solutions, to some extent, a correlation between those values was shown (Fig. 10). The measured results for strontium were between 0.1 and 13 mg/L and between 0.07 and 380 mg/L for magnesium.

Plotting illustrated that zinc and strontium did not correlate in the industrial solutions. In many cases either zinc or strontium were beneath the detection limit, and are therefore not shown in the graph (Fig.11). The comparison of the aluminium and zinc concentrations (Fig. 12) also did not show any significant correlation.

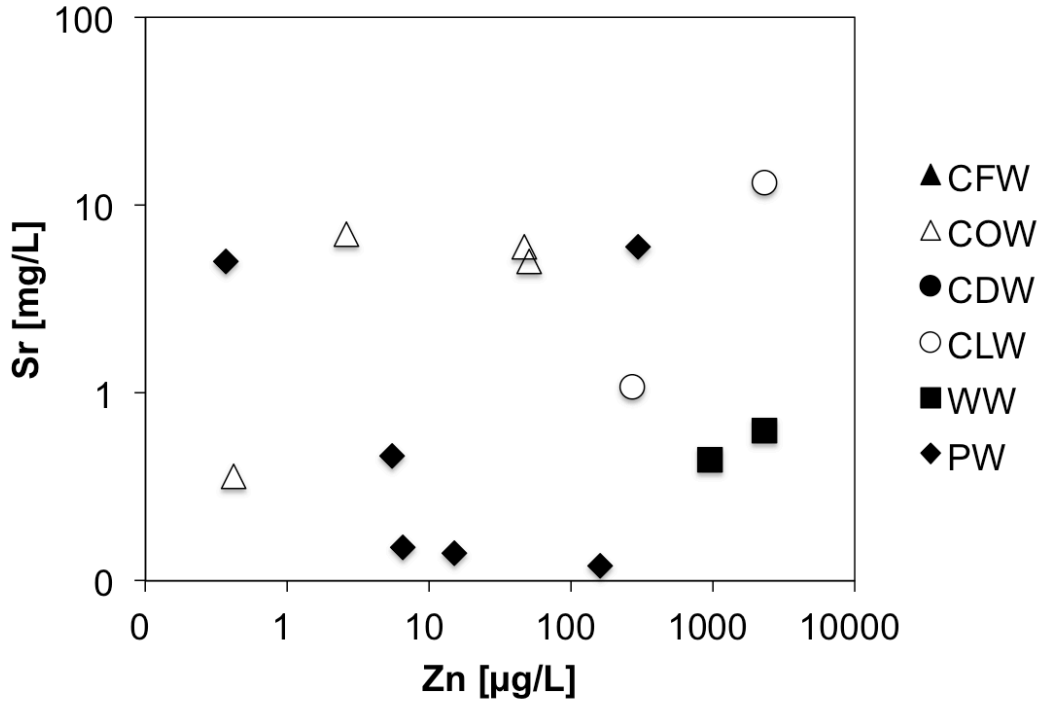

Figure 11: zinc concentrations plotted against strontium concentrations. CFW…Centrifuge Water, COW...Compressor Water, CDW...Condensate Water, CLW...Cleaning Water, WW...Waste Water, PW...Process Water

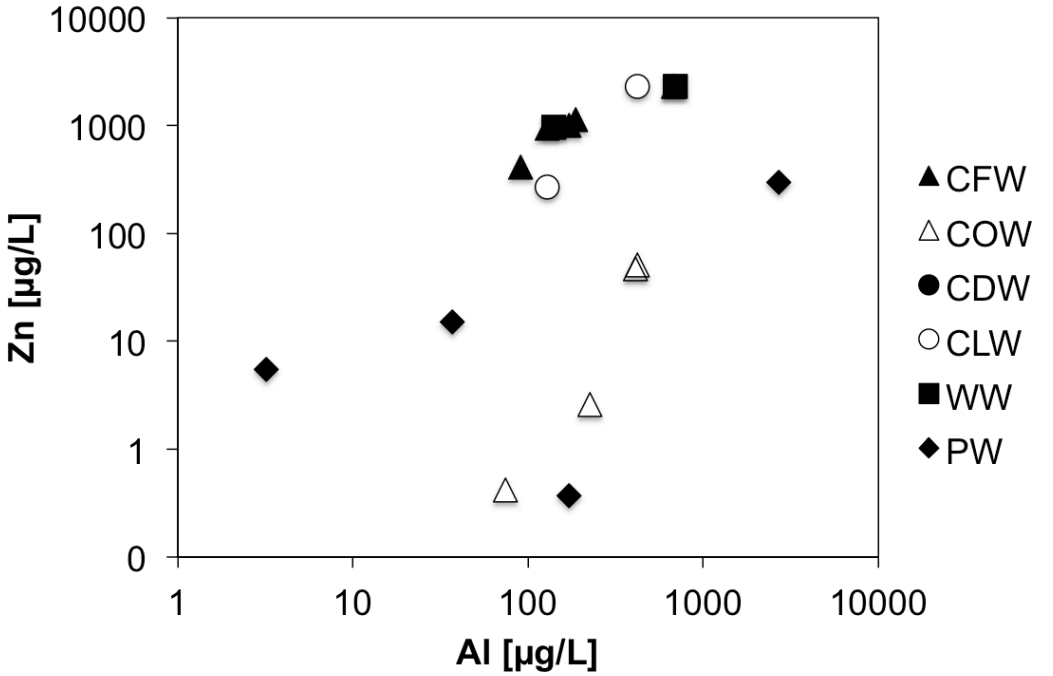

Figure 12: Aluminium concentrations plotted against zinc concentrations. CFW…Centrifuge Water, COW...Compressor Water, CDW...Condensate Water, CLW...Cleaning Water, WW...Waste Water, PW...Process Water

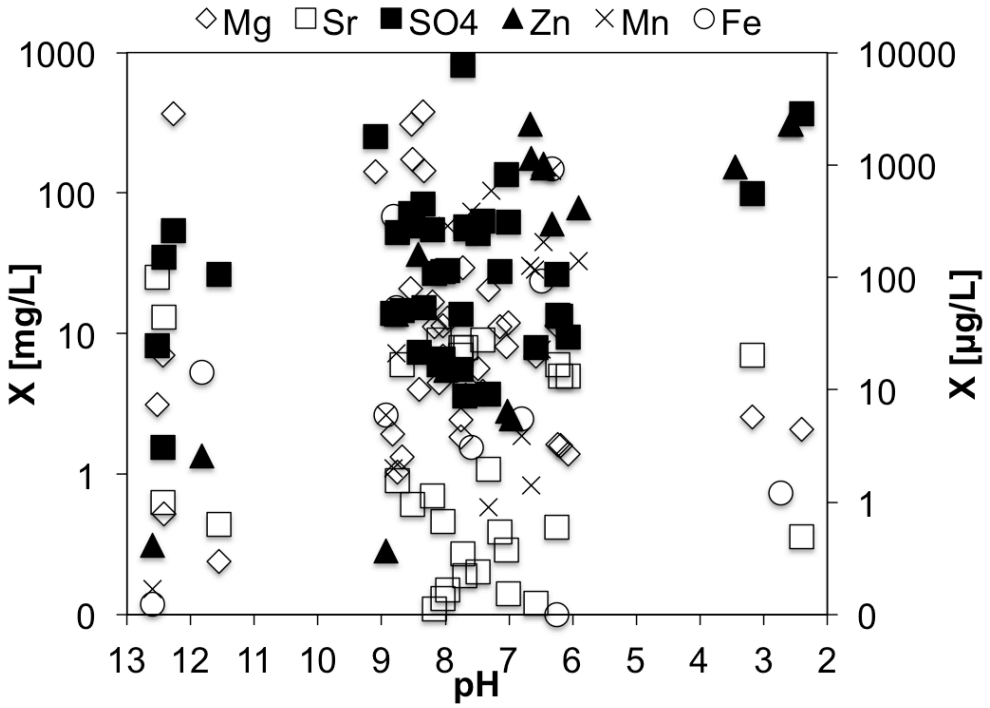

Figure 13: Concentrations of dissolved ions in mg/L (Mg, Sr, SO_4, Mn) or µg/L (Zn, Fe) plotted against pH

In Figure 13 the ion content of the elements, which had subsequently been used for the precipitation experiments were plotted against the pH. The magnesium concentrations lay between 0.1 and 379 mg/L, strontium up to 35 mg/L, zinc up to 2331 µg/L, manganese up to 3.9 mg/L, sulphate between 1.6 and 815 mg/L, and finally, iron up to 14 µg/L.

As can be seen in Fig. 13 most of the investigated industrial solutions indicated a pH between 6 and 9. The concentrations of the ions exhibited as rather inhomogeneous. However, for each element only a small number of solutions displayed an exceptionally increased concentration. The waters from the centrifuge (CFW) showed a mean value for magnesium of 167 mg/L. Comparing that to the mean value of 7 mg/L of all samples exhibited that apparently in those waters the magnesium was higher in concentration. The same was valid for the zinc concentrations in the CFWs. Whereas most solutions contained very little or no zinc at all the waters from the centrifuge showed values ranging from 414 to 2318 µg/L. The cleaning waters (CLW) revealed slightly elevated strontium values up to 13 mg/L and elevated zinc concentrations with a maximum of 2320 µg/L. The waters from the compressors (COW) were characterised by increased sulphate concentrations of 100 and 364 mg/L. For the process waters (PW) no visible trend of elevated ion concentrations could be observed. The same was valid for the waters from the condensers (CDW). Remarkable was the high pH of about 12 for the waste waters.

4.2. Precipitation experiments

The following graphs in figure 14 depict the slaking curves for all samples by plotting the change in temperature over time. For each experiment the slaking process was started when a temperature of 40 °C was reached. During slaking the temperature was taken five times throughout the experiment (at 2, 5, 10, 20 and 25 minutes).

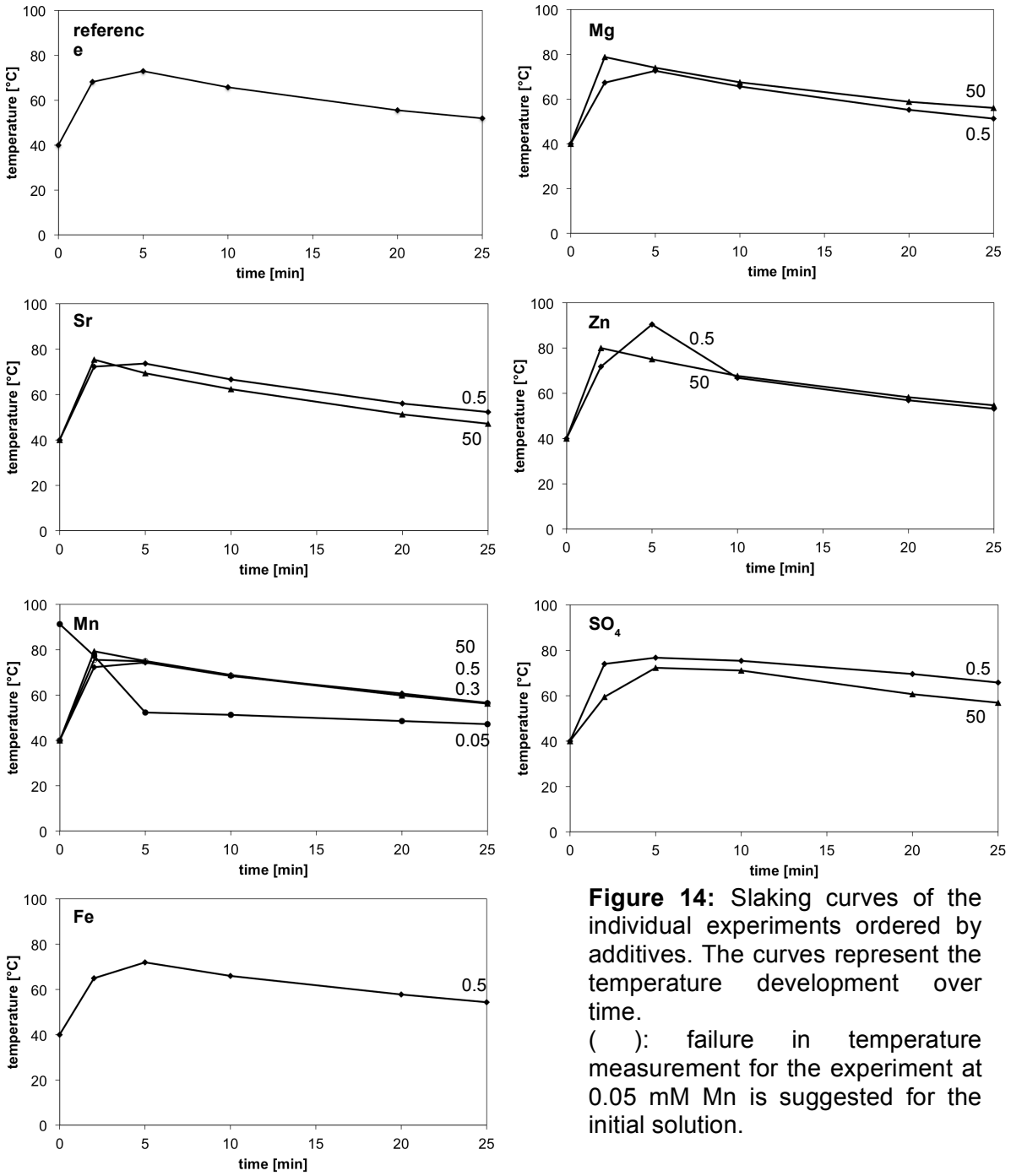

Figure 14: Slaking curves of the individual experiments ordered by additives. The curves represent the temperature development over time.
( ): failure in temperature measurement for the experiment at 0.05 mM Mn is suggested for the initial solution.

All samples with the exception of 0.05 mM Mn reached their maximum temperature within the first five minutes. For said experiment a failure in the temperature measurement is suggested.

The slaking curves in Fig. 14 do not resemble typical slaking curves due to non-adiabatic conditions in the case of the conducted experiments, leading to a loss of temperature due to emission.

4.2.1. Solid phase characterisation

The Figs. 15a and b display the XRD patterns of the precipitates from the experiments containing either 0.5 or 50 mM additive after filtration through 0.45 µm membrane (final product). The Fig. A-2 in the appendix shows the XRD pattern for all experiments before they were filtered through the 0.45 µm membrane. The $CaCO_3$ phase in all 0.5 mM additive bearing experiments for both steps was characterised as calcite by its distinctive peaks, e.g. d_{104} = 3.04 Å. All samples except precipitates from initial 50 mM of Sr solution the XRD pattern revealed 100 % calcite. For the latter sample aragonite was detected according to its peaks, e.g. d_{221} = 1.97 Å, besides calcite. The equations 24 and 25 were used to quantify the calcite (X_{Cc}) and aragonite (X_{Ar}) fractions of this sample after carbonation in wt. % according to the XRD pattern. Aragonite dominates with 94 wt. % and calcite occurs with 6 wt. %.

The XRD results of the final product were confirmed by FTIR pattern (Fig. 16). The FTIR pattern verified calcite in all precipitates except for initial 50 mM Sr. Calcite was detected by a wave number at 712 cm^{-1}, whereas aragonite was detected by 1083 cm^{-1}.

Furthermore, the results concerning the chemical composition, which were measured via XRF, can be found in Tab. A-3. The CaO content of the final product for all conducted experiments was 54 ±5 wt.% and for MgO 1 ± 0.5 wt.%. Concerning the other components the initially added additive was to some extent reflected in the composition of the final product. Notably, in the case of 50 mM Sr the value of 2.1 wt.% lay significantly above the average of 1.5 wt.%.

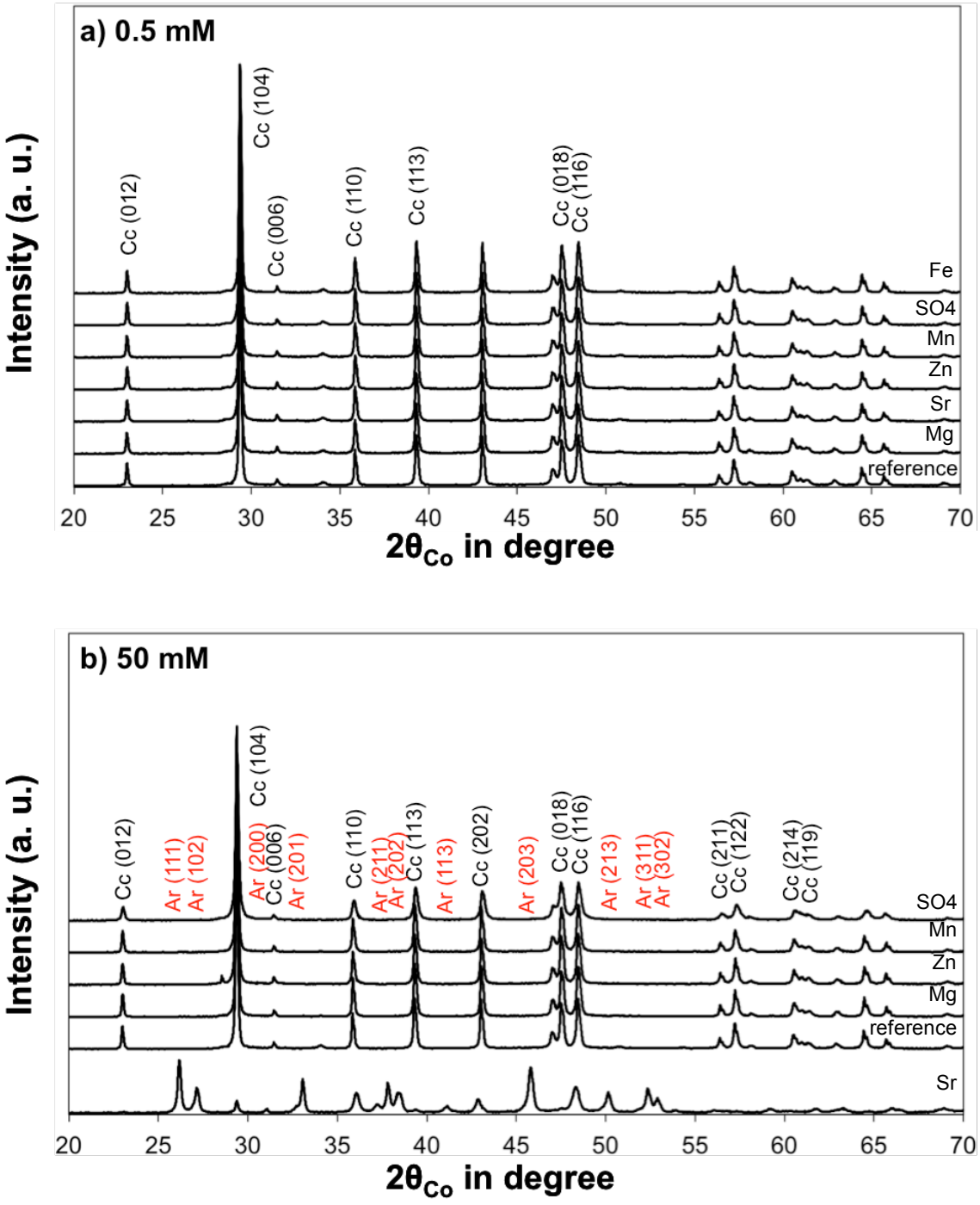

Figure 15: XRD patterns of the filter (final product) for **a)** 0.5 mM and **b)** 50 mM additives showing the calcite (Cc) and aragonite (Ar) indices.

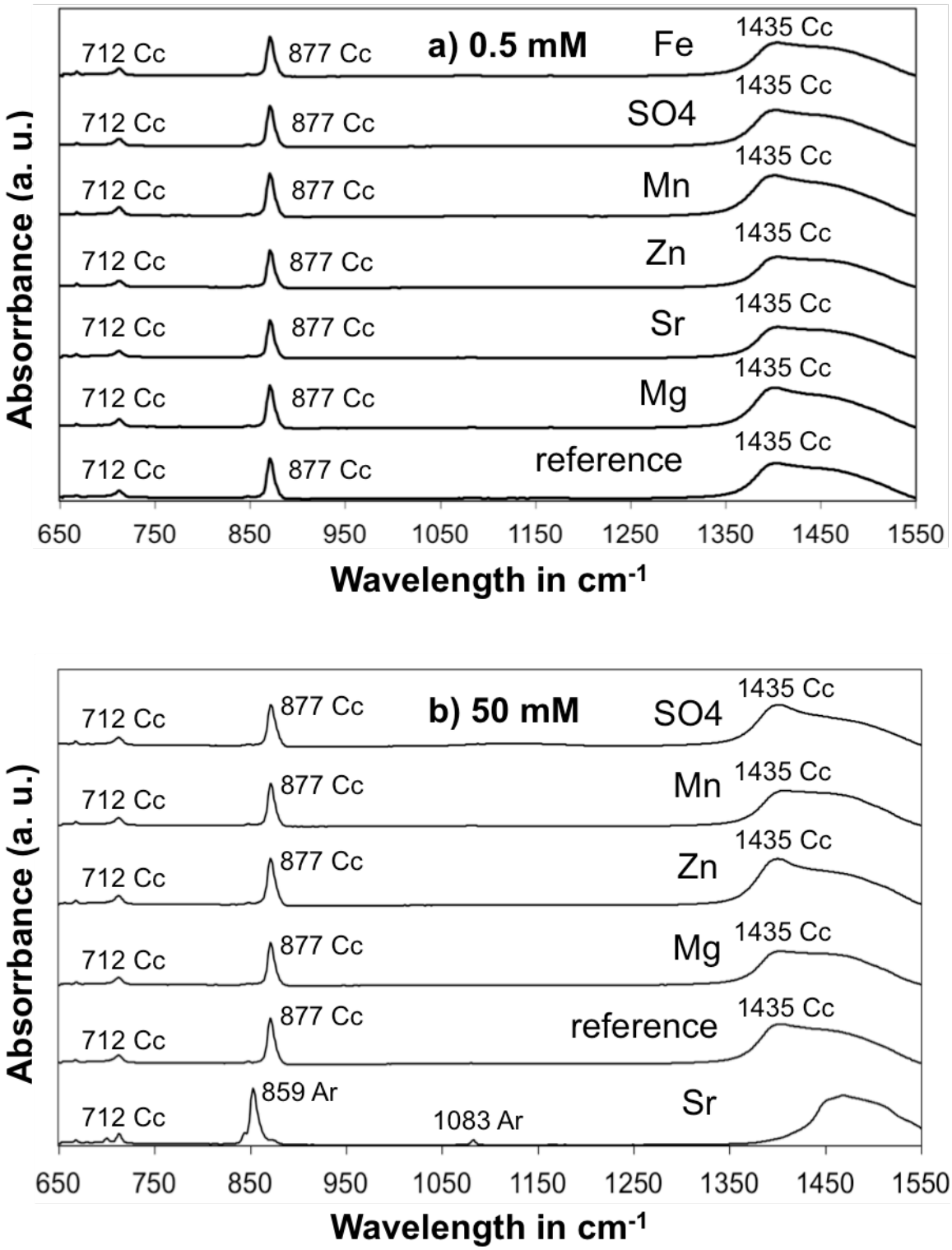

Figure 16: FT-IR spectra of the final product for **a)** 0.5 mM and **b)** 50 mM additives showing characteristic peaks for calcite (Cc) and aragonite (Ar).

The SEM pictures were taken at two stages after the precipitation process. Firstly after sieving the solution through a 45 µm mesh and then after filtering it through a 0.45 µm filter (referred to as final product). Due to the similar results only the pictures of the final product are going to be discussed (Figs. 17 and 18). The other pictures can be found in the appendix (Figs. A-3a and b).

At 0.5 mM additives the final products showed a rather similar behaviour compared to the reference concerning crystal size and shape. All experiments delivered the required conglomerated scalendoedral calcitic PCC (S-PCC) with 2 to 3 µm in size. The samples showed an average SSA of 5.9 m^2/g.

In contrast to the 0.5 mM samples the crystals for 50 mM additive mostly did not resemble the reference sample in shape and size. Magnesium and manganese, however, still had high similarities to the reference. With strontium ions at an elevated level aragonite precipitated, which was reflected in the SEM image. The crystals were considerably smaller in size (0.5-1 µm) and thinner than the reference. For the addition of zinc ions the image showed clusters with a size up to 2 µm. The addition of 50 mM of sulphate resulted in a highly clustered structure with clusters of about 5 µm in size. In Figure 20 the precipitates from 50 mM strontium and 50 mM sulphate solution are represented at a higher magnification to document the difference in shape.

Furthermore, the SSA (specific surface area) was established. The values lay between 4.7 and 8.8 % excluding the 50 mM samples of strontium and sulphate. The values for 50 mM Sr and SO_4 were 20.9 and 13.9, respectively. A complete list can be found in the appendix (Tab. A-4).

Concerning the brightness according to R457 the reference sample had a value of 97.2 %. With 0.5 mM additive the greatest difference to the reference's value, apart from manganese, was shown by iron with 96.1 %. For manganese only a brightness of 86.4 % was achieved. 50 mM magnesium, strontium and zinc had a brightness of ca. 96 %. PCC in the presence of 50 mM sulphate had a value of 90.7 %, whereas in the presence of 50 mM manganese a value of 26.7 % was observed. The experiments with a Mn addition of 0.3 and 0.05 mM resulted in a brightness of 86.4 and 92.9 %, respectively. The latter still showed a loss of brightness of 4.3 % compared to the reference sample. The brightness was not only measured at the final product but also after the slaking process and before filtration to gain the final product. A list of all the values for the brightness can be found in Tab. A-5.

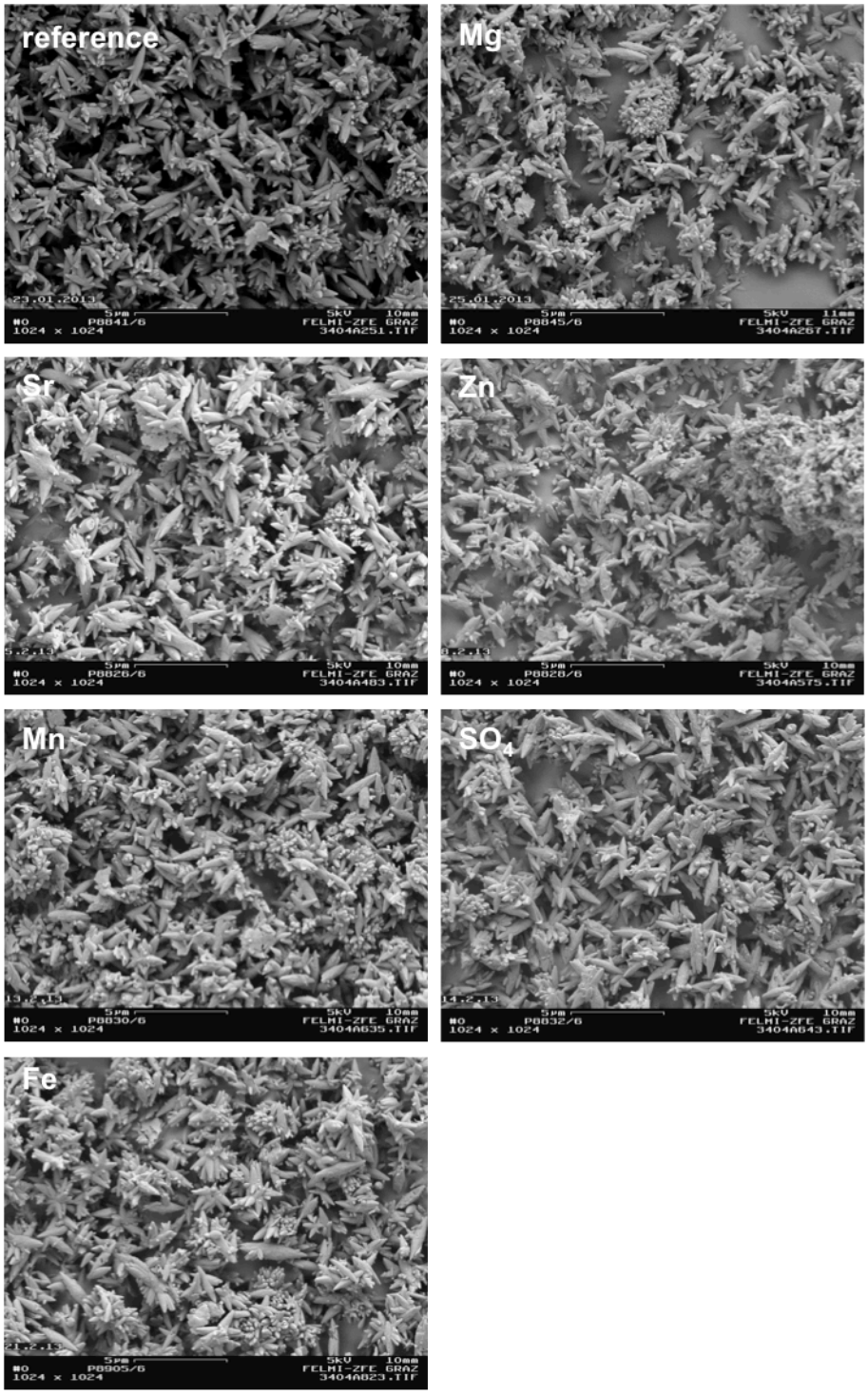

Figure 17: SEM imaging for the final products including the reference sample and precipitates from solutions with 0.5 mM of either Mg, Sr, Zn, Mn, SO_4 or Fe after the filtration through 0.45 µm membrane.

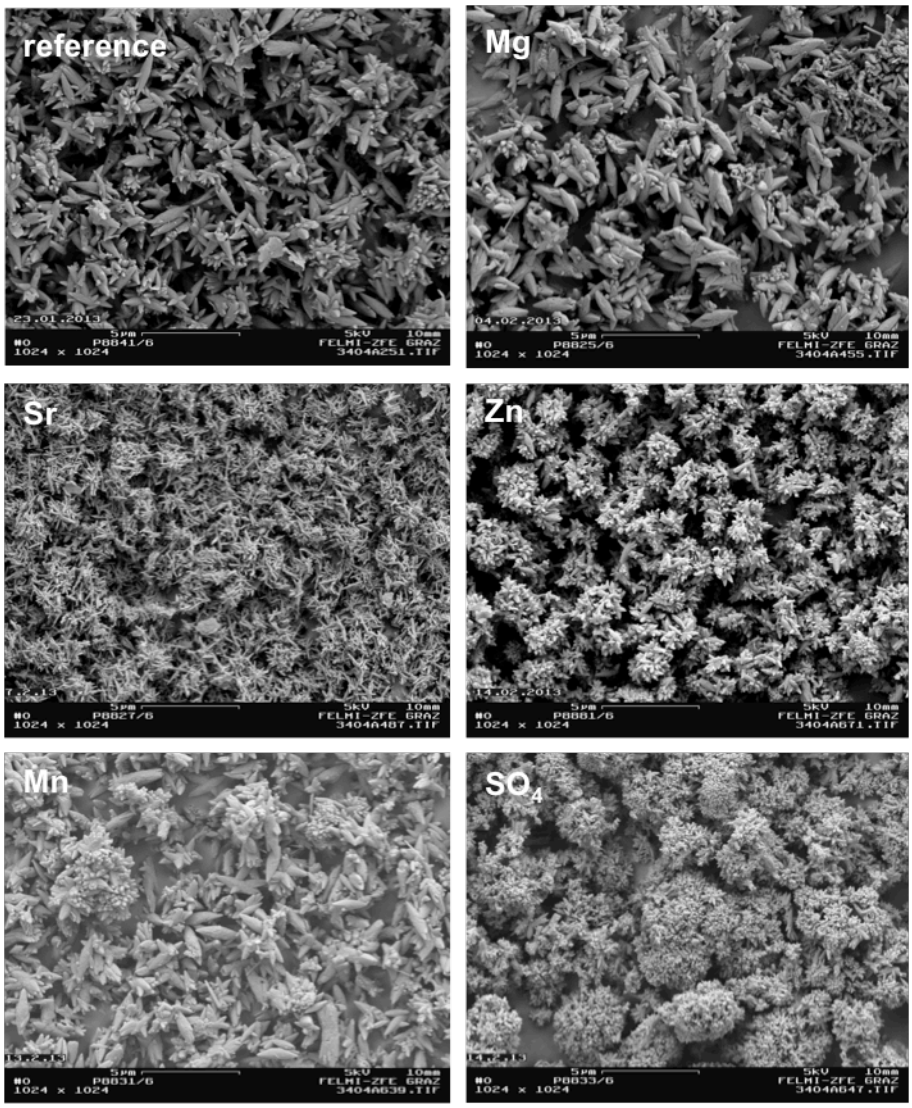

Figure 18: SEM imaging for the final products including the reference sample and precipitates from solutions with 50 mM of either Mg, Sr, Zn, Mn, SO_4 or Fe after the filtration through 0.45 µm membrane.

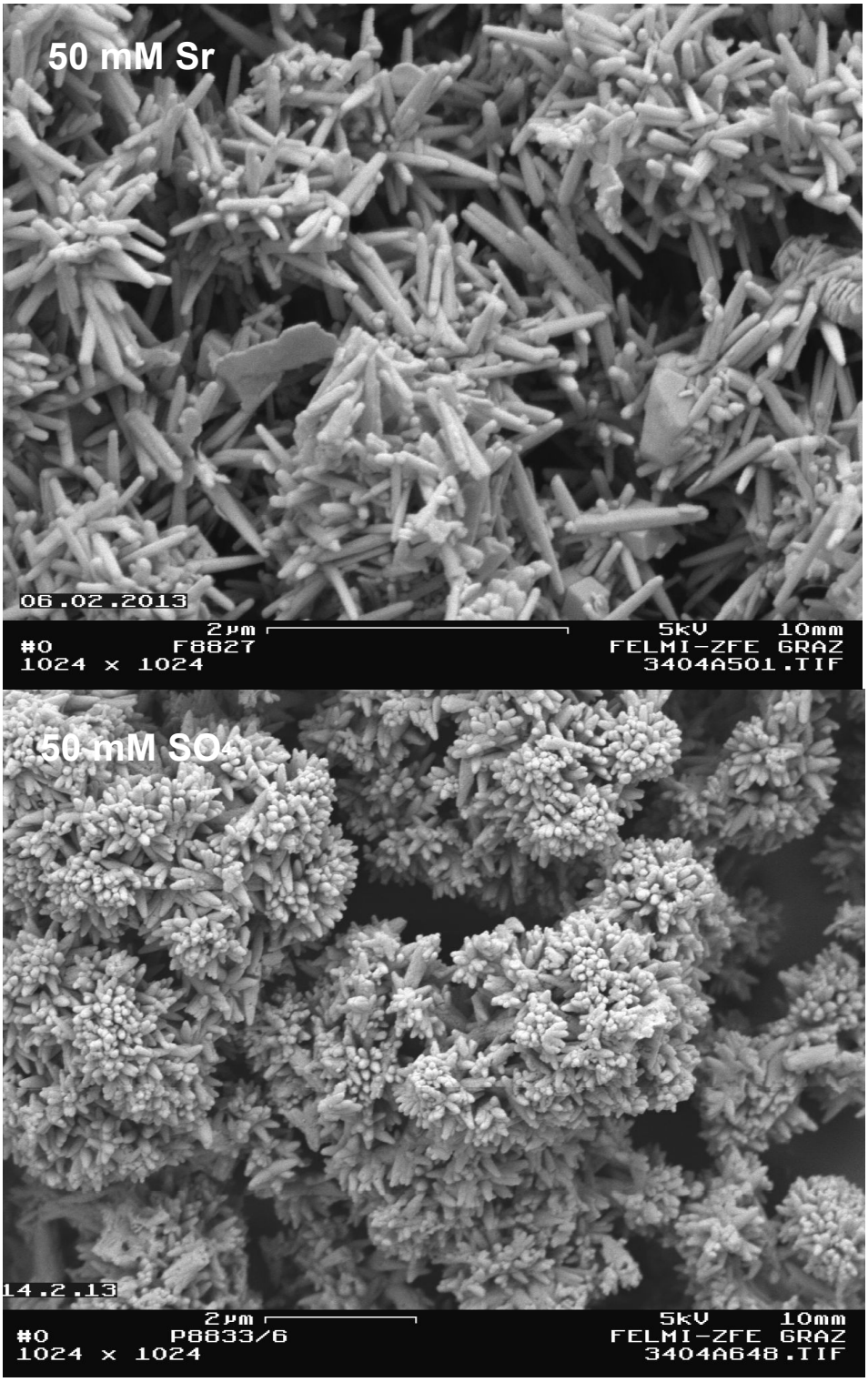

Figure 19: SEM imaging of precipitates from solutions with 50 mM Sr and SO_4

4.2.2. Solution chemistry

The complete list of the chemical analysis of the three solutions which were taken at different stages during each experiment (initial solution, after slaking (MoL) and after carbonation) are given in the Table A-6 in the Appendix. Most of the charge balance values were in the acceptable range of ± 5 % but some are significantly higher, probably due to the addition of the sodium citrate and its lost during the carbonation process (see discussion in methodology).

Figure 20 depicts the ion content of the main components in mg/L for the solution after the carbonation process. Most solutions were magnesium enriched and showed very low concentrations of Ca and Na+K.

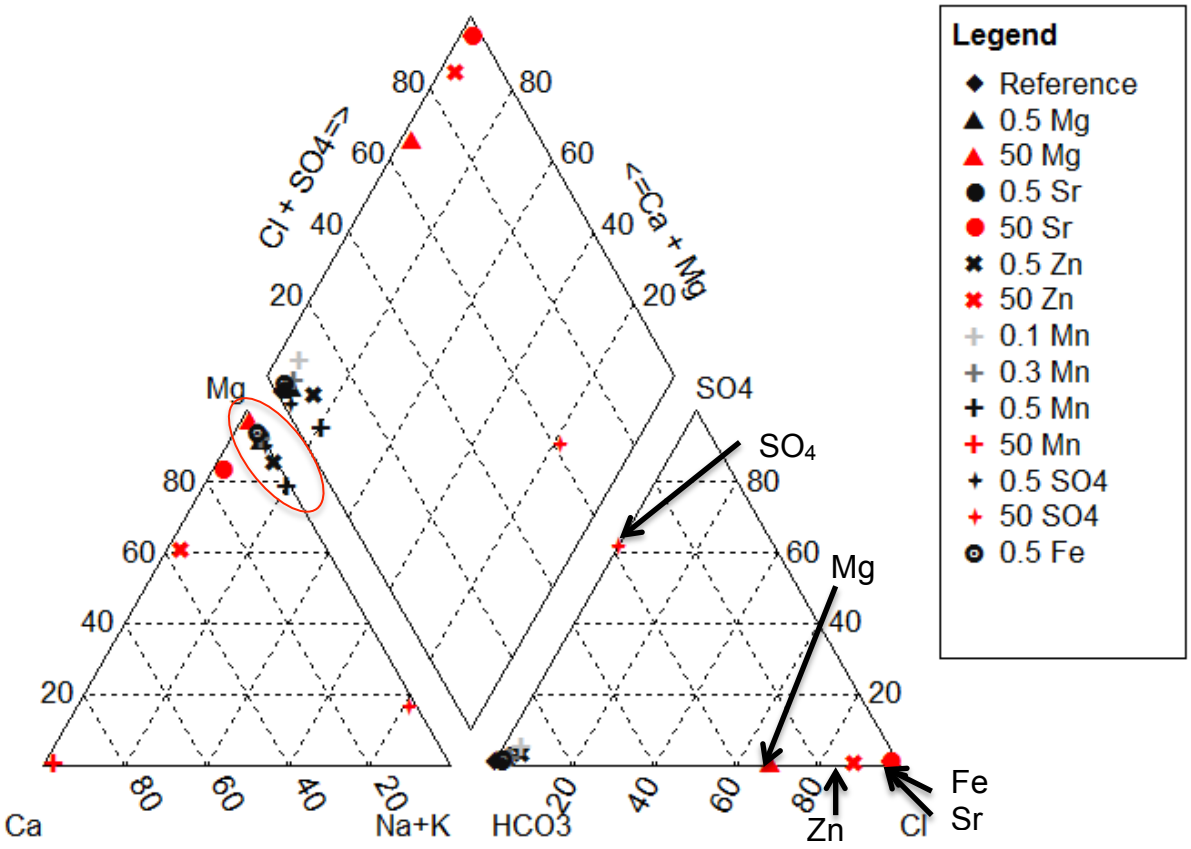

Figure 20: Piper plot of the concentrations of the precipitation experiments after the carbonation in mol/L.

The concentrations in mg/L for each cation were between 2 and 2200 for calcium, 1 and 200 for magnesium, and 72 and 2500 for sodium plus potassium. The anions were dominated by bicarbonate. The solutions with initial 50 mM magnesium, strontium and zinc showed high chloride concentrations, which were caused by the initial addition of the respective chloride salt (see methods). The concentrations lay

between 95 and 4000 for bicarbonate, 3 and 3900 for chloride and 12 and 4000 for sulphate in mg/L.

The solution chemistry for the solution containing 50 mM of SO_4 differed significantly compared to all other solutions. This sulphate containing solution showed elevated Na (2500 mg/L) and SO_4 (4000 mg/L) concentrations, which was referred to the initial addition of sodium sulphate.

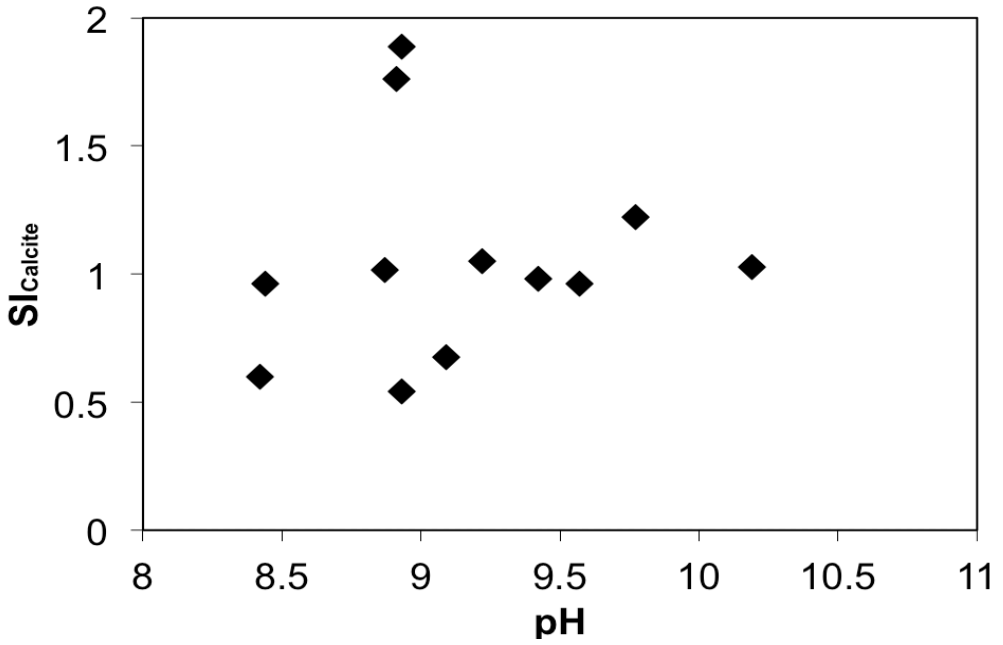

Figure 21: The saturation index of calcite of the final experimental solutions plotted against their pH.

Comparing the $SI_{calcite}$ to the pH of the final solution a correlation trend was not clearly visible (Fig. 21). Most solutions had a SI of about 1 and the complete range was from 0.5 to 2. Therefore, all samples were supersaturated with respect to calcite. In Figure 22 the $SI_{calcite}$ was plotted against the calcium concentrations in mg/L of the final solutions, indicating a correlation between the SI and the concentration of calcium. The samples built a cluster around the saturation index of 1 and a Ca concentration between 2 and 6 ± 0.5 mg/L. The two dots outside this cluster were the solutions with initial 50 mM magnesium (at 19mg/L Ca) and 0.5 mM sulphate (at 55 mg/L Ca). The final solutions of 50 mM strontium, 50 mM zinc and 0.5 mM manganese showed a distinctively higher Ca concentration (266 mg/L, 712 mg/L, 2200 mg/L,) and were therefore only indicated with arrows.

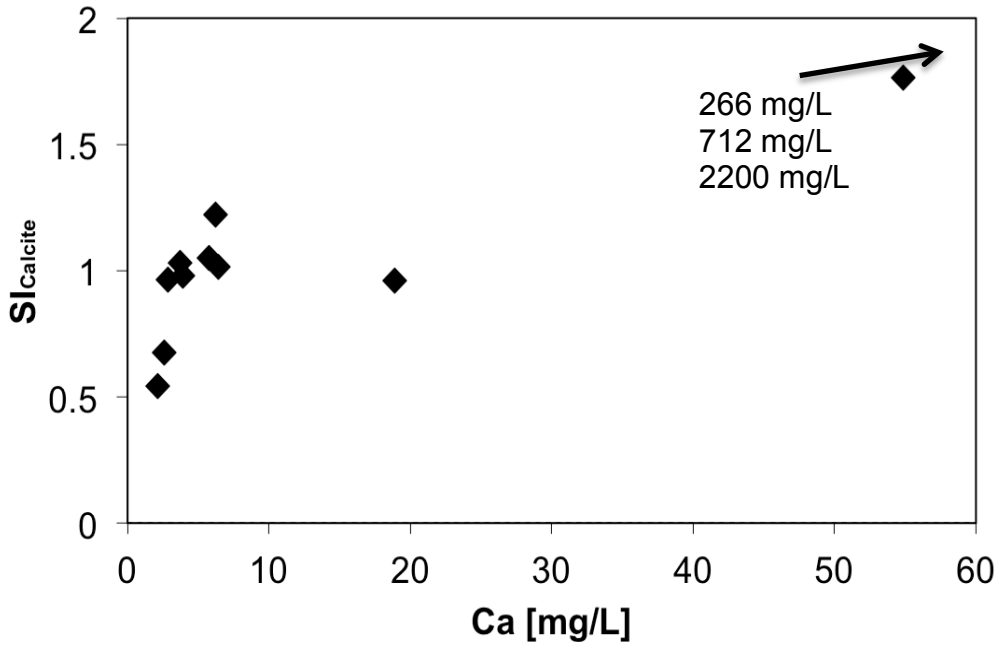

Figure 22: The saturation index of calcite of the final experimental solutions plotted against their calcium concentrations in mg/L.

In Figure 23 the calcium concentrations were plotted against the pH. The individual stages (inital solution, milk of lime (MoL) (and final solution) showed similar results for each group. The initial solutions are plotting in the lower left-hand side corner with a pH between 7 and 10. The MoLs were closely located in the upper right-hand side of the diagram separating themselves from the other solutions by a high pH ranging from 11 to 13. The final solutions, however, were relatively widespread within a separate area of the diagram. Most of the latter solutions presented a pH from 8.5 to 9.5.

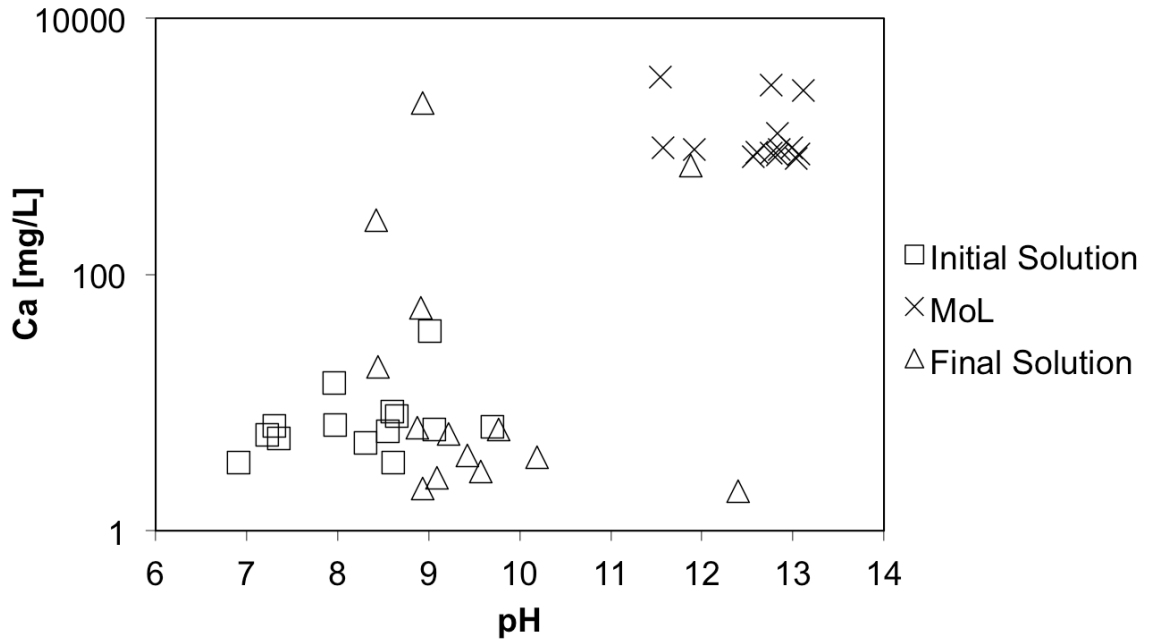

Figure 23: The calcium concentrations of the different experimental solutions plotted against their pH.

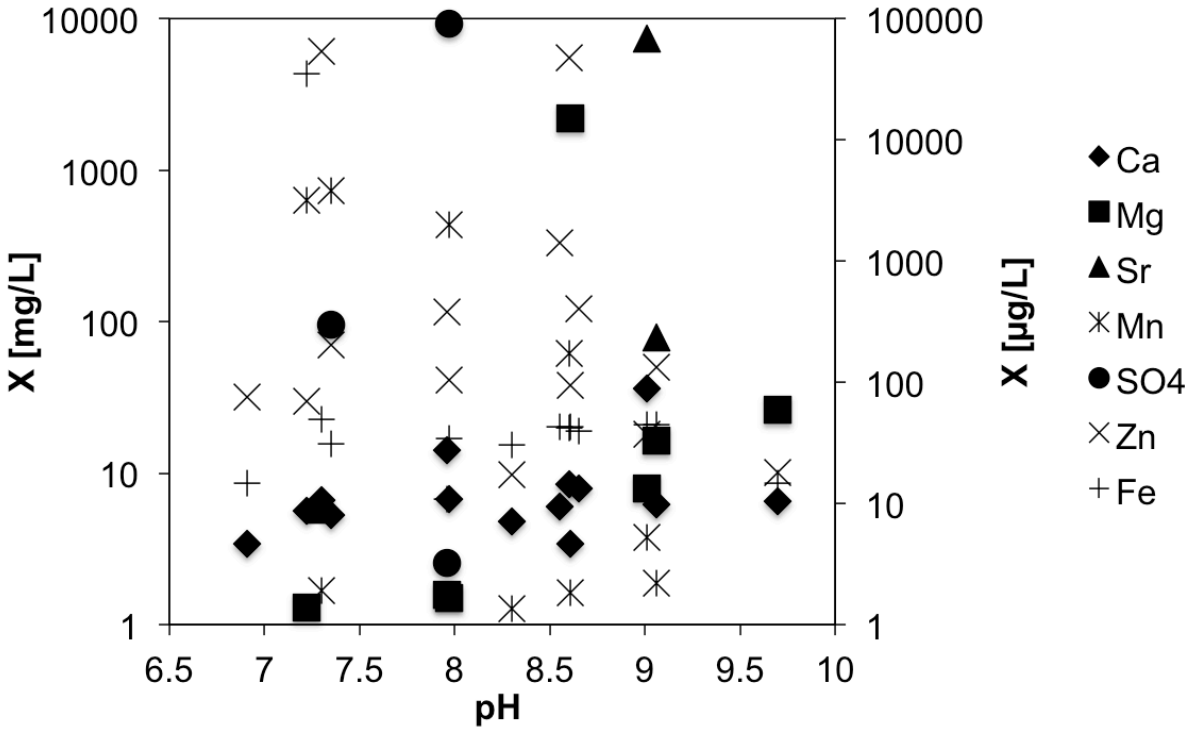

Figure 24: Selected ions of the initial experimental solution in either mg/L (Ca, Mg, Sr, Mn, SO_4) or µg/L (Zn, Fe) plotted against pH.

The concentrations of the selected ions for the initial solutions plotted against their pH were depicted in Figure 24. The pH values varied from 7 to 10. Ranging only from 4 to 36 mg/L the calcium concentrations were fairly low. The magnesium concentrations were rather constant between 0.5 and 26 mg/L with the exception of

the square, which reflected the 50 mM magnesium (2180 mg/L) solution. For strontium and sulphate the concentrations were also quite constant except for the experiments with 50 mM of these ions. The manganese concentrations (0.7 to 49000 mg/L) depicted in this graph did show increased values for the samples where manganese chloride was added due to precipitation that occurred in the container before conducting measurements. The results for zinc and iron were given in µg/L and ranged from 17 to 53200 and 11 to 35270.

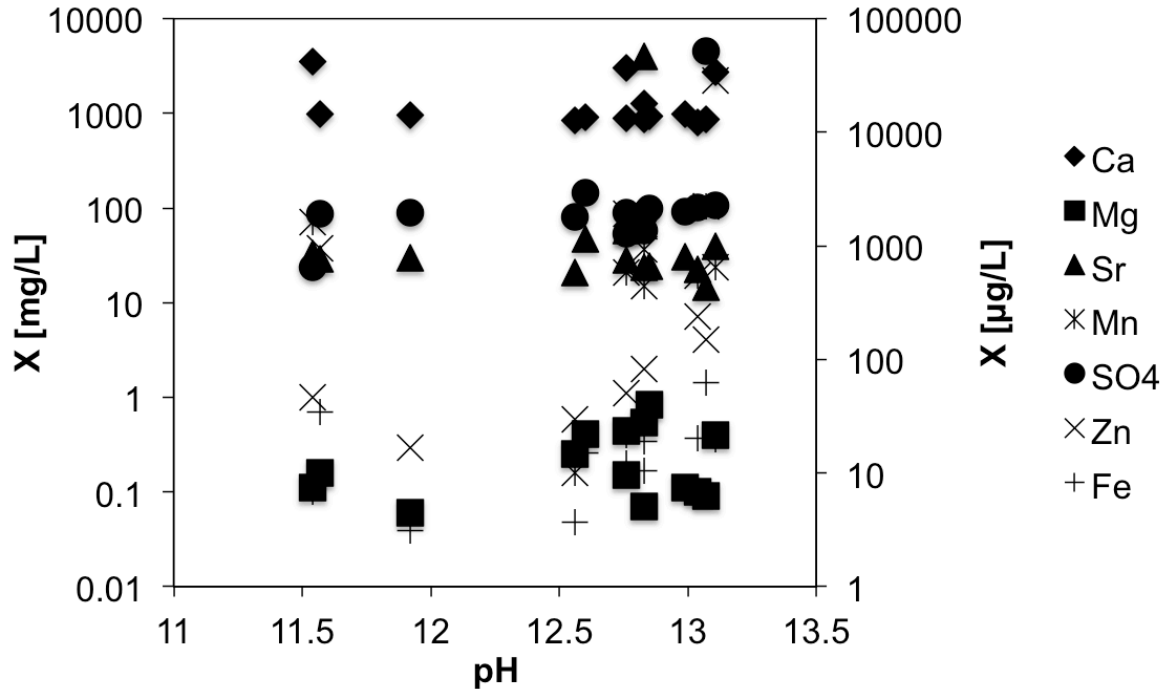

Figure 25: Selected ions of the milk of lime in either mg/L (Ca, Mg, Sr, Mn, SO_4) or µg/L (Zn, Fe) plotted against pH.

The ion composition of aqueous solution from the milk of lime with regard to the Ca, Mg, Sr, Mn, SO_4, Zn and Fe was plotted in Figure 25. The calcium concentrations were noticeably higher compared to the other ions. Moreover, a distinction within those concentrations was possible. Most solutions included an average of 1400 mg/L Ca. Four solutions contained very high concentrations of calcium. The solutions concerned were the samples containing 50 mM of magnesium, strontium, zinc and sulphate. The manganese sample was the only one not showing the same high concentration level. Magnesium presented fairly constant concentrations throughout the experiments ranging from 0.1 to 0.9 mg/L. According to the chemical analysis the average strontium and sulphate concentrations were

315, 404 in mg/L and 2250 for zinc in µg/L. The maximum concentrations of 4000 mg/L for Sr, 28500 µg/L for Zn and 4600 mg/L for SO_4 represented the solutions containing 50 mM of the specific ion. The manganese values reached values up to 105 mg/L. It is noteworthy, that three out of the four manganese experiments did not show any Mn concentrations above the detection limit of 0.4 µg/L in those solutions. Only the experiment using 50 mM presented manganese in the milk of lime with 71 mg/L. Iron occurred in fairly small concentrations within a range of 0-63 µg/L. All solutions were alkaline with a pH between 11.54 and 13.11.

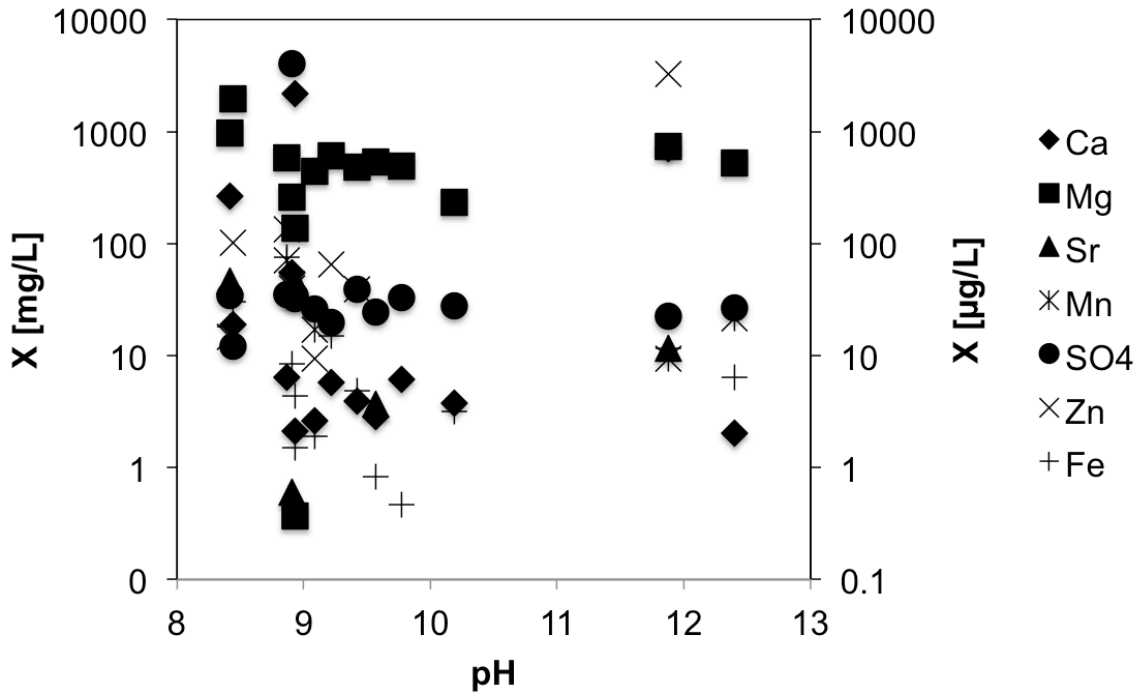

Figure 26: Selected ions of the final experimental solution in either mg/L (Ca, Mg, Sr, Mn, SO_4) or µg/L (Zn, Fe) plotted against pH.

Analysing the final solutions the pH had dropped again to values between 8.4 and 12.4 (Fig. 26). The 0.5 mM experiments showed very low calcium concentrations ranging from 2 to 6 mg/L, whereas the 50 mM ones had an average of 650 mg/L. The magnesium concentrations presented a mean value of 570 mg/L. Fairly high values were reached for 50 mM magnesium (2000 mg/L) and 50 mM strontium (980 mg/L). Compared to those high concentrations 0.5 and 50 mM manganese experimental solutions show Mg concentrations between 140 and 0.4 mg/L. Strontium was only detected in five solutions and ranged from 0.6 to 74 mg/L. Manganese was measured in half the samples with concentrations from 10 to 70 mg/L. The highest Mn concentration was measured in 0.5 mM iron. The sulphate concentrations

presented a mean value of 30 mg/L excluding the sample where 50 mM SO_4 were added, which has 4050 mg/L of of SO_4. Six samples did not show zinc above the detection limit of 1 µg/L in the final solutions. For all other experimental solutions the values were between 9 and 135 mg/L. The highest value of 3285 mg/L zinc was reached in the sample 50 mM Zn. The measurements for iron resulted in a mean value of 13 mg/L for all samples.

5. Discussion

5.1 Industrial solutions

The various plants show very different results according to the chemical composition of the waters (Fig. 4; Table A-1). No satisfying grouping according to the process states could be observed. The values have been within a certain frame but were more likely defined by the local situations worldwide than the process itself. In the following some waters with outstanding compositions are exemplarily discussed.

Compared to other plants G showed relatively high concentrations of sulphate. This could be caused by the limited water supply in this area. Omya plant G receives its waters from a paper factory, which uses aluminium sulphate for water purification. This also leads to a rise in the Al concentration. Furthermore, Zn concentration is also elevated for this plant. All these parameters may have an influence on the morphology of $CaCO_3$ and consequently on the product's quality (see results).

The plant J uses 95 % compressor water of the total amount. The concentrations of SO_4, Fe and Mn in the analysed solutions were relatively high compared to the solutions from other plants. Mn can result in a significant decrease of the brightness of the final product. The high conductivity resulted from the low pH of 2.4 (see Tab. A-1).

The centrate water from plant F contained comparatively high concentrations of K, Mg, Na, Zn, SiO_2 and especially Cl.

In plant B the Sr content was up to 10-times higher compared to other plants.

The plant H contained high nitrate concentrations. Those are very likely caused by fertilisation through agriculture. Furthermore, the wastewater showed an elevated alkalinity and calcium content. This water, however, is used as splashing water for the slaker, and therefore, influences the slaking process with special regard to $Ca(OH)_2$ (Pohl, 2014, personal communication, Omya).

5.2. Precipitation experiments

5.2.1. Chemical composition

The chemical composition of the experimental solutions revealed that magnesium concentrations in the initial solutions and the MoLs were low compared to the final solutions (Tab. A-6). The increase in the latter suggested that the magnesium content derived from the CaO added at the beginning of the experiment. The low concentrations of the MoLs indicated that at this stage the magnesium was still bound in the solid phase, whereas it had been very limited incorporated into the calcite crystal lattice of the final product. Therefore, no significant impact of Mg could be observed. Only the experiment with initial 50 mM of Mn seemed to have incorporated the magnesium in its bulk solid phase with only 0.37 mg/L of Mg left in the final solution (Tab. A-6). Nevertheless, no magnesium phases could be detected via XRD, FT IR, SEM or XRF.

The strontium values for the initial solution barely exceeded 1 mg/L. However, in the MoL the strontium content rose significantly. For the final solutions only five solutions still included strontium above the detection limit. Those fluctuations suggested that the strontium detected in the MoLs descended from the reaction with calciumoxide. Finally, the strontium had to be incorporated into a solid phase otherwise it would have still occurred in the final solution (see section basic concepts). It either had to be in the sieving grit or the final product. Examinations revealed that the latter was not the case with the exception of the experiment with initial 50 mM of Sr (Figs. 15 and 16; Tab. A-3). In this case aragonite precipitated.

Zinc did not show consistent results concerning its concentration. It appeared that most of the zinc derived from the distilled water used for the slaking process and not from the added calciumoxide. The SEM results revealed an affect on the structure of the precipitate at higher concentrations. The individual needles were smaller in size and appeared clustered.

The manganese concentration in the aqueous solutions was below the detection limit because manganese oxide/hydroxide precipitated in most solutions prior to chemical analysis (Tab. A-6). However, even traces revealed a dramatic impact on the brightness. With an initial 0.05 mM Mn the brightness R457 was decreased by about 4 %.

The sulphate content appeared to have derived from the calciumoxide, just as in the case of magnesium and strontium. The initial solutions did not have a high

sulphate concentration. Other than for magnesium the concentrations rose significantly for the MoLs suggesting that it was no longer incorporated into the solid phase. In the final solution the sulphate values decreased again (Tab. A-6). The slaking process already resulted in a large amount of precipitates. This suggested that sulphate has a major impact on, for example, the reactivity and in further consequence the PCC properties.

The iron measured in the experimental solutions originated from the used slaking water. The values for the initial solutions were the highest throughout the experiments. The iron content seemed to have gradually decreased during the trials. The addition of initial 0.5 mM Fe did not lead to a recognisable decrease in brightness. Furthermore, no separate Fe mineral phases could be verified. It was, however, assumed possible that badly crystalline oxide/hydroxide phases were formed. This is also valid for manganese causing the coloration. The SEM imaging for intial 0.5 mM Fe did not show a noticeable behaviour.

Taking the chemical composition of all solutions (Tab. A-4 and XRF analysis of the Tagger (CaO) as well as the final products (Tab. A-3)), an ion distribution between solution and solids for their calcium, magnesium and additive concentrations in percentages throughout the experiments was calculated (Tab. A-7).

The diagrams in Figs. 27 to 29 depict the calculated calcium, magnesium and additive distribution in percentage between solution and bulk solid phase for all stages of the experiments.

Calcium showed constant values for each stage. The initial solution had an average value of 0.01 % and the solid phases (Tagger) 99.99 % of Ca in respect to the total amount. According to the equations 30 to 35

$$[X]_{Tagger} + [X]_{distilled\ water} + [X]_{additive} = [X]_{total} \tag{30}$$

$$\frac{100}{[X]_{total}\ mg/L} * [X]_{\ Tagger} = \%\ [X]_{\ Tagger} \tag{31}$$

$$\frac{100}{[X]_{total}\ mg/L} * [X]_{\ distilled\ water+additive} = \%\ [X]_{\ Initial\ solution} \tag{32}$$

$$\frac{100}{[X]_{total}\, mg/L} * [X]_{MoL} = \%[X]_{MoL} \quad (33)$$

$$\frac{100}{[X]_{total}\, mg/L} * [X]_{final\ solution} = \%[X]_{final\ solution} \quad (34)$$

$$\frac{100}{[X]_{total}\, mg/L} * [X]_{final\ product} = \%[X]_{final\ product} \quad (35)$$

those had to give a total of 100 % (where [X] is referred to the concentration of Ca in this case). A mean value of 1.97 % was obtained for the milk of lime (MoL) in respect to the Ca budget. The sieving grit, which had been taken away at this stage, had not been measured via XRF, and, therefore, the respective percentage could not be estimated. For the final solution and the end product the calculations resulted in mean values of 0.3 and 60.1 %, respectively, for the Ca budget.

The estimated mass balance for magnesium in Fig. 28 was not as constant as the calcium ones. Only the first stage, initial solution and Tagger, showed an average of 0.22 and 99.78 % of Mg of total magnesium in the system. Exceptions to that were the experiments where 0.5 or 50 mM magnesium chloride were added to the initial solution. In those cases the magnesium concentration of the solutions increased to 2.1 and in the solid phase decreased to 64.3 %, whereas they decreased to 98 and 35.7 %, respectively, for the Tagger. For the MoL the average Mg percentage in respect to total Mg was 0.02 %. The final solution presented values between 0.03 and 80 % of Mg and the end products' values ranged from 13.8 to 74.8 % of Mg. The heterogeneous distribution of magnesium was very likely caused by the various additives. It seemed that a lot of magnesium was incorporated into the zinc-bearing sample (experiment with 0.5 mM of Zn in the initial solution). The precipitate from the 50 mM Zn experiment, on the other hand, showed a comparatively low Mg percentage. This result showed that a higher magnesium content would replace more calcium by magnesium in the crystal lattice of calcite.

In Figure 29 the Me and SO_4 content for each individual stage and sample was given. The experiments with added magnesium chloride have already been discussed above. Only for six of all the experiments the percentage of the additive

measured in the initial solution reached 100 % (50 mM Sr, 50 mM Zn, 0.05, 0.3, 0.5 and 50 mM Mn and 50 mM SO_4).

The addition of 0.5 mM Sr made up about 85 % of the initial solution and the other 15 % resulted from the Tagger. For 0.5 mM Zn, 0.5 mM SO_4 and 0.5 mM Fe the values for the initial solution were about 95 %, 65 % and 45 %, respectively. Regarding the total amount of available additive 4 samples built in less than 20 % in the final precipitates (50 Mg, 0.3 and 0.5 mM Mn and 50 mM SO_4). The precipitates from the experiments with 50 mM Sr, 0.5 and 50 mM Zn and 0.05 mM Mn incorporated between 20 and 40 % of the available additives. The precipitates from the experiments with 0.5 mM Mg, 50 mM Mn, 0.5 mM SO_4 and 0.5 mM Fe included between 40 and 65 % of the total sum of the available ion.

For the calculation of the mass balance for an element throughout the experiment and respective values in percentages the concentrations in the Tagger, the distilled water and those from individual additive were used, which refers in sum to 100 % considering the whole system (equation 30). To get the percentages for the individual values, the chemical composition in mg/L of the individual compound within a certain stage had to be calculated as described in equations 31-35. Afterwards, 100 was divided by $[X]_{total}$ from equation 30 in mg/L and multiplied with the value that wanted to be transformed into percentages (equations 31 to 35). In equations 31 and 32 the X given as distilled water could also be written as X in *initial solution* (composition of water before adding the calcium oxide. *MoL* of (equation 33) refers to the solution received after the slaking process and *final solution* (equation 34) to the solution after the precipitation or carbonation process.

Taking the above-discussed results a flow chart was created (Fig. 30). The program e!Sankey was used for the visual representation. Its purpose was to display exemplarily for 0.5 mM Zn (initial solution) the distribution of selected compounds between solids and fluids at the different experimental stages in percentages. The flowcharts for all other experiments can be found in the appendix (Fig. A-4a to k). Creating this flowchart the chemical compositions of the initial solution, the milk of lime and the final solution of the solutions were used. Concerning the solids the analysis results of the Tagger and the final product (end product) were used (Tab. A-3). It is, however, noteworthy that the above calculations did not include the slaking grits (see discussion above). It is important to mention that the values for the ions in the final stage (final solution + end product) do not add up to 100 %. However, it has to be kept in mind that none of the slaking grits were looked upon, and therefore, might have a bigger influence on the total mass balance.

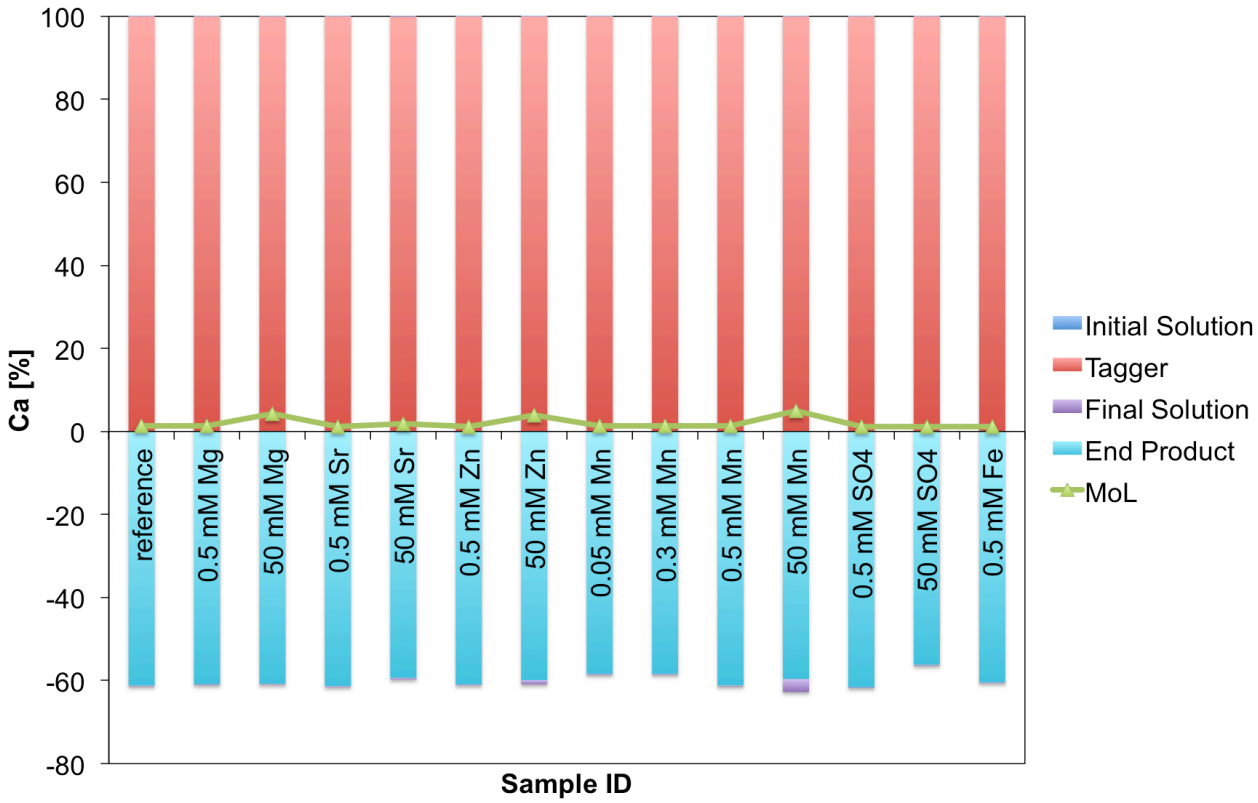

Figure 27: Calcium mass balance throughout precipitation experiment in percentage. The calculation basis for the diagram were the chemical compositions of the solutions and solids (see Tabs. A-3; A-6).

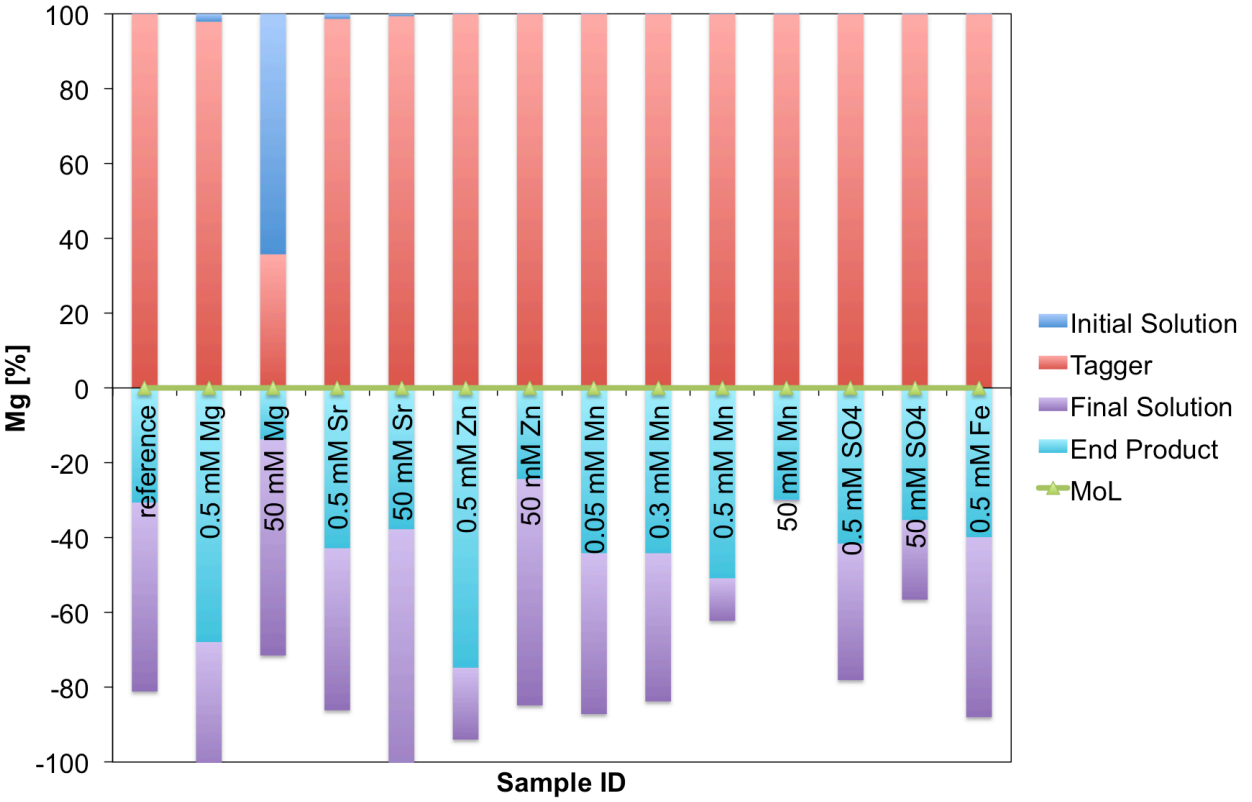

Figure 28: Magnesium mass balance throughout precipitation experiment in percentage. The calculation basis for the diagram were the chemical compositions of the solutions and solids (see Tabs. A-3; A-6).

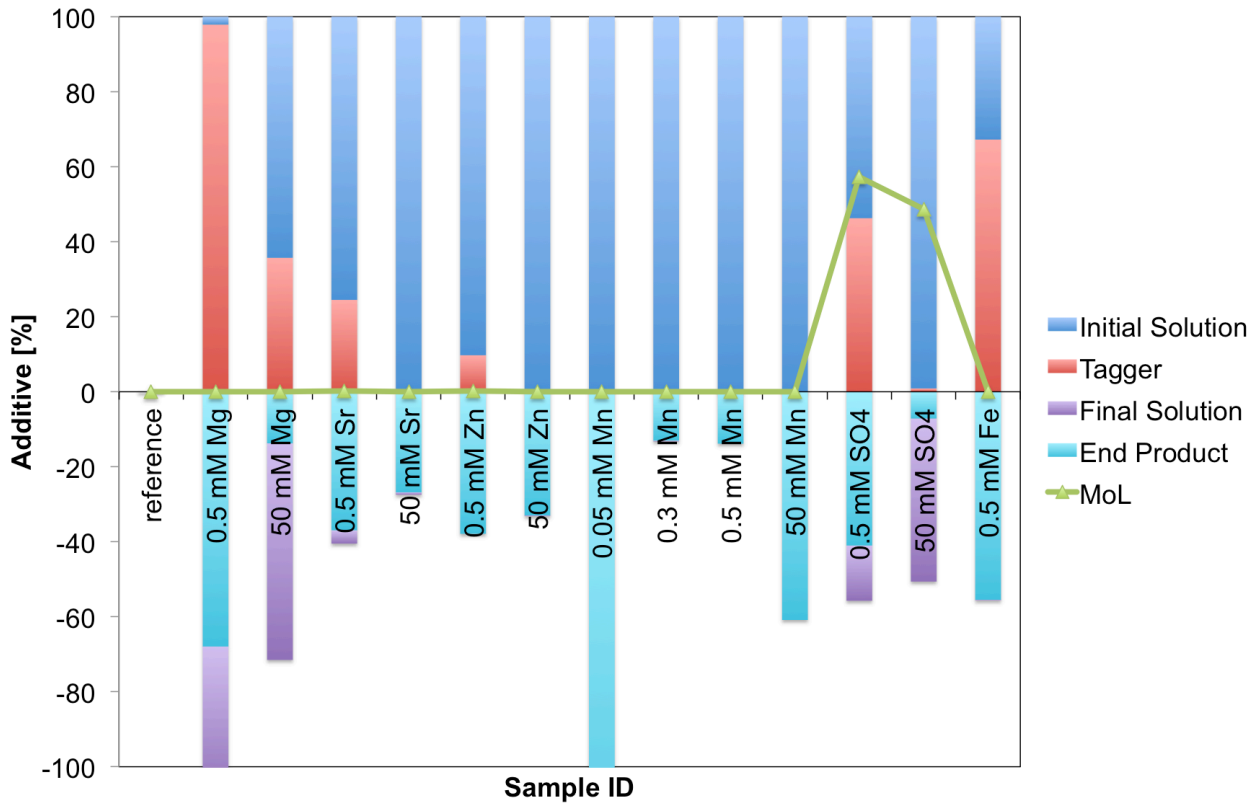

Figure 29: Additive mass balance throughout precipitation experiment in percentage. The calculation basis for the diagram were the chemical compositions of the solutions and solids (see Tabs. A-3; A-6).

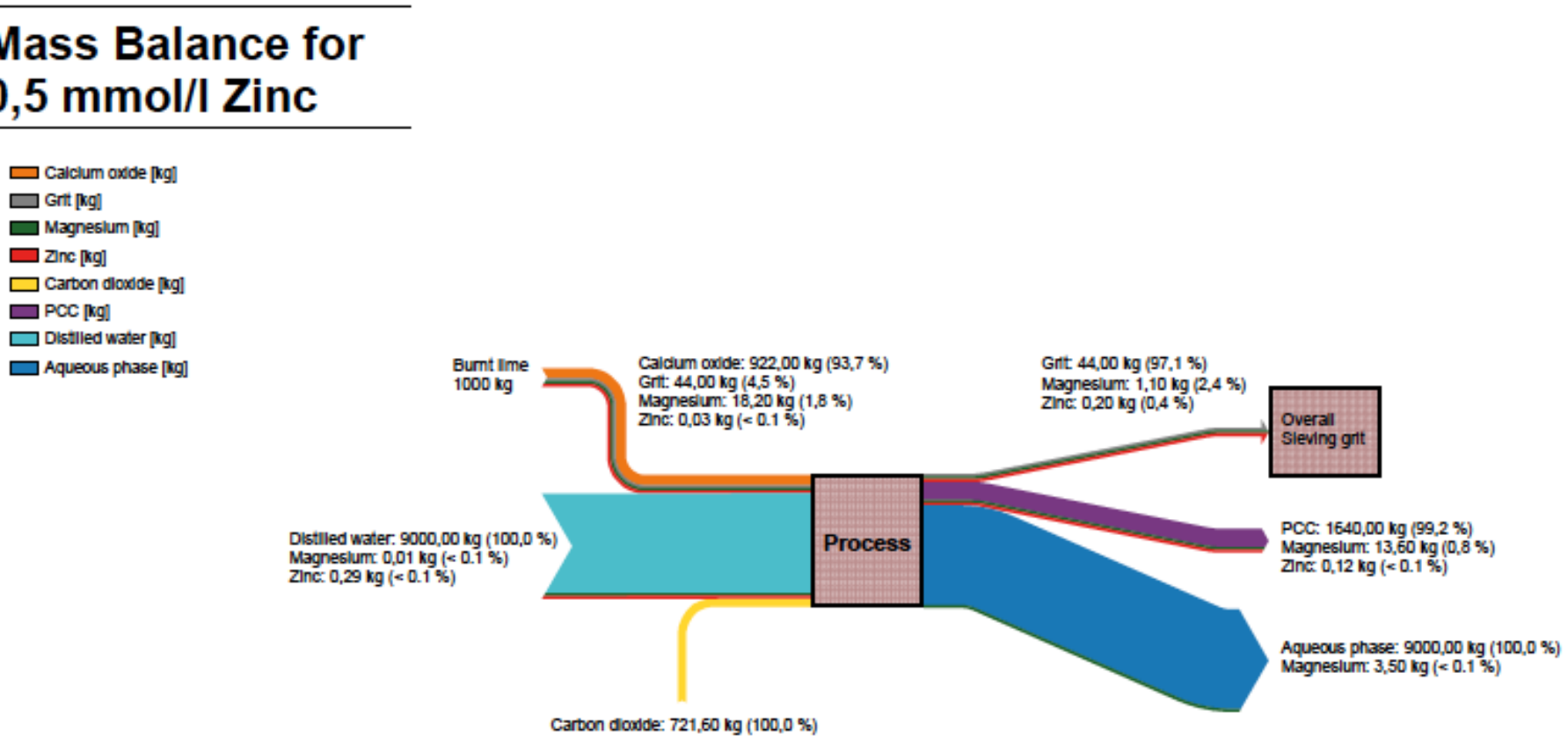

Figure 30: Flowchart for mass balance calculation for experiment with 0.5 mM Zn in the initial solution. Given values represent the percentage according to equations 30 to 35.

5.3. Slaking water specification

Taking the results of the precipitation experiments, especially with regard to brightness and crystal structure and comparing them to measured concentrations of the chosen ions a chart concerning recommended maximum upper limits for concentrations at which no impact on the S-PCC process- and quality data is to be expected was created (Tab. 2).

Considering the observed impacts on the final products caused by the used concentrations of either 0.5 or 50 mM of the used ions (additionally 0.05 and 0.3 mM for Mn) in the precipitation experiments estimated maximum values at which no negative influence on the final product is to be expected were determined.

For magnesium no limiting values were estimated because analysis did not reveal an influence on the final product, therefore the magnesium concentrations in the used industrial waters do not need to be limited (the vast bulk of Mg remains in the solution at the end of carbonation). Due to the precipitation of aragonite instead of calcite in the presence of strontium at a limiting value of < 0.6 mM (≙ 50 ppm) was suggested for Sr. Zinc causing variations in the crystal shape a maximum limit of 0.2 mM (≙ 10 ppm) was recommended. The significant reduction of the brightness with only initial 0.05 mM manganese led to setting the limit at < 0.002 mM (≙ 0.1 ppm). The results of the experiment with initial 50 mM SO_4 revealed a significant impact on the crystal shape and also the brightness. Hence, the maximum upper limit for sulphate was set at < 5 mM (≙ 500 ppm). The limit for iron was determined at < 0.02 mM (≙ 1 ppm) due to possible brightness reduction. For chloride the limiting value was set at < 1.4 mM (≙ 50 ppm), but it has to be said that chloride was not explicitly investigated in the experiments. Hence, the value is based on practical experience by Omya.

Table 2: Recommended maximal upper concentration limits for the ions in industrial solutions
*not explicitly investigated in experiments; based on practical experience by Omya.

Element contamination	Recommended Upper Limit		(Impact on)
	[ppm]	[mM]	Remarks
Sr	< 50	< 0.6	- aragonite formation
Zn	< 10	< 0.2	- crystal shape
Mn	< 0.1	< 0.002	- brightness
SO_4	< 500	< 5	- crystal shape - brightness
Fe	< 1	< 0.02	- brightness
Cl	< 50*	< 1.4	- corrosion

5.4. Modelling approach

The program PhreeqC (with modified database minteqv4 in respect to citrate complexes, see section methods) was used to simulate the precipitation process in the carbonation reactor. The program code (Fig. A-5) was based on: (i) a defined solution chemistry including the starting amount of sodium citrate and additives, (ii) a stated amount of portlandite and of Mg to reach equilibrium with portlandite and various Mg-phases (such as brucite, $Mg(OH)_2$), (iii) equilibrium with respect to calcite, which corresponds to precipitation of calcite throughout the on-going delivery of gaseous CO_2 at the measured rate in the experimental approach (at a temperature of 50°C). The aim was to determine and monitor various hydrochemical parameters as a function of reaction time and to compare the modelled results to the ones measured during the carbonation experiments.

In more detail: The experimental solutions were saturated in respect to calcite and portlandite over the whole experimental run, hence, they were set to be at thermodynamic equilibrium. This means that as soon as a state of supersaturation is reached calcite is formed. Additionally, due to the high magnesium content of the Tagger used for the experiments various Mg-phases (brucite, nesquehonite, $Mg(OH)_2$ (active), hydromagnesite) were tested to determine their impact on the dissolution/precipitation reactions. The amount of Mg, which could be dissolved was limited according to the measured amount of MgO in the Tagger.

The reactions are suggested to occur spontaneous as thermodynamic equilibrium in respect to solid-liquid interaction (see above) and the on-going reaction progress was simulated via the CO_2 addition. By adding CO_2 portlandite is progressively dissolved and “transformed” to calcite via precipitation. The CO_2 rate reflects the transformation time. The end of the modelling of the carbonation process was reached as soon as a P_{CO2} of $10^{-0.2}$ atm was calculated (CO_2 concentration of the gas phase used in the carbonation experiments).

In Fig. 31 the final modelling results for pH and conductivity (SpC) evolution compared to the measured values were displayed. Generally the pH and SpC curve could be divided into three parts (i) dissolution and transformation of $Ca(OH)_2$ into $CaCO_3$ (ii) consumption of the Tagger and re-dissolution of Mg-phases (in the present case brucite) (iii) dissolution of $Ca(OH)_2$ relicts which might have been covered by Mg-phases. To fit the modelled curves even better the modelled values

were adjusted (6% shift with respect to the CO_2 addition). The data of the monitored values for each carbonation experiment can be found on the enclosed CD.

At the beginning of the experiment a slight decrease for the modelled pH from the measured pH was observed. Considering the temperature curve it was suggested that the difference in pH had been linked to the change in temperature of the experiments. The decrease in the pH curve indicated the end of the first phase. Up to that point $Ca(OH)_2$ was continuously consumed until limited amounts of $Ca(OH)_2$ was left to be transformed into $CaCO_3$. At that point the measured pH generally correlated with the pH modelled via PhreeqC. Once nearly all of the $Ca(OH)_2$ was consumed the pH started to drop. The decrease of pH initiated the dissolution of magnesium phases (e.g. brucite). Moreover, calcium hydroxide relicts, which had been coated with brucite or other solids, dissolved causing an increase of the pH. The third phase was referred to this dissolution of relicts. The experiment terminated once a pH of about 7 was reached.

To be able to compare the values' development over time they were plotted versus the amount of CO_2, which was added to the system. Those values were taken from the net consumption measured for one of the precipitation experiments. Furthermore, the temperature curve of the precipitation experiment as well as the modelled end of the precipitation due to reaching the limiting $P_{CO2} = 10^{-0.2}$ atm (dashed line) were illustrated in the diagrams.

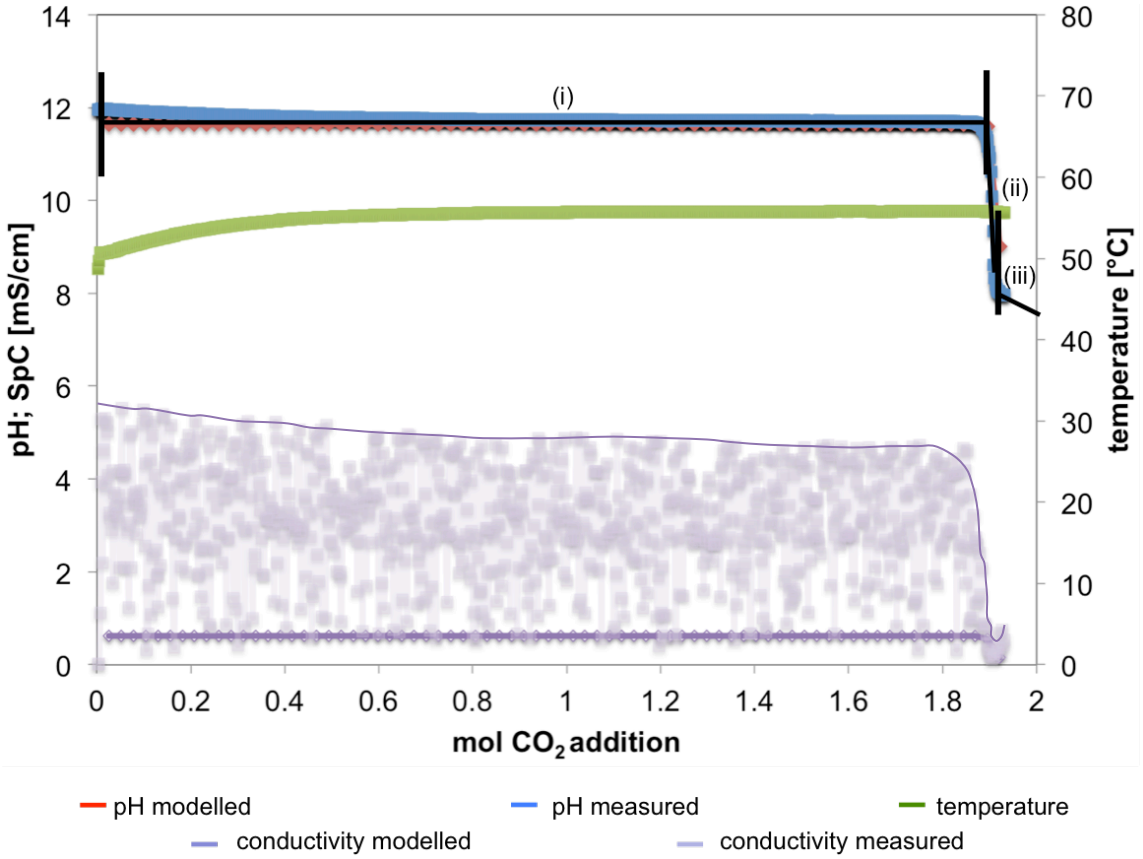

Figure 31: Graphical depiction of the three different stages during the carbonation process. (i) dissolution and transformation of $Ca(OH)_2$ into $CaCO_3$; (ii) consumption of the Tagger and re-dissolution of Mg-phases (in the present case brucite); (iii) dissolution of $Ca(OH)_2$ relicts which might had been covered by Mg-phases. Modelled evolution is shifted by a factor of 0.6 with respect to the CO_2 addition (from the left to the right) to fit the measured values.

For the reference experiment a more detailed modelling was developed (Fig. 32). Due to the high magnesium content of the used Tagger it was to be assumed that magnesium played an important role in the overall formation of $CaCO_3$. However, as mentioned above a major percentage of the magnesium was not incorporated into the bulk $CaCO_3$ solid but stayed in the solution. Therefore, in the following modelling approach a closer look had been taken at the dissolution and formation behaviour of four different magnesium phases: brucite, hydromagnesite, nesquehonite and $Mg(OH)_2$ (active; a less ordered $Mg(OH)_2$ with a higher solubility). Figure 32 depicted the comparison of the pH and conductivity values obtained from the precipitation experiment of the reference (no additives) and the values gained from the modelling approach for the distinct formation of above Mg-phases.

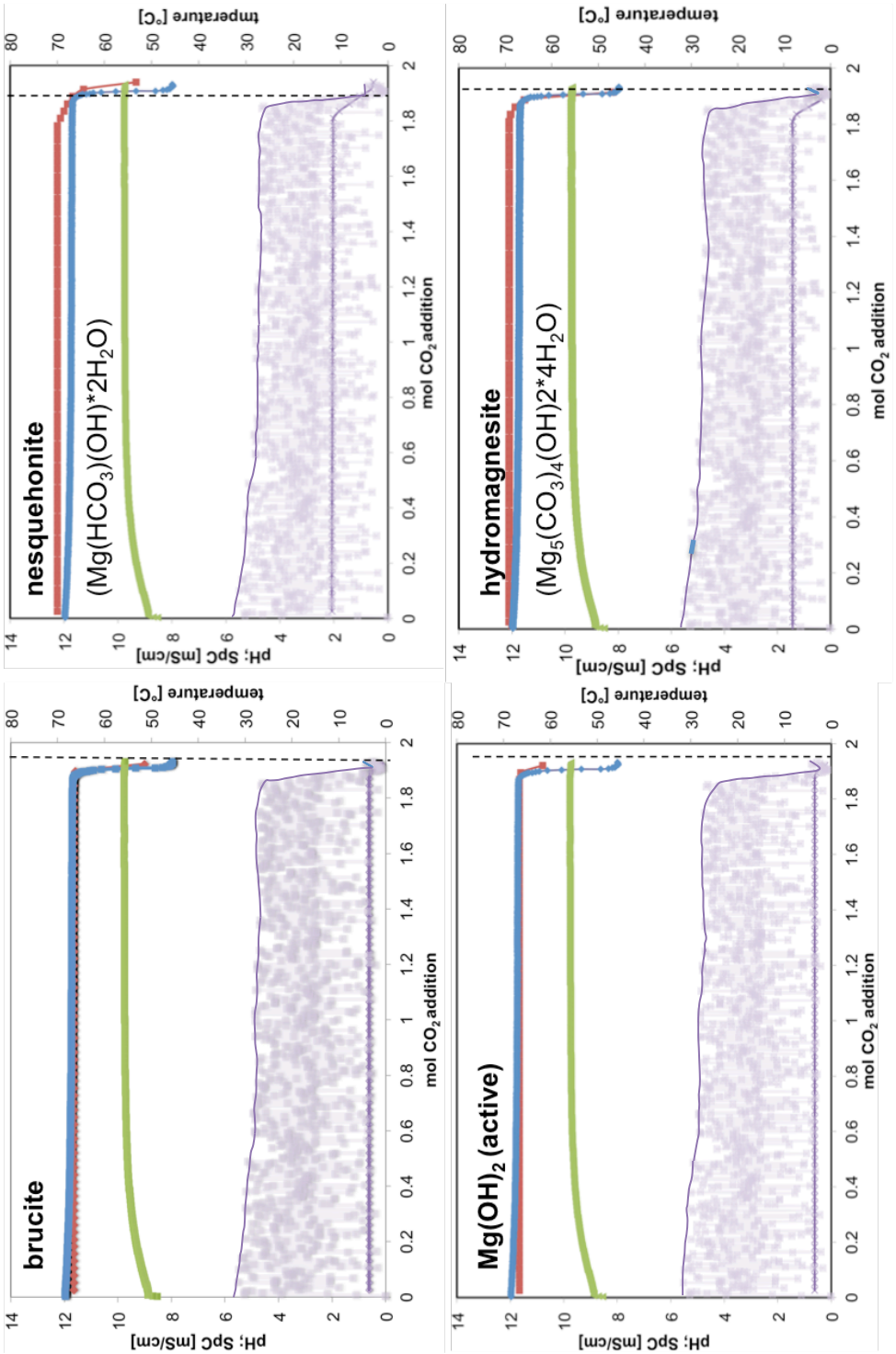

Figure 32: Comparison of modelled and measured carbonation trends regarding pH and conductivity in µS/cm. Graph shows the results for the four model approaches with respect to the four different magnesium phases which are allowed to be precipitated and dissolved. Modelled evolution is shifted by a factor of 0.6 with respect to the CO_2 addition (from the left to the right) to fit the measured values.

In general, the models presented fairly good compliance with the measured data. To fit the modelled curves to the measured values the modelling results were accordingly adjusted by a shift factor with respect to the CO_2 addition of 6 % from the left to the right. Comparing the individual results for the different modelling approaches the one allowing brucite to precipitate and dissolve showed the best correlation with the experimental data. The graphs showed, as already described in Fig. 33, the three stages of the carbonation process (see discussion above).

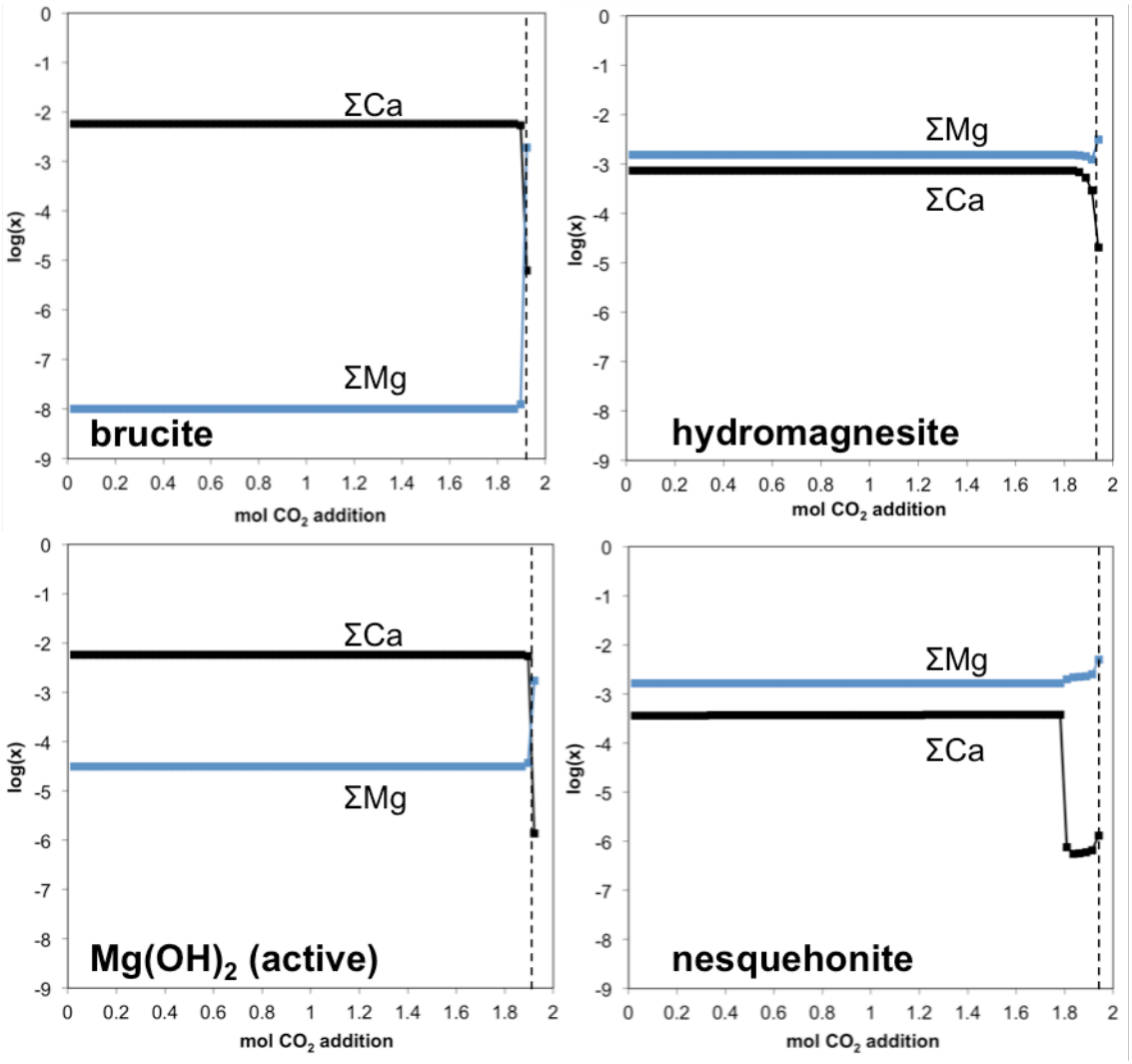

Figure 33: Total calcium and magnesium concentration plotted versus the CO_2 addition over time obtained by the applied modelling approach considering the four distinct Mg-phases. Modelled evolution is shifted by 6 % with respect to CO_2 addition (from the left tot he right).

In the graphs in Figure 33 the modelled total concentrations of Ca and Mg were plotted versus the CO_2 addition in order to analyse their behaviour over time. The obtained relationships confirmed the linkage between coupled $Ca(OH)_2$

dissolution and $CaCO_3$ precipitation and the $Mg(OH)_2$ precipitation and re-dissolution process. The graphs showed that at the same time as the total calcium concentrations dropped the total magnesium concentrations rose.

The modelled individual distribution of the calcium aquo-complexes considering brucite, $Mg(OH)_2$ (active), hydromagnesite and nesquehonite during the run of the experiment can be found in Fig. 34. Brucite and $Mg(OH)_2$ (active) showed a rather similar behaviour, as did hydromagnesite and nesquehonite. At the beginning of the experiment Ca^{2+} was the dominant dissolved species for brucite and $Mg(OH)_2$ (active) followed by $CaCO_3^0$, $Ca(OH)_2^0$, and finally, $CaHCO_3^+$. For hydromagnesite and nesquehonite Ca^{2+} and $CaCO_3^0$ were equal until the turning point where $Ca(OH)_2^0$ and $CaHCO_3^+$ increased. At the end of the experiment the order in respect to concentrations of the aquo-complexes was the same for all experiments. The dominant one was $CaHCO_3^+$, followed by Ca^{2+}, $Ca(OH)_2^0$ and $CaCO_3^0$.

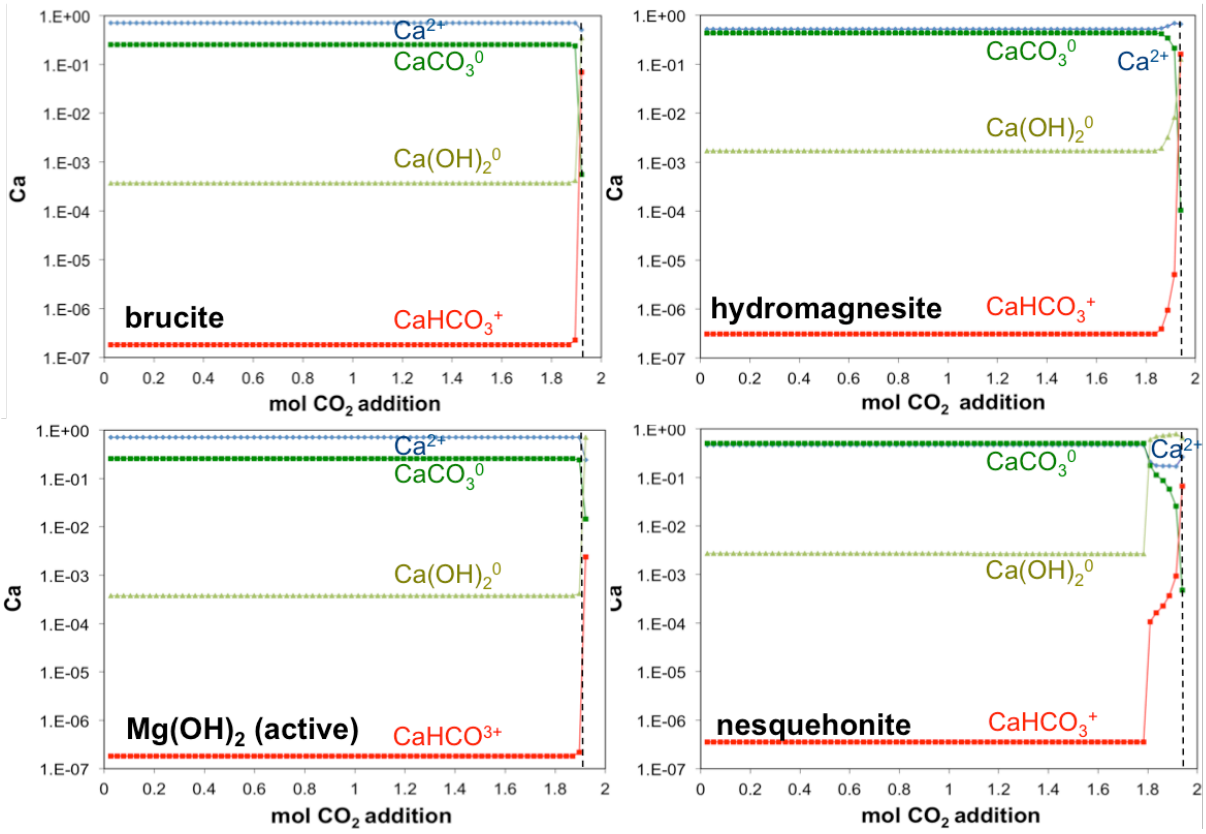

Figure 34: Depiction of the evolution of the calcium aquo-complexes over time for the different modelling approaches. Modelled evolution is shifted by a factor of 0.6 with respect to the CO_2 addition (from the left to the right).

The aquo-complex evolution for magnesium at the beginning of the carbonation process was nearly the same for all modelling approaches for the reference experiment (Fig. 35). $MgCO_3^0$ started as the dominant dissolved species followed by Mg^{2+}, $Mg(OH)_2^0$ and $MgHCO_3^+$. At the end $MgHCO_3^+$ was the dominant aquo-complex followed by Mg^{2+}, $Mg(OH)_2^0$ and $MgCO_3^0$.

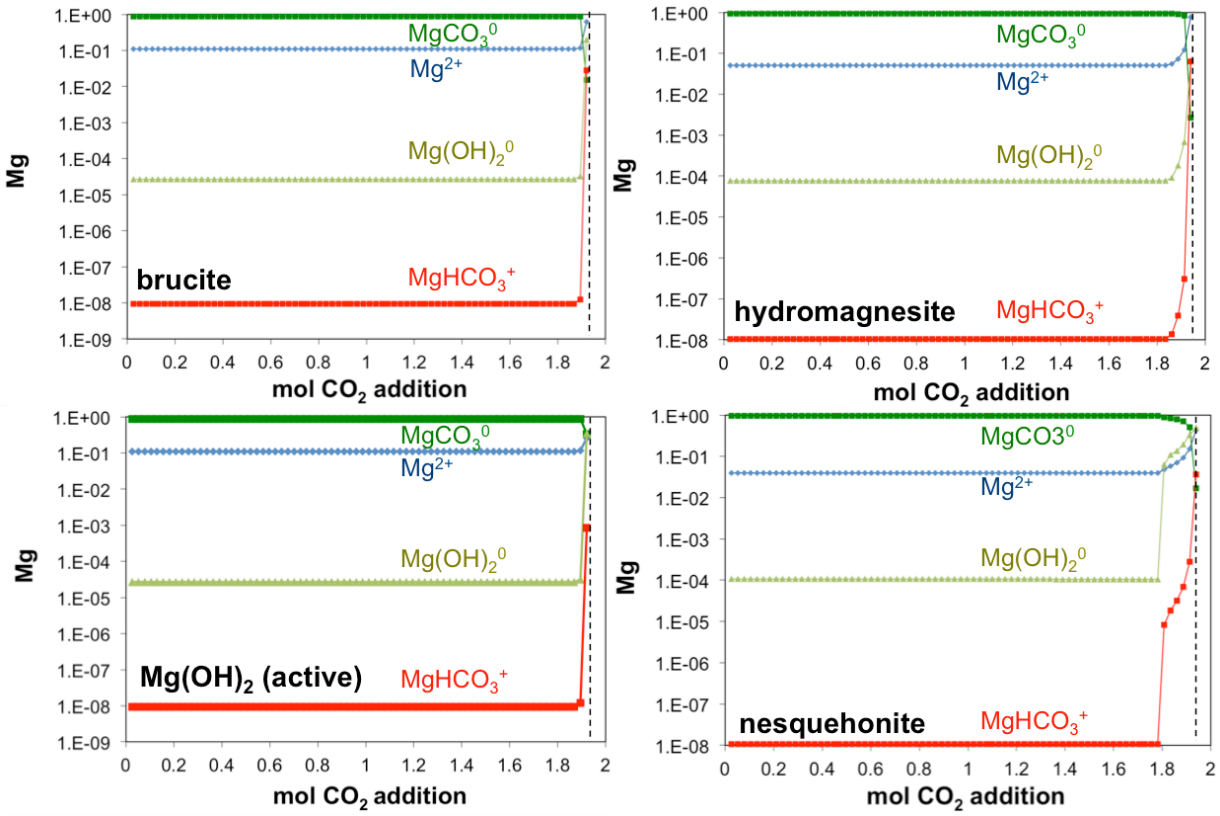

Figure 35: Depiction of the evolution of the magnesium aquo-complexes over time for the different modelling approaches. Modelled evolution is shifted by a factor of 0.6 with respect to the CO_2 addition (from the left to the right).

Figure 36 depicted the aquo-complexes of calcium and magnesium plotted versus the pH. The graphs were shown to evaluate the evolution of the aquo-complex evolution. Keeping in mind that the experiments were started at a pH of about 12 the dominant aquo-complex for calcium was Ca^{2+} and $Mg(OH)_2^0$ for magnesium. $Ca(OH)_2^0$ and Mg^{2+} were the lower represented complexes. As the experiment proceeded and the pH decreased so did Ca^{2+} and $Mg(OH)_2^0$, whereas the concentrations of $Ca(OH)_2^0$ and Mg^{2+} increased. Furthermore, the values for $CaCO_3^0$, $CaHCO_3^+$, $MgCO_3^0$ and $MgHCO_3^+$ displayed a slight increase.

The comparison of the modelled pH and conductivity curves over time (as mol CO_2 addition) with the measured pH and conductivity curves for the additives Mg, Sr, Zn, Mn and SO_4 for both 0.5 and 50 mM of the initial solution is shown in the Figures 37 a to e.

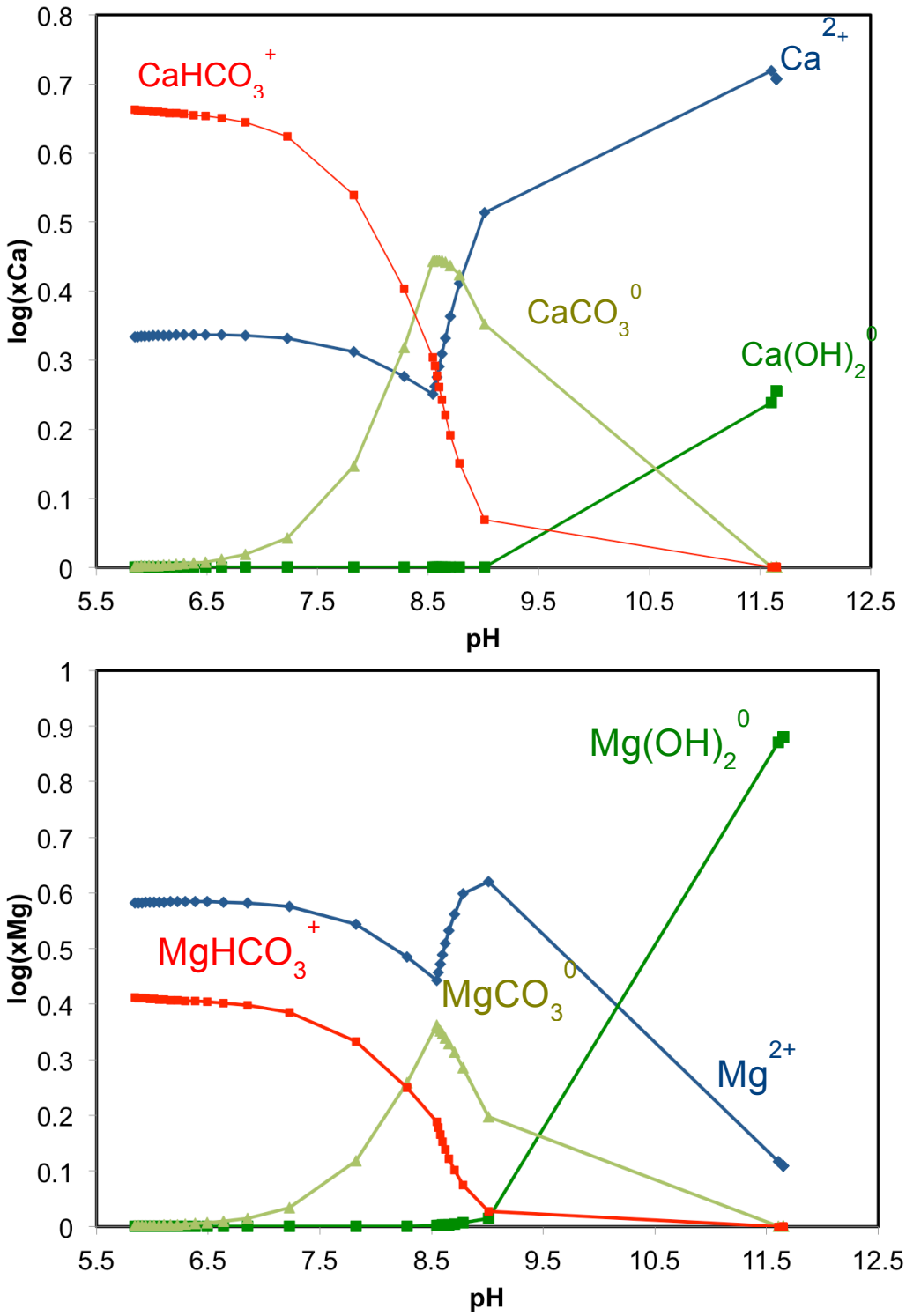

Figure 36: Depiction of the calcium and magnesium aquo-complexes plotted versus the pH. Graph shows the evolution of the complexes according to pH. Modelled evolution is shifted by a factor of 0.6 with respect to the CO_2 addition (from the left to the right).

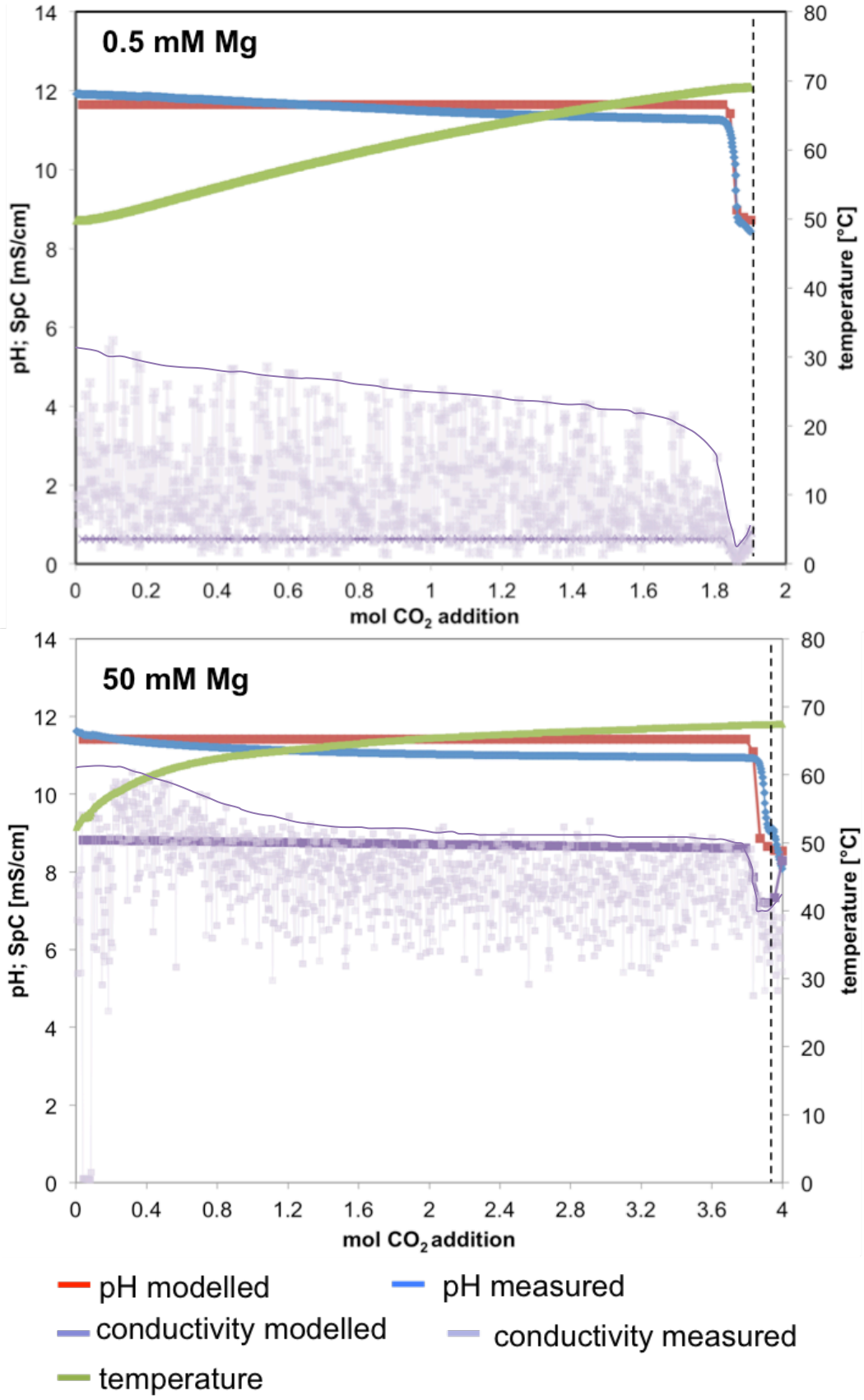

Figure 37a: Depiction of the modelled and measured carbonation curves for the experiments with initial 0.5 and 50 mM of Mg. The modelled values for 0.5 mM Mg were adjusted by 0.2 (from right to left), the values for 50 mM Mg by 0.7 (from left to right) (for mol CO_2 addition). Additionally the SpC was adjusted by the factor 14 (with respect to mS/cm).

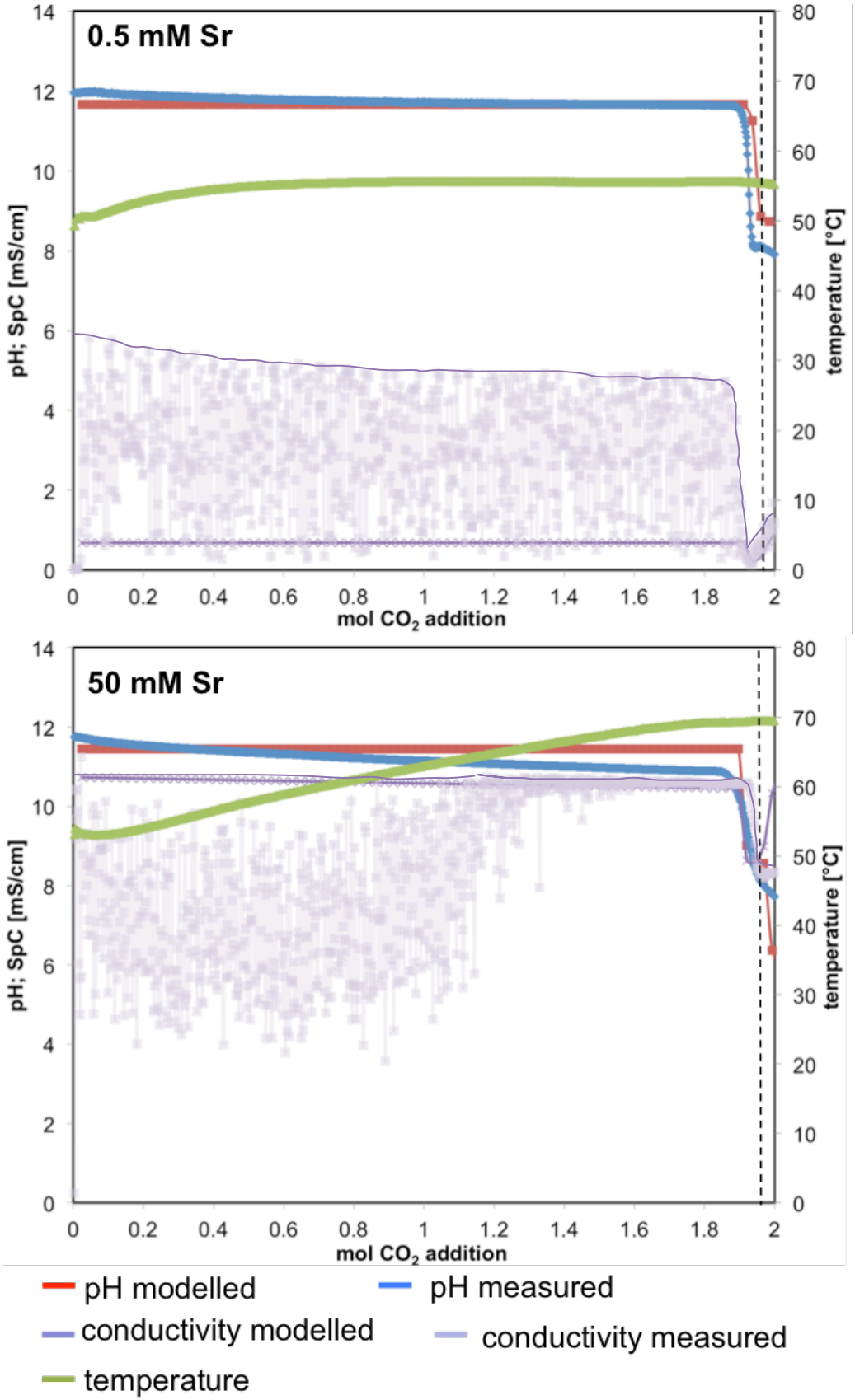

Figure 37b: Depiction of the modelled and measured carbonation curves for the experiments with initial 0.5 and 50 mM of Sr. The modelled values for 50 mM Sr were adjusted by 0.7 (from left to right) (for mol CO_2 addition). Additionally the SpC was adjusted by the factor 14 (with respect to mS/cm).

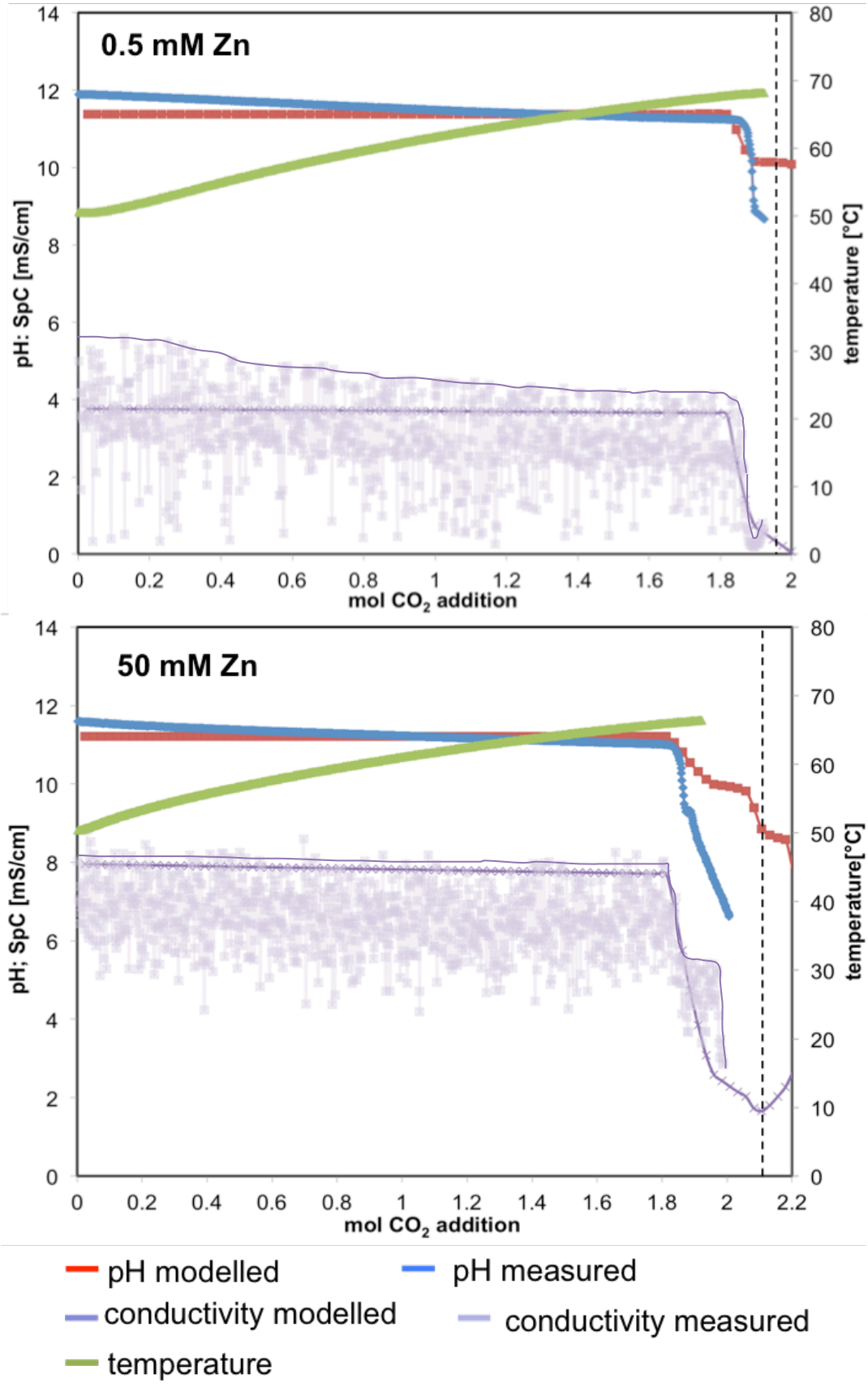

Figure 37c: Depiction of the modelled and measured carbonation curves for the experiments with initial 0.5 and 50 mM of Zn. The modelled values for 0.5 mM Zn were adjusted by 0.6 (from left toright) (for mol CO_2 addition). Additionally the SpC was adjusted by the factor 14 (with respect to mS/cm).

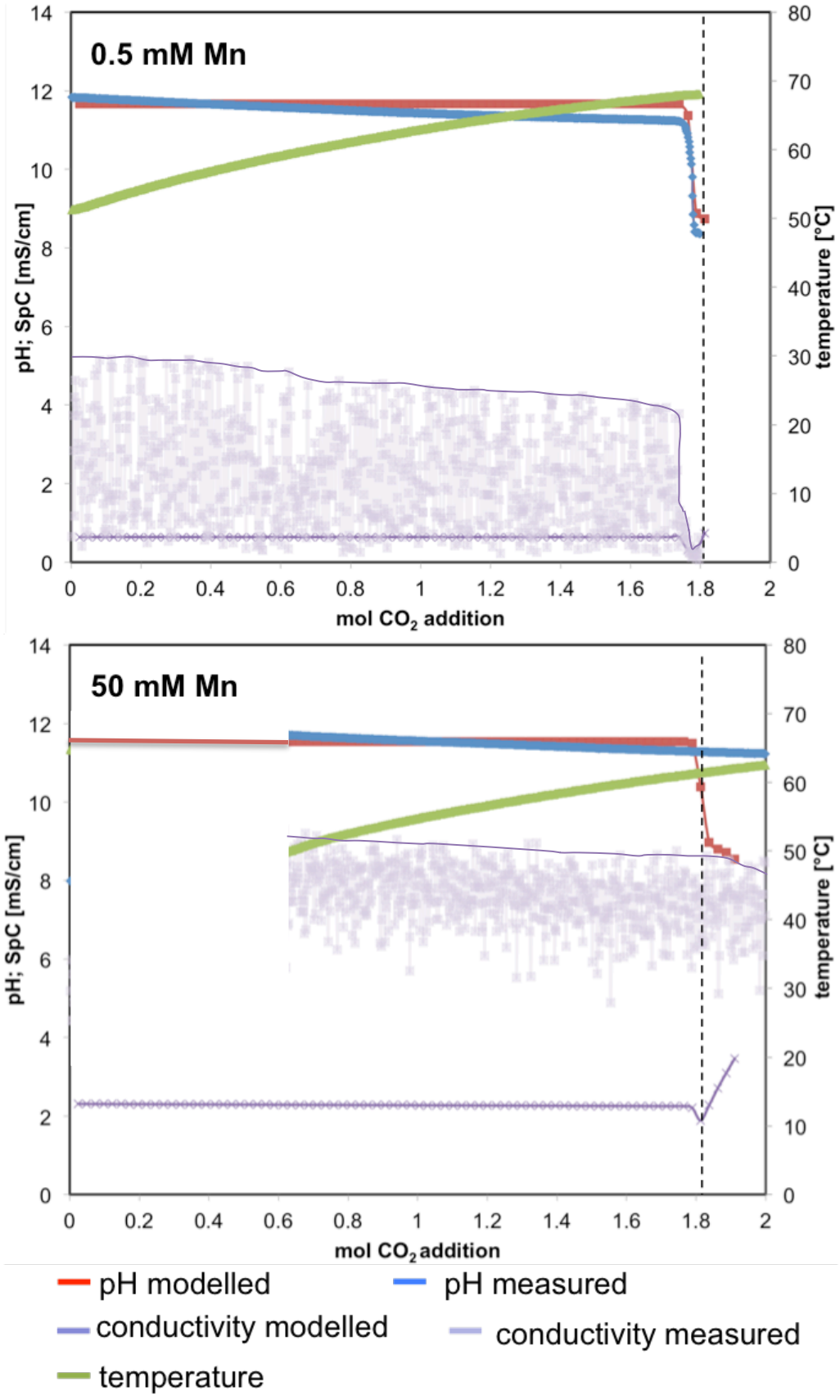

Figure 37d: Depiction of the modelled and measured carbonation curves for the experiments with initial 0.5 and 50 mM of Mn. For the experiment with initial 50 mM Mn the laboratory data are unreliable due to a monitoring error. The SpC was adjusted by the factor 14 (with respect to mS/cm).

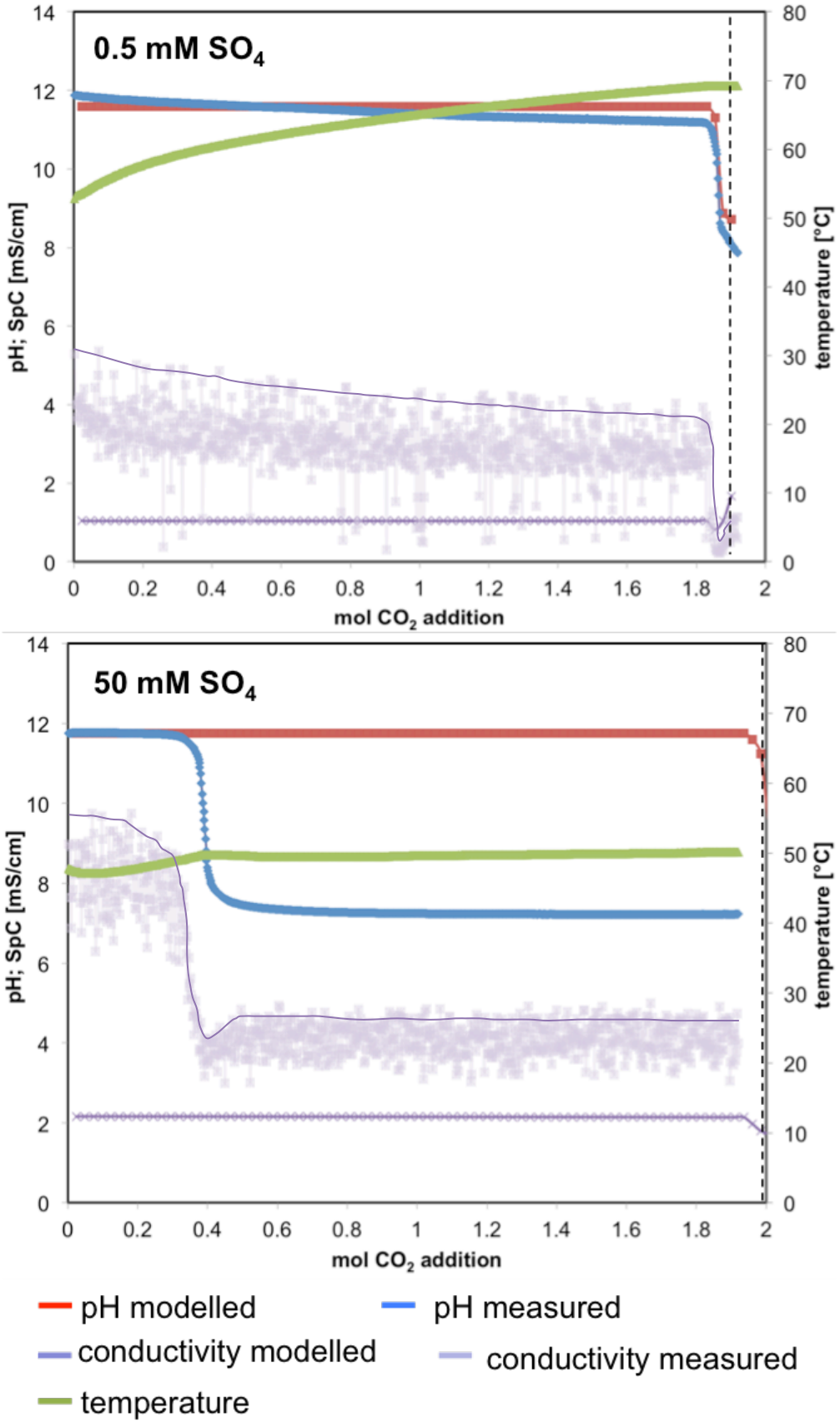

Figure 37e: Depiction of the modelled and measured carbonation curves for the experiments with initial 0.5 and 50 mM SO_4. The modelled values for 0.5 mM SO_4 were adjusted by 0.3 (from left to right) to get a better visual fit. Additionally the SpC for initial 0.5 mM SO_4 was adjusted by the factor 14 (with respect to mS/cm). For 50 mM SO_4 the end of the measured reaction was at 0.5 mol CO_2. Due to the unexpected early finish gas addition was going of too long.

5.4.1. Hydrochemical modelling for distinct salt additions

Most experiments presented a satisfying fit between measured and modelled results (see Figs. 39a to e). However, experiments with 0.5 and 50 mM zinc of the initial solution revealed a differently shaped curve for the pH of the modelled one than for the measured one. The modelled pH curves did not show a gradually decreasing line but had a plateau like phase in the middle, where the pH was decreasing more slowly or remained constant before rapidly decreasing again. This phenomenon seemed to be linked to the formation and dissolution of zinc phases (Fig. 38a). Zincite (ZnO) was highly supersaturated at high pH and was suggested to have precipitated. The saturation states over time for smithsonite ($ZnCO_3$) equal the shape of the modelled pH curve. Unfortunately, for the experiment with initial 50 mM manganese the laboratory data were unreliable due to precipitation of presumably manganese oxide/hydroxide before chemical analysis, and therefore, a matching of the curves was not possible. However, the results for initial 0.5 mM manganese showed that the curves would fit if the data was complete (if no pre-analysis precipitation would have taken place). The experiment with the highest discrepancy of measured and modelled results, was the experiment with initial 50 mM sulphate. In that case the measured carbonation process ended much earlier than the modelled one. This might have been due to the fact that in this experiment the slaking process in the laboratory generated a high amount of slaking grit (>200 µm). This volume of solids was missing for the carbonation process reducing the amount of solids, which could precipitate and dissolve significantly during the on-going carbonation process.

Figures 38a and b depict the saturation indices for the various solid phases during the individual carbonation processes over time. For the experiments with initial 0.5 and 50 mM magnesium the saturation states of brucite ($Mg(OH)_2$), nesquehonite ($MgCO_3$), huntite ($Mg_3Ca(CO_3)_4$), hydromagnesite, $Mg(OH)_2$ (active) and magnesite ($MgCO_3$) was discussed in more detail. For the modelling brucite was set at thermodynamic equilibrium (SI = 0). For initial 0.5 mM Mg all magnesium phases stayed highly undersaturated for the entire experiment. For the experiment with initial 50 mM Mg magnesite, huntite and nesquehonite are supersaturated, but only at the end of the experiment. Thus, brucite can reasonably be suggested to have formed at the start of the experiments.

The experiments with initial 0.5 and 50 mM strontium were investigated with respect to their aragonite ($CaCO_3$) and strontianite ($SrCO_3$) saturation indices. At the

beginning of the experiment aragonite stayed slightly undersaturated with a SI = -1.3 and strontianite had a SI = 0 for the whole experiment. The latter revealed a SI = 0 for both strontianite and aragonite throughout the run of the experiment (Fig. 38).

Quite interesting saturation indices were observed for the experiment with added zinc chloride (Fig. 38a). At the beginning both experiments (initial 0.5 and 50 mM zinc) were supersaturated with respect to zincite (SI = 5) and undersaturated with respect to smithsonite (SI = - 4). Over the course of the experiment smithonite first reached SI = 0 and stayed constant. At the same time as the latter, equilibrium value was reached. According to those observations zincite instead of smithonite was likely to precipitate at alkaline pH and was suggested to not have re-dissolved as soon as the pH decreased. However, from the XRD analysis of the end product no crystalline Zn phase could be detected, which may have been due to low crystalinity degree of ZnO. It is noteworthy, though, that the zinc concentrations in the end product were fairly high (see Figs. 29 and Tab. A-6c). In the case of initial 0.5 mM zinc the zinc concentration in the final solution was even below the detection limit.

In the case of manganese it was observed that at the beginning of the experiment pyrochroite ($Mn(OH)_2$) was supersaturated with a SI of 5, rhodochrosite ($MnCO_3$) had a SI close to 0. Thus it is suggested that pyrochroite was formed. However a rhodochrosite formation could not be ruled out throughout the whole experimental run (see evolution of SI values in Fig. 38b).

The results for the experiment with added sodium sulphate were as follows: For the experiment with initial 0.5 mM sulphate neither gypsum nor mirabilite reached a supersaturated state during the run of the experiment. The same observations were valid for the experiment with initial 50 mM sulphate. The saturation state for gypsum stayed at SI close to 0 throughout the entire experiment. After reaching the pH decrease stage of the experiment gypsum became highly undersaturated (Fig.38b). Thus a sulphate-bearing phase was not suggested to have been formed, but keeping in mind that prior to the carbonation process a large amount of calcium sulphate was separated from the solution (slaking grit > 200 µm; see results) influenced the results concerning sulphate phases during the carbonation process drastically.

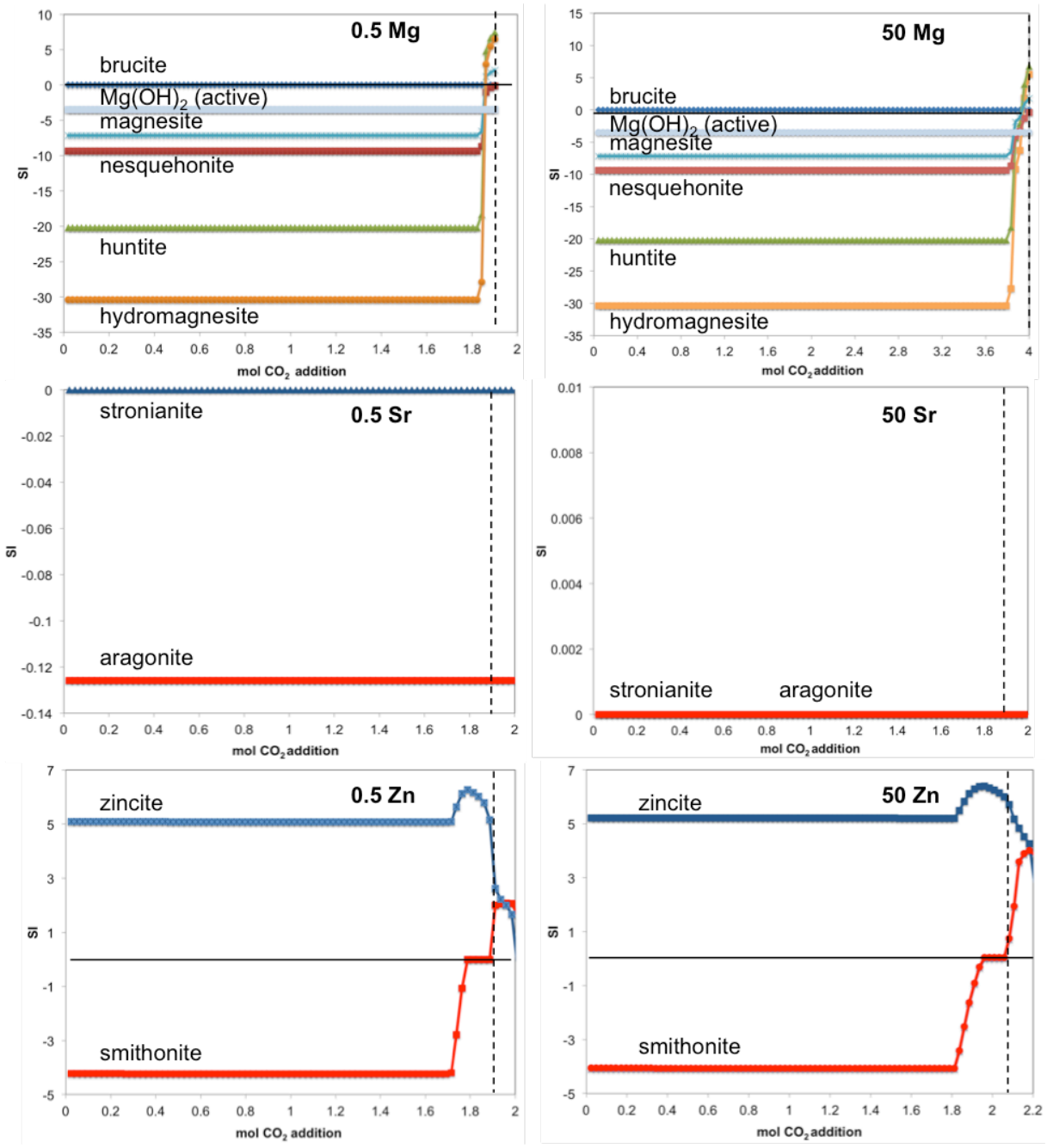

Figure 38a: Evolution of the saturation indices for the individual solid phases for the experiments with initial 0.5 and 50 mM Mg, Sr and Zn throughout the experiment.

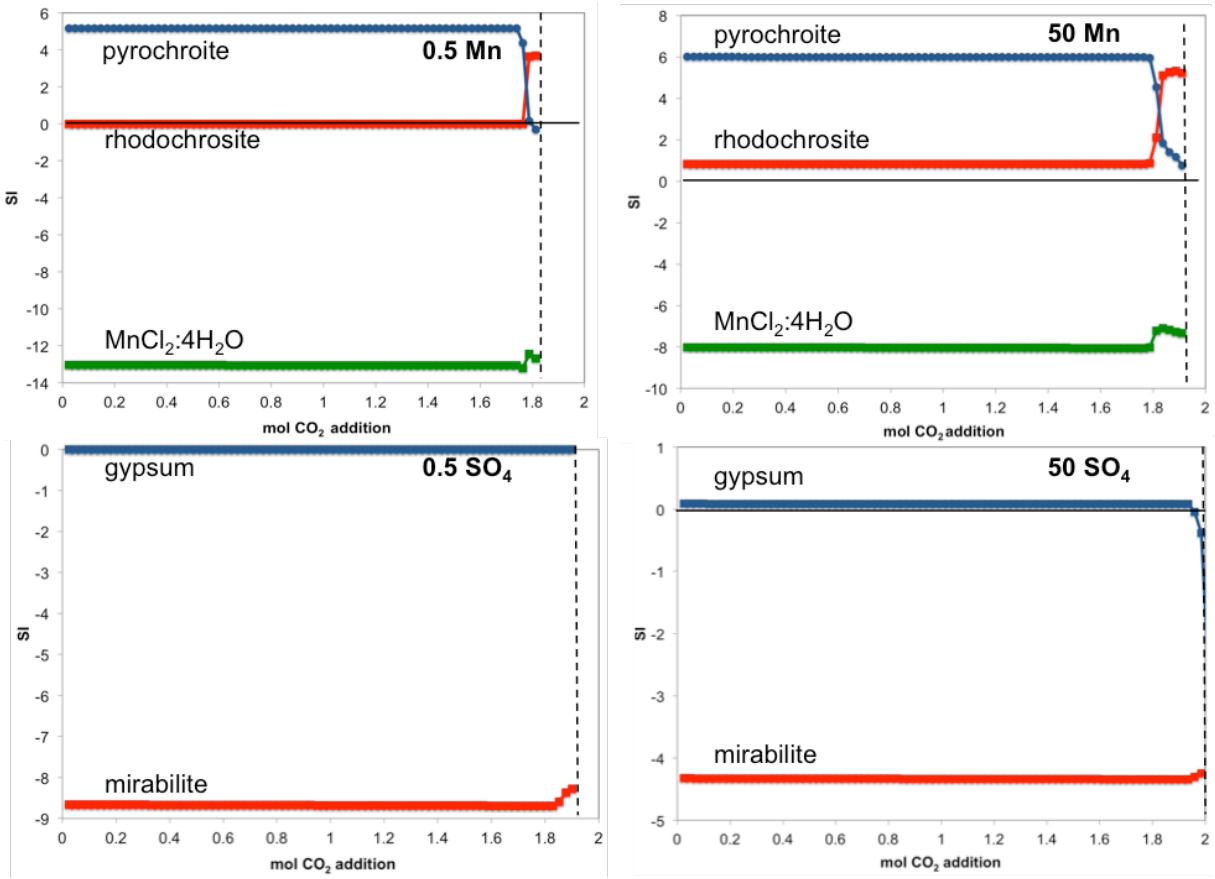

Figure 38b: Evolution of the saturation indices for the individual solid phases for the experiments with initial 0.5 and 50 mM Mn and SO_4 throughout the experiment.

6. Summary and Conclusion

The objective of the present thesis was to decipher the impact of selected dissolved ions on the $CaCO_3$ formation by PCC processing. Focus was given on chemical and in particular morphological attributes of the final product. Those attributes are essential factors for the usability, and quality in industrial applications of PCC (e.g. rubbers, papers, fillers).

In this study fourteen experiments with six distinct dissolved compounds were conducted. The used compounds Mg, Sr, Zn, Mn, SO_4 or Fe were selected from their (i) high concentration in solutions from numerous industrial waters from worldwide subsidiaries of Omya (e.g. Mg) or (ii) known negative effect on the end product as required by Omya (e.g. Mn, reducing the brightness). The industrial waters investigated were taken at six different stages during the carbonation process: process water (PW), wastewater (WW), water from the centrifuge (CFW), water from the compressor (COW), cleaning water (CLW) and flue gas condesate (CDW). Depending on their origin the pH varied from 2.5 to 12.5.

For the precipitation experiments Mg, Sr, Zn, Mn, SO_4 or Fe (chlorides and sodium sulphate) were added to the initial solution as well as 0.1 % sodium citrate in each case. This solution was mixed with the Tagger (burned lime) for slaking. After separating the solution from the solids > 200 µm the carbonation process was started by introducing CO_2.

The XRD and FT-IR results showed that calcite was precipitated in all experiments except for the experiment with initial 50 mM Sr. In the latter case aragonite was dominant in comparison to calcite despite the addition of the sodium citrate to the initial solution, which was added to inhibit aragonite precipitation. Further experiments are required to investigate the Sr limit for calcite versus aragonite precipitation.

SEM imaging concurred with the previous results and calcitic PCC was obtained at 0.5 mM of additives with similar shape and size. The experiments delivered the required scalendohedral calcitic PCC (S-PCC) with 2 to 3 µm in size. The samples showed an average specific surface area of 5.3 m^2/g, which was slightly lower than the 5.6 m^2/g that were measured after sieving.

In contrast to the final product at 0.5 mM additive concentration the crystals at 50 mM additive mostly did not resemble the reference sample in shape and size. The experiments with initial magnesium and manganese at 50 mM, however, still showed

similar crystal shapes compared to the calcite reference (precipitated without additive). With strontium ions at the elevated concentration level of 50 mM the additional aragonite precipitates were considerably smaller in size (0.5-1 µm) and thinner than the calcite reference. SEM imaging for 50 mM zinc revealed that the addition of zinc in high concentrations influences the structure. Imaging showed calcite clusters with smaller crystals of a size up to 2 µm. The addition of 50 mM of sulphate resulted in an even more highly clustered structure (see also Fig. 18), and therefore, also influenced the properties of the final product.

By introducing the burned lime (Tagger) into the solution the magnesium content of the system rose significantly. Thus, a main percentage of the dissolved Mg in the final solution derived from the added burned lime (natural limestone with a Mg content of 1.8 wt. %). In the final solution (after $CaCO_3$ precipitation) the magnesium concentration was high due to dissolution of Mg phases. Furthermore, the concentration of the other additives in the final solution was mostly decreased compared to the initial solution. At the end of the carbonation process Mg remained in the solution and was non-significantly incorporated into the calcite. No distinct Sr - rich solids were detected but the formation of e.g. strontianite at high alkaline solutions cannot be ruled out. However, in the case of Sr aragonite was formed at elevated Sr concentrations instead of calcite. All PCC products from experiments with initial Mn showed a significant decrease in brightness. Even 0.05 mM Mn resulted in a brightness R457 decrease of about 4 %. The addition of 0.5 mM Fe did not show any significant colouring, even though iron is known to cause yellow coloration. In the case of manganese and iron it was assumed that separate X-ray amorphous oxides/hydroxides were formed causing colouring at varying concentrations. Experiments with initial 50 mM SO_4 resulted in a large amount of slaking grit (presumably gypsum). Subsequent to the precipitation of $CaSO_4$ no significant incorporation of SO_4 into the calcite occurred. In conclusion sulphate in high concentrations had a strong impact on the conversion and reactivity of the milk of lime.

Comparing the influences on the end product caused by varying initial concentrations of the selected ions to the maxima, minima and mean values of the industrial solutions recommended maximum upper limits were set at which no impact on the S-PCC process and the quality of the products is to be expected (Tab. 2). For magnesium no limit was suggested due to no significant influence on the final

product and the remaining of Mg in the final solution. The limit for strontium was set to < 0.6 mM (≙ 50 ppm) due to the observed precipitation of aragonite instead of calcite at high strontium values. High zinc concentrations lowered the brightness, and therefore, the limit was estimated at < 0.2 mM (≙ 10 ppm). A significant reduction in brightness for low manganese concentrations (already at initial 0.05 mM) caused a maximum upper limit of < 0.002 mM (≙ 0.1 ppm) Mn. For sulphate < 5 mM (≙ 500 ppm) were considered because of its significant influence on brightness and crystal structure at high initial concentrations. For iron a limit of < 0.02 mM (≙ 1 ppm) was suggested due to its brightness reducing effect. The limiting values for chloride were set at 1.4 mM (≙ 50 ppm) but it has to be mentioned that chloride was not explicitly investigated in the experiments. The value is based on practical experience by Omya.

The modelling approach in most cases provided a good correlation between monitored and modelled pH/conductivity curves, and thus, a better understanding of the processes occurring during the carbonation process. The precipitation of brucite instead of hydromagnesite and nesquehonite during carbonation gave the best modelling results. The modelling results were as follows in chronological order: (i) the transformation of $Ca(OH)_2$ into $CaCO_3$ via on-going dissolution and precipitation and brucite precipitation at alkaline pH (ii) as soon as all the $Ca(OH)_2$ from the Tagger was consumed the pH decreases and re-dissolution of brucite occured and (iii) in some cases the dissolution of $Ca(OH)_2$ relicts, which might have been covered by e.g. brucite.

The modelling approach lead to the conclusion that at elevated Mg content hydromagnesite might have been formed at an intermediate stage. Even at high strontium concentration the modelling revealed that strontianite could not precipitate. In the case of experiments including zinc and manganese the modelling exposed that zincite and rhodochrosite may have precipitated, which could not be verified by analyses of the precipitates. For the experiments with the addition of sulphate, especially at initial 50 mM of sulphate, gypsum precipitated after the slaking process causing a high amount of slaking grit. However, throughout the carbonation gypsum was not supersaturated and accordingly not detected in the final PCC product.

Future studies on PCC formation should be focused in more detail on the individual reaction kinetics during the carbonation process. This includes sampling throughout the process in order to develop the evolution of solids and solution

composition. This might be also done by in-situ monitoring e.g. by Raman spectroscopy or ion sensitive electrodes. In addition, future projects should include the analyses of the slaking grit.

References

Appelo C. A. J. and D. Postma (2009). *Geochemistry, groundwater and pollution*. Rotterdam: Balkema. 178-183.

Böttcher M.E. and M. Dietzel (2010). “Metal-ion partitioning in carbonates and sulphates“. In: *Ion partitioning in ambient-temperature aqueous systems (eds.* Manuel Prieto and Heather Stoll). London: EMU and the Mineralogical Society of Great Britain & Ireland: Vol. **10**: 139-187.

Dietzel M. (2011). “Carbonates”. In: *Encyclopedia of Geobiology (eds.* Reitner, J. and Thiel V.). Berlin: Springer. 261-266.

Fernandéz-Díaz L. et al. (2010). „The role of sulfate groups in controlling $CaCO_3$ polymorphism“. *Geochimica et Cosmochimica Acta* **75**: 6064-6076.

Franklin M.L and J.W. Morse (1983). The interaction of manganese (II) with the surface of calcite in dilute solutions and seawater. *Mar. Chem*. **12**: 241-254.

Gautier Q. (2012). *Cinétiques de precipitation de minéraux carbontatés magnésiens influence de ligands organiques, et consequences pour la sequestration minérale du CO_2*. Doctoral Thesis. 69-72.

Isopescu R. et al. (2009). „The effects of organic additives on induction time and characteristics of precipitated calcium carbonate“. *Chemical Engineering Research and Design* **88**: 1450-1454.

Jung W.-M. et al. (2010). „Precipitation of calcium carbonate particles by gas-liquid reaction: Morphology and size distribution of particles in Couette-Taylor and stirred tank reactors“. *Journal of Crystal Growth* **312**: 3331-3339.

Kadota K. et al. (2013). “Effect of surface properties of calcium carbonate on aggregation process investigated by molecular dynamics simulation”. *J Mater Sci* **49**: 1724-1733.

Knights A.V. and R. D. Stenner (1999). “The role of ion balances in examining the reliability of analytical data: a case study of mendip streams”. *Proc Univ Bristol Apelaeol Soc* **21**: 235-249.

Kosma V. K. and K. G. Beltsios (2012). “Simple solution routes for targeted carbonate phases and intricate carbonate and silicate morphologies“. *Materials Science and Engineering C* 33: 289-297.

Kotoyannis C.G. and N. V. Vagenas (2000). “Calcium carbonate phase analysis using XRD and FT-Raman spectroscopy”. *Analyst* **125**: 251-255.

Matsumoto M. et al. (2010). “Polymorph control of calcium carbonate by reactive crystallization using microbubble technique”. *Chemical Engineering Research and Design* **88**: 1624-1630.

Morse J. W. and F. T. Mackenzie (1990). “Geochemistry of Sedimentary Carbonates”. *Developments in Sedimentology* **48**: 4, 24, 36.

Morse John W. et al (2007). “Calcium Carbonate Formation and Dissolution”. *Chem. Rev.* 107. **2**: 355, 356.

Nehrke G. et al. (2007). “Dependence of calcite growth rate and Sr partitioning on solution stoichiometry: Non-Kossel crystal growth”. *Geochimica et Cosmochimica Acta* **71**: 2240-2249.

Niedermayr, A. et al. (2013). “Impacts of aqueous carbonate accumulation rate, magnesium and polyaspartic acid on calcium carbonate formation (6-40°C). *Chemical Geology* **340**: 105-120.

Parkhurst D. L and C.A.J. Appelo (1998). “User’s guide to PHREEQC (Version 2) – A computer program for speciation, batch-reaction, one-dimensional transport, and inverse geochemical calculations”. *US Geological Survey Water-Resources Imvestigations Report*.

Pingitore N. E. et al. (1988). “The Co-precipitation of Manganese(II) with Calcite: an Experimental Study”. *Marine Chemistry* **25**: 107-120.

Saulnier S. et al. (2012). “Mg isotope fractionation during calcite precipitation: An experimental study”. *Geochimica et Cosmochimica Acta* **91**: 75-91.

Stumm W. and J.J. Morgan (1996). *Aquatic Chemistry: chemical equilibria and rates in natural waters*. New York: Wiley-Interscience. 1022 p.

Tang J. et al. (2008). “Sr^{2+}/Ca^{2+} and $^{44}Ca/^{40}Ca$ fractionation during inorganic calcite formation: I. Sr incorporation”. *Geochimica et Cosmochimica Acta* **72**: 3718-3732.

Ukrainczyk M. et al. (2008). “Precipitation of different calcite crystal morphologies in the presence of sodium stearate”. *Journal of Colloid and Interface Science* **329**: 89-96.

Walter Lynn M. and E. L. Dromgoole (1989). “Iron and manganese incorporation into calcite: Effects of growth kinetics, temperature and solution chemistry”. *Chemical Geology* **81**: 311-336

Zhang G. et al. (2012). “Effect of the lattice ions on the calcite flotation in presence of Zn(II)”. *Minerals Engineering* **40**: 24-29.

Zhang Y. and R.A. Dawe (2000). “ Influence of Mg^{2+} on the kinetics of calcite precipitation and calcite crystal morphology”. *Chemical Geol*ogy **163**: 129-138.

Appendix

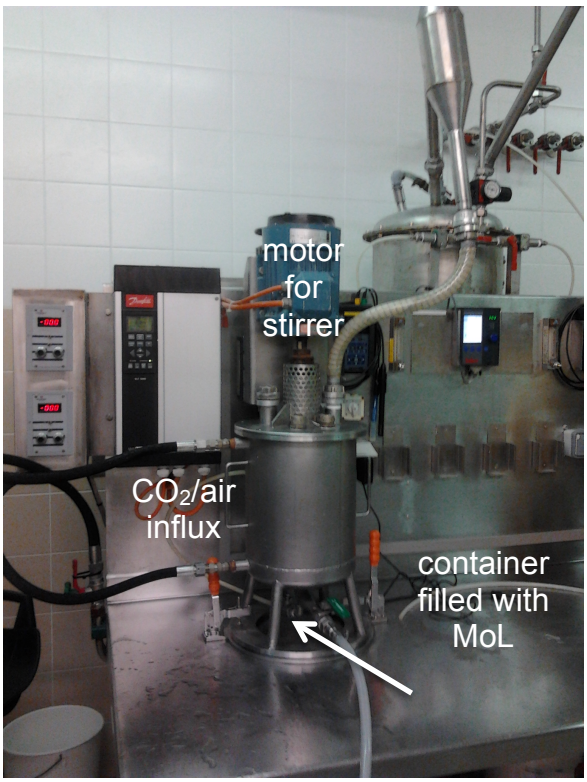

A - 1: setup/equipment for precipitation process. Showing the CO_2 and air influx, the container in which the milk of lime (MoL) was put and the motor for the stirrer.

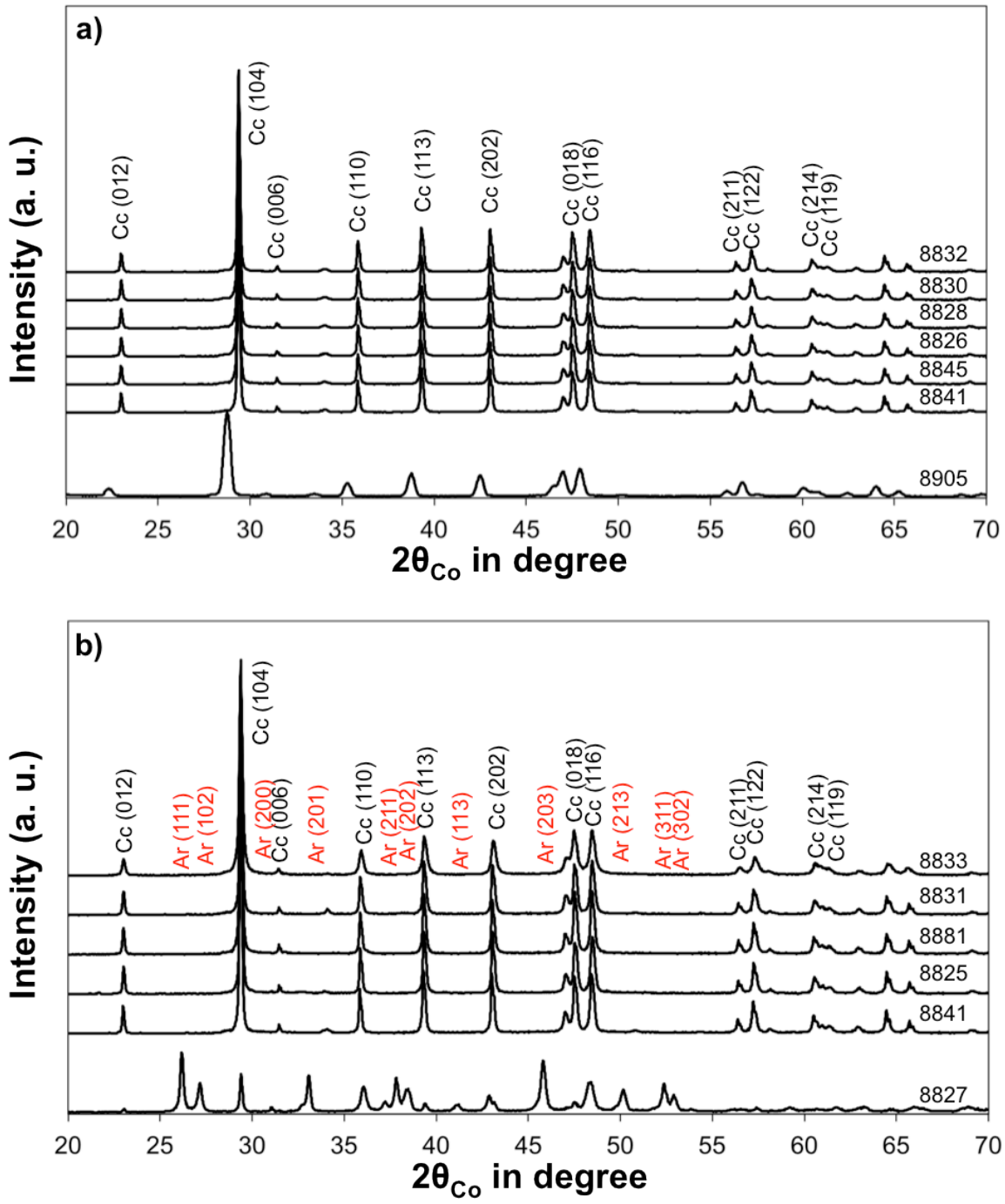

Figure A - 2: XRD patterns of the filter cakes after sieving through 45 m mesh for **a)** 0.5 mM and **b)** 50 mM additives showing the calcite (Cc) and aragonite (Ar) indices. The shift to the left of sample 8905 is probably due to a preparation failure.

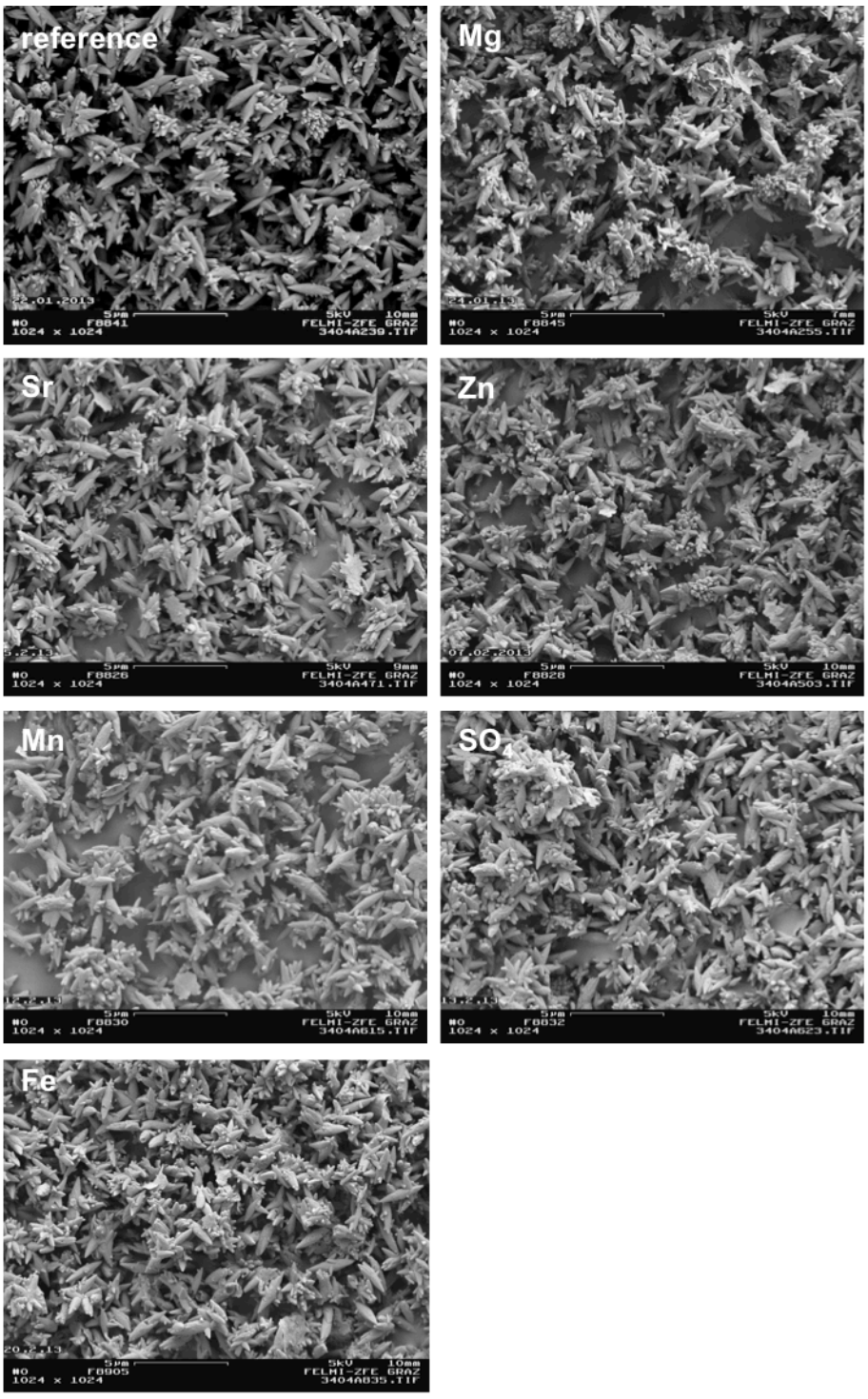

Figure A-3a: SEM results showing the reference sample and samples including 0.5 mM of either Mg, Sr, Zn, Mn, SO_4 or Fe after sieving through 45 µm mesh.

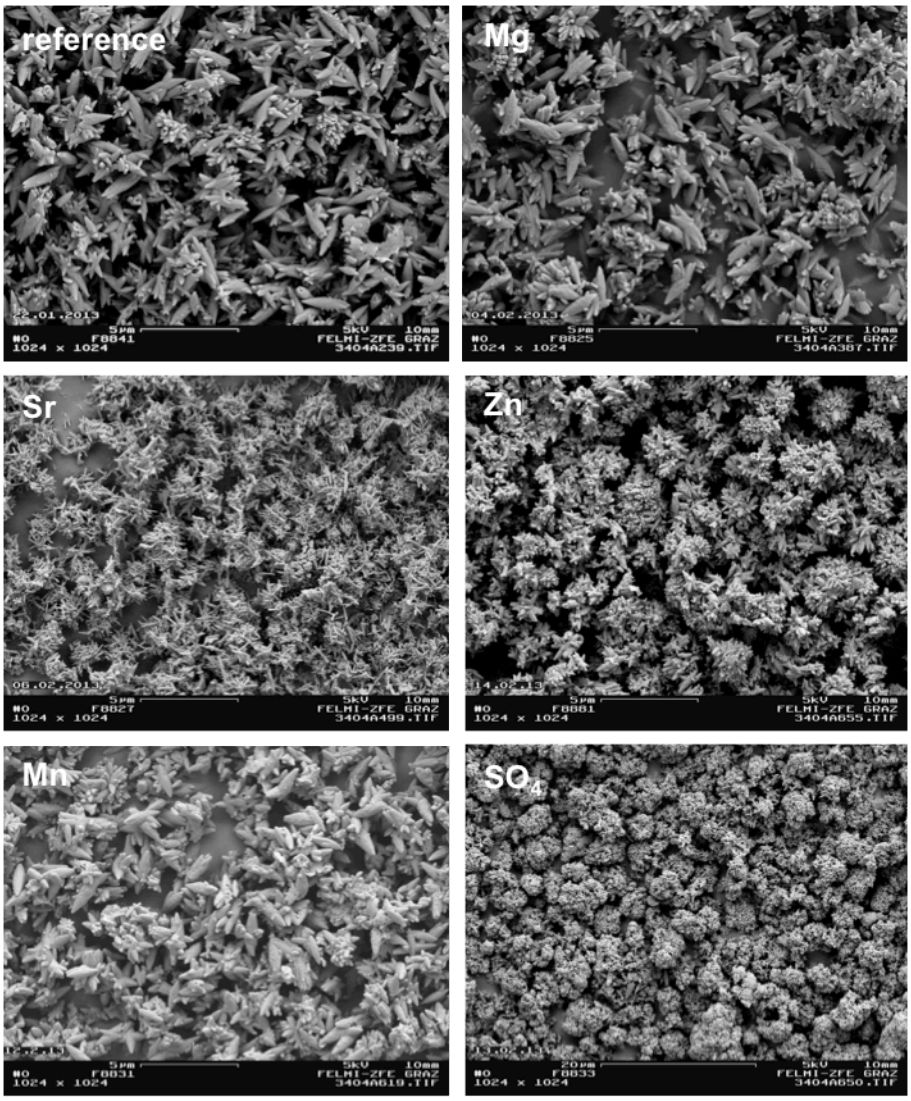

Figure A-3b: SEM results showing the reference sample and samples including 50 mM of either Mg, Sr, Zn, Mn, SO_4 or Fe after sieving through 45 µm mesh.

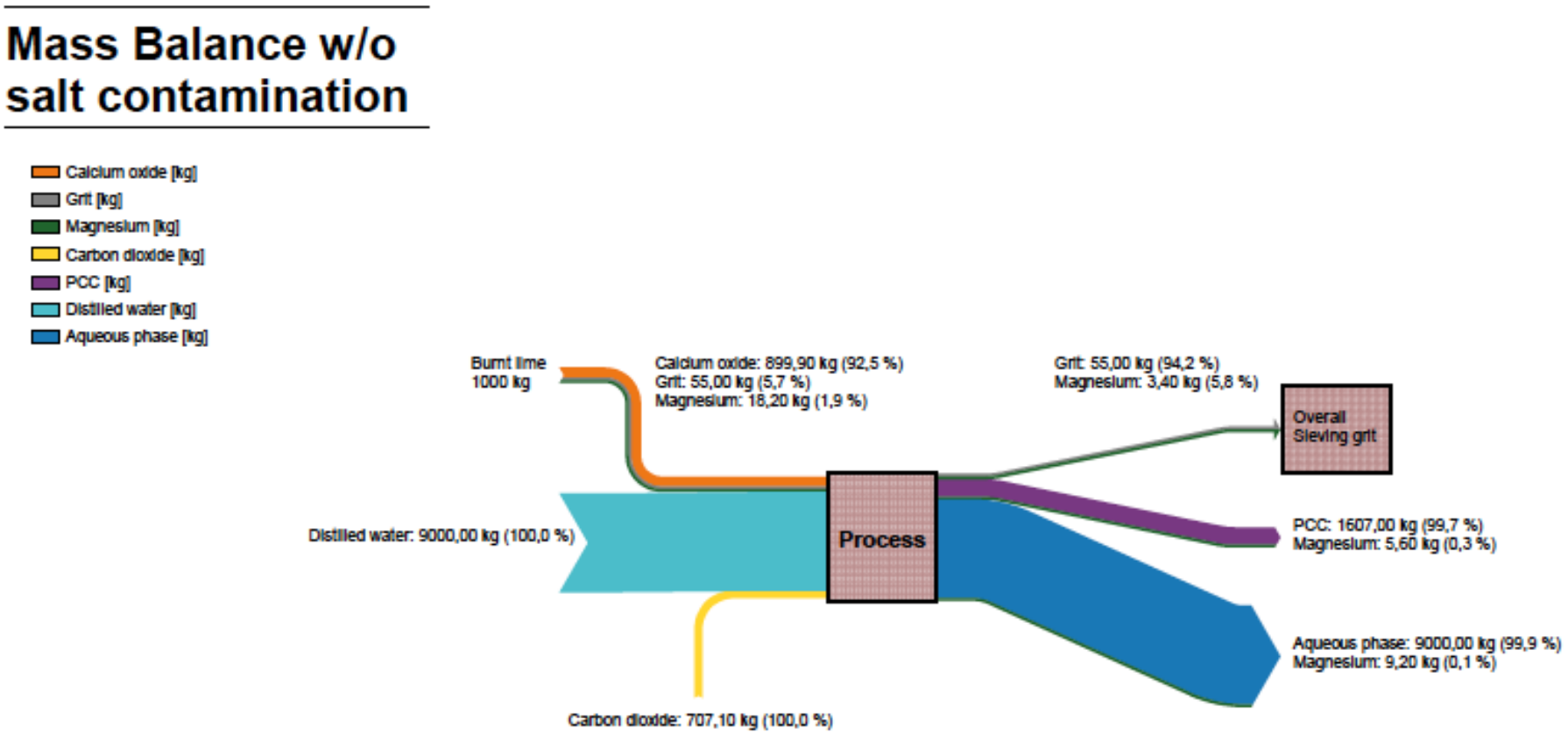

Figure A-4a: Flowchart for mass balance calculation for reference experiment without initial additives. Given values represent the percentage according to equations 30 to 35.

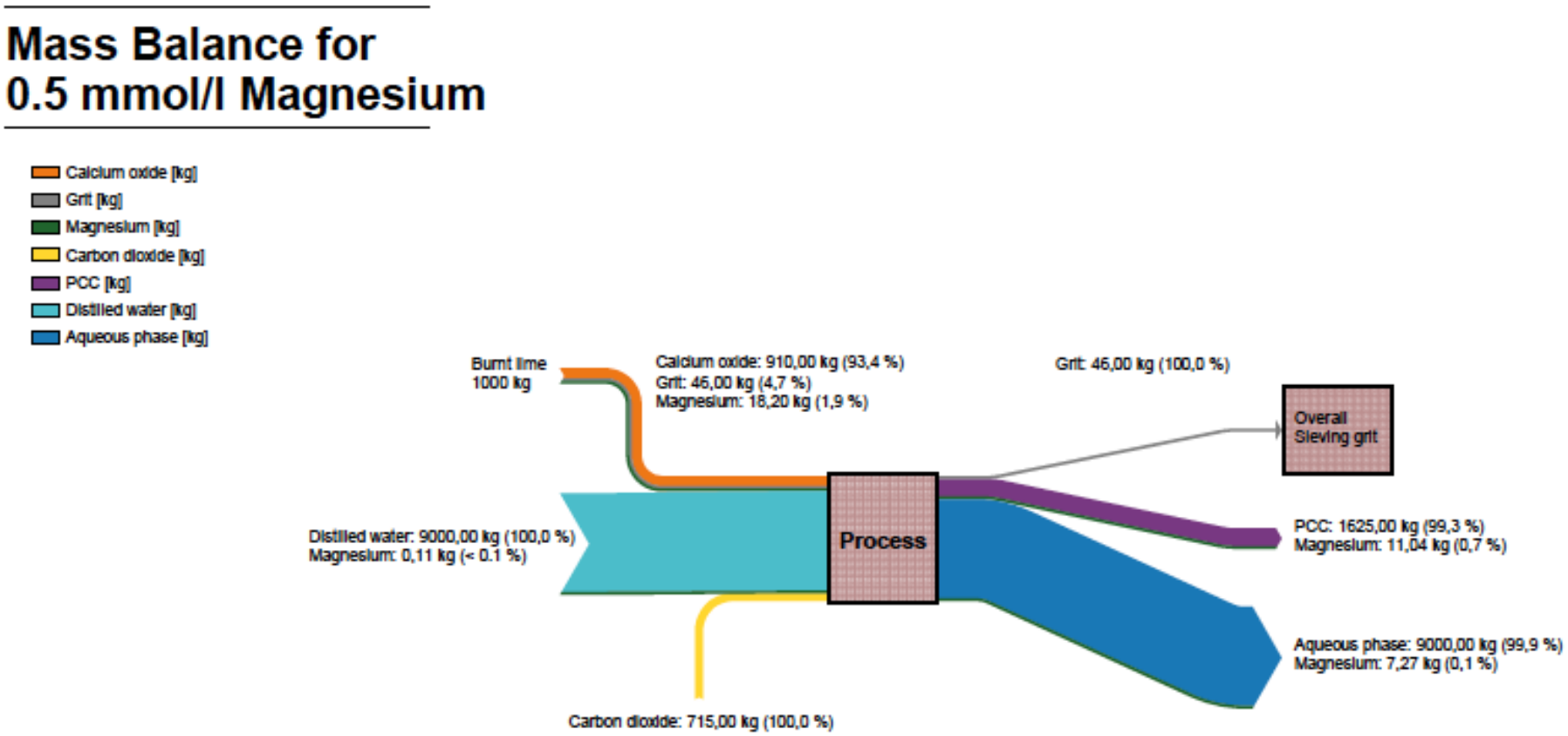

Figure A-4b: Flowchart for mass balance calculation for the experiment with initial 0.5 mM Mg. Given values represent the percentage according to equations 30 to 35.

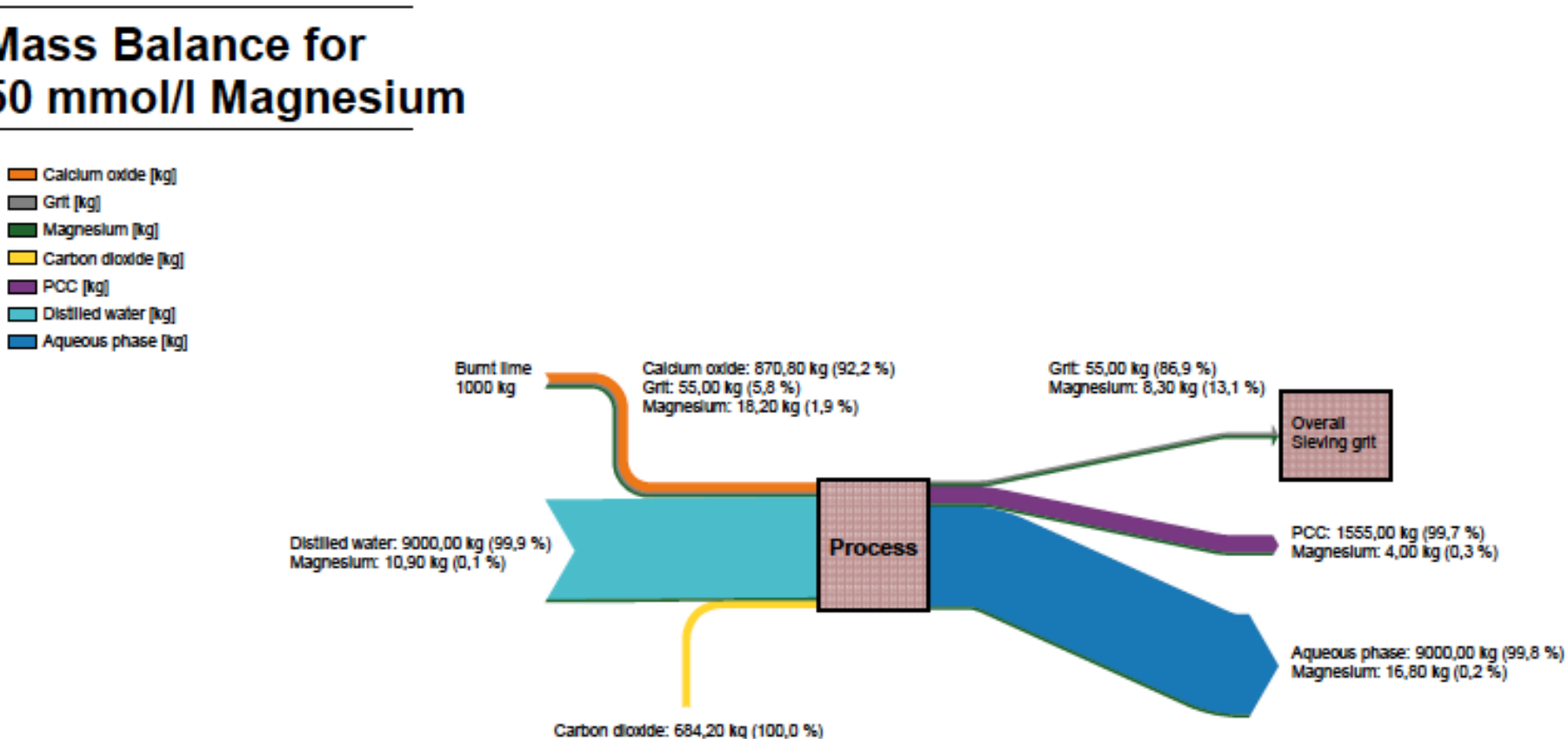

Figure A-4c: Flowchart for mass balance calculation for the experiment with initial 50 mM Mg. Given values represent the percentage according to equations 30 to 35.

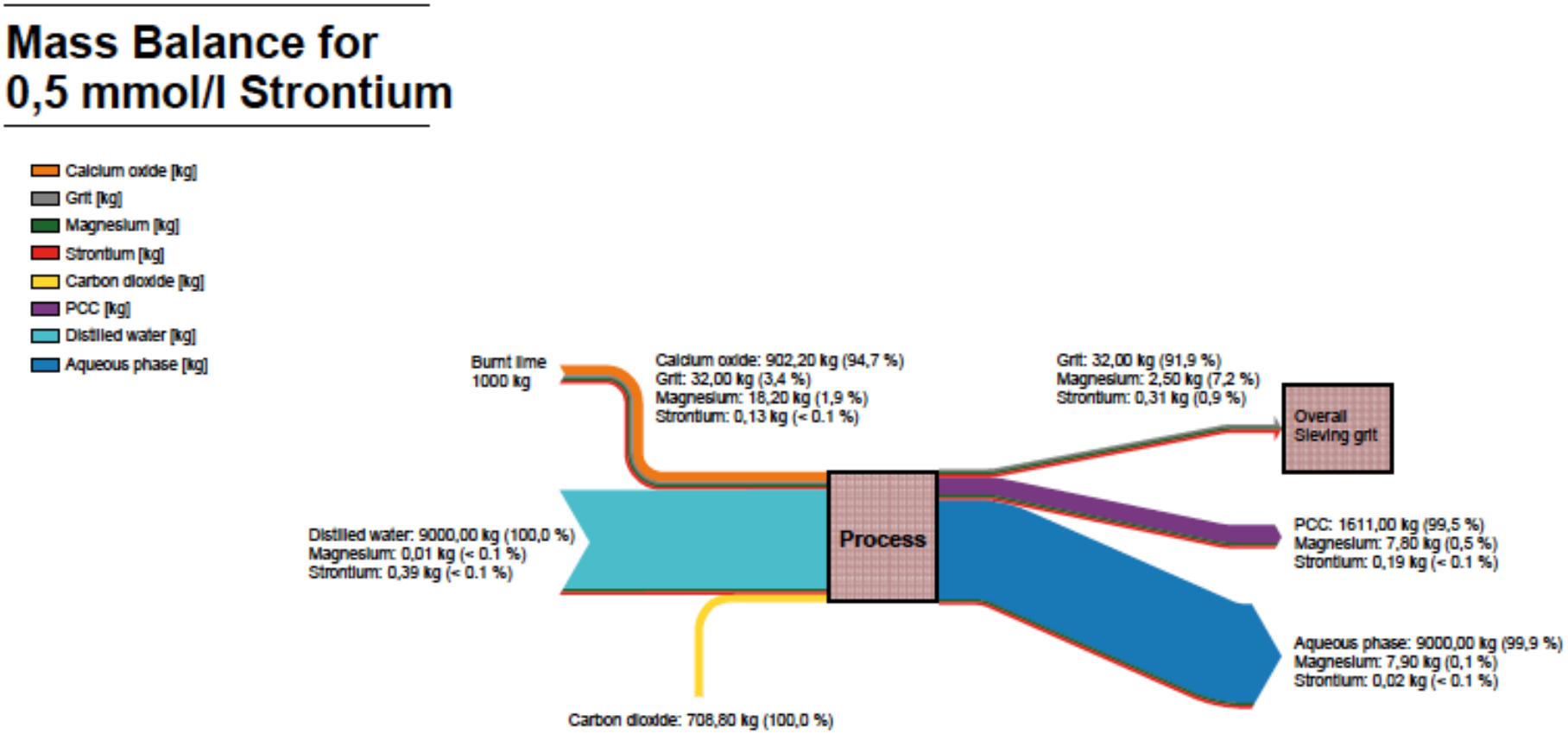

Figure A-4d: Flowchart for mass balance calculation for the experiment with initial 0.5 mM Sr. Given values represent the percentage according to equations 30 to 35.

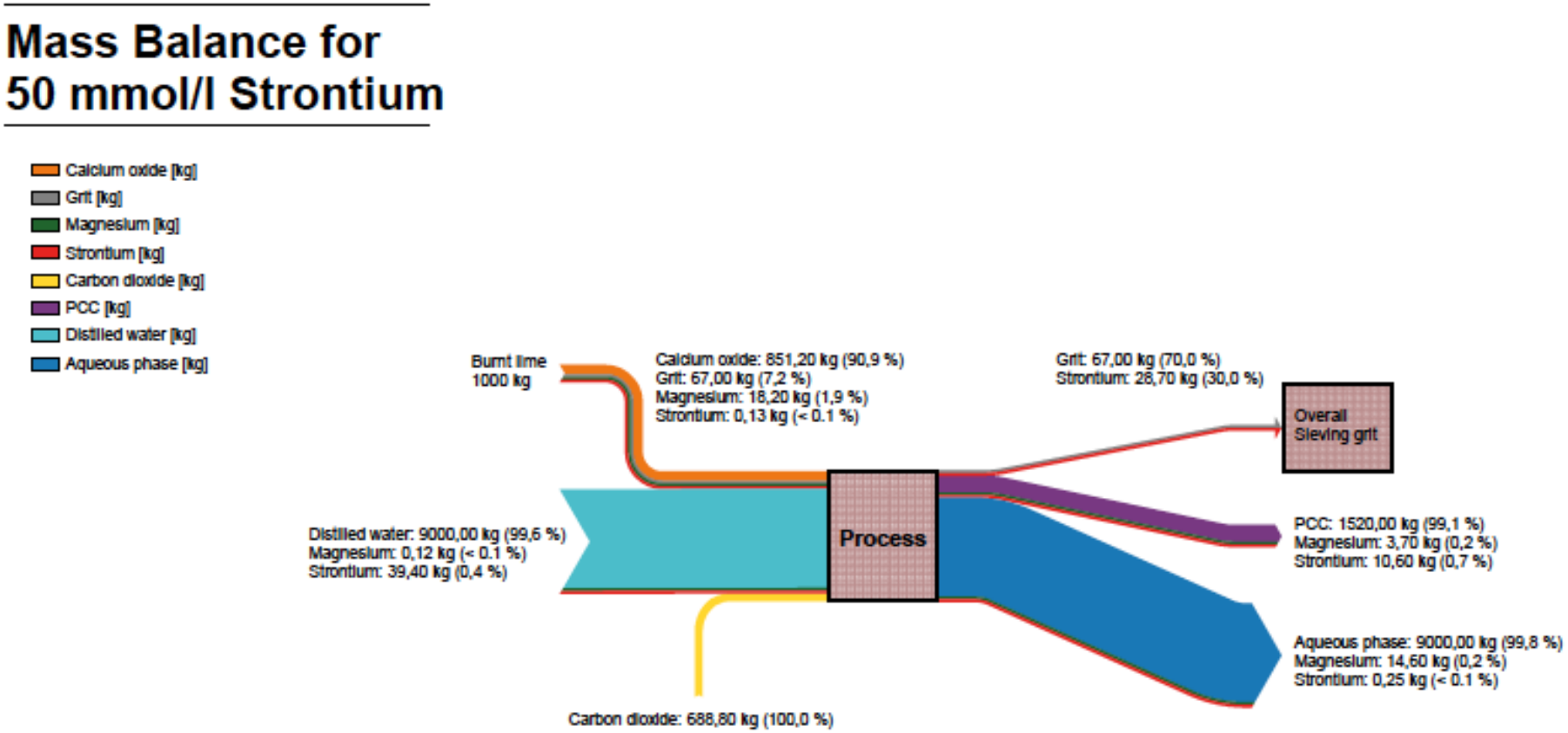

Figure A-4e: Flowchart for mass balance calculation for the experiment with initial 50 mM Sr. Given values represent the percentage according to equations 30 to 35.

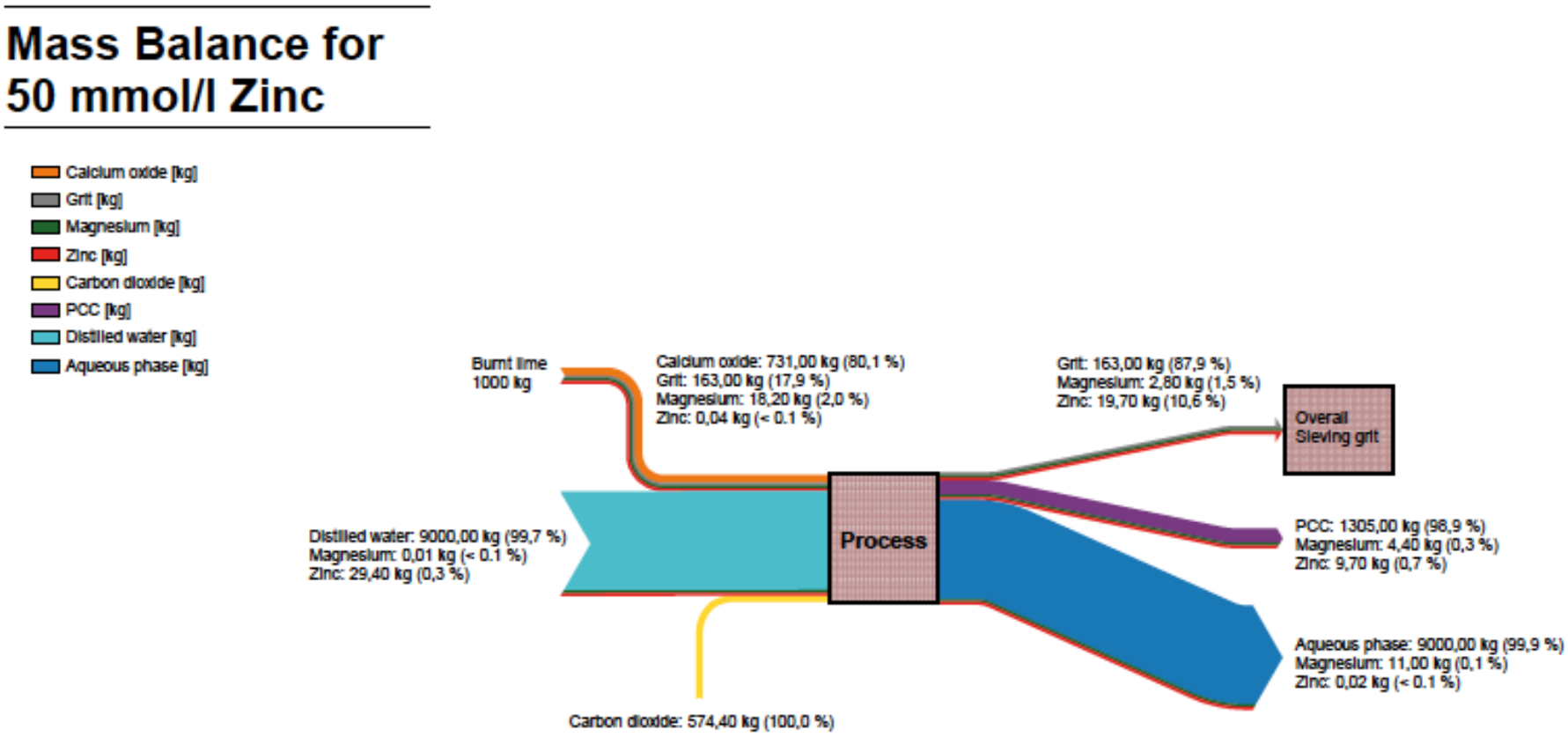

Figure A-4f: Flowchart for mass balance calculation for the experiment with initial 50 mM Zn. Given values represent the percentage according to equations 30 to 35.

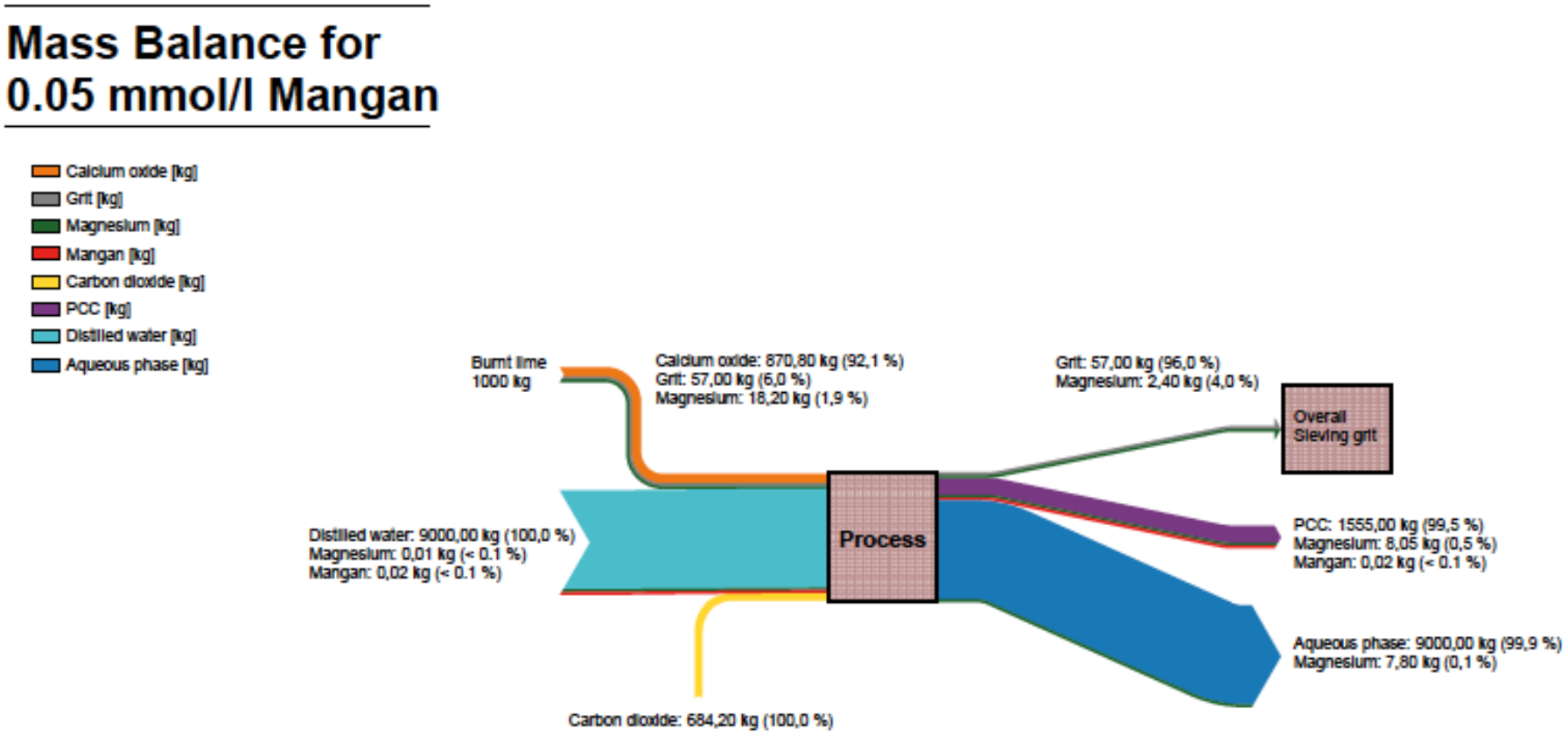

Figure A-4g: Flowchart for mass balance calculation for the experiment with initial 0.05 mM Mn. Given values represent the percentage according to equations 30 to 35.

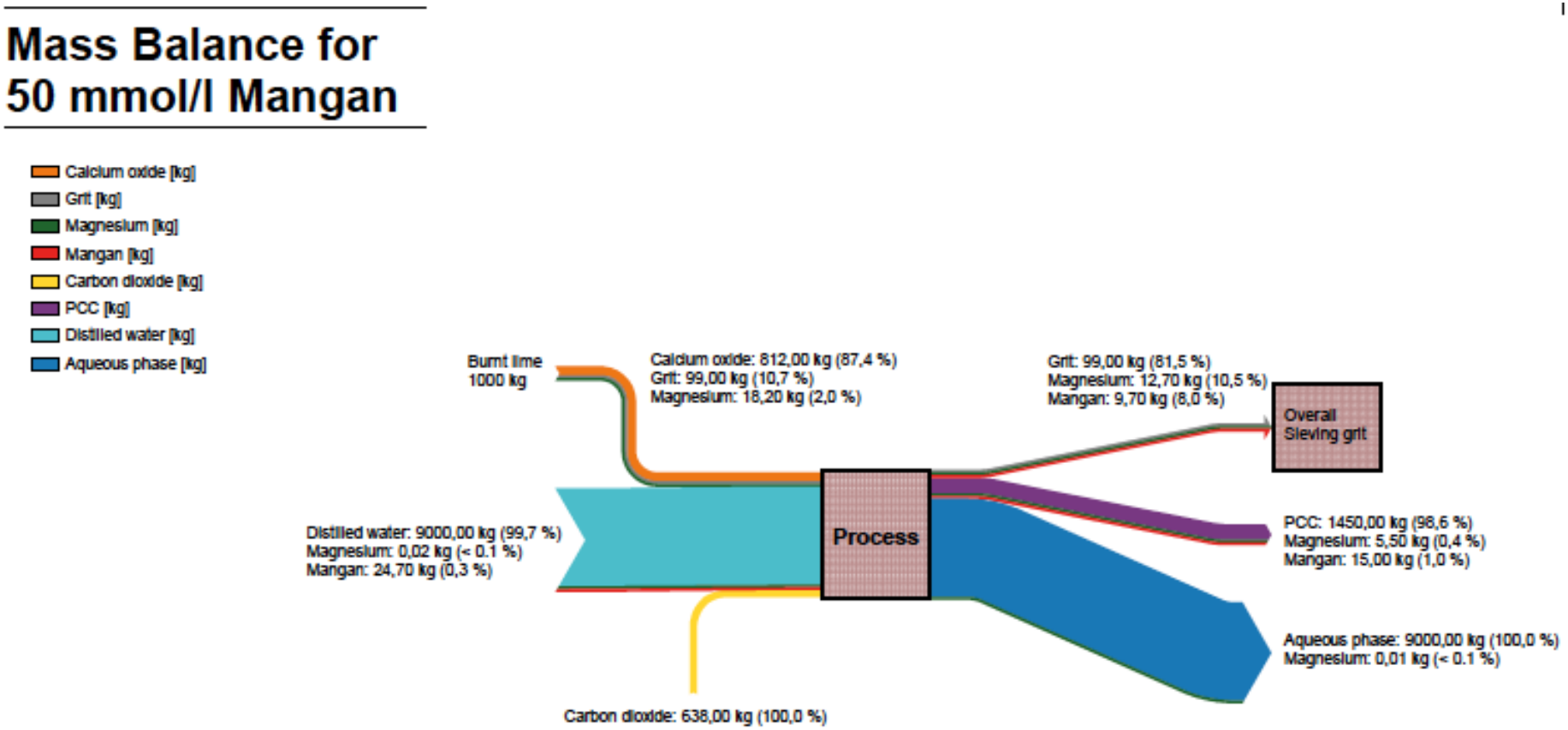

Figure A-4h: Flowchart for mass balance calculation for the experiment with initial 50 mM Mn. Given values represent the percentage according to equations 30 to 35.

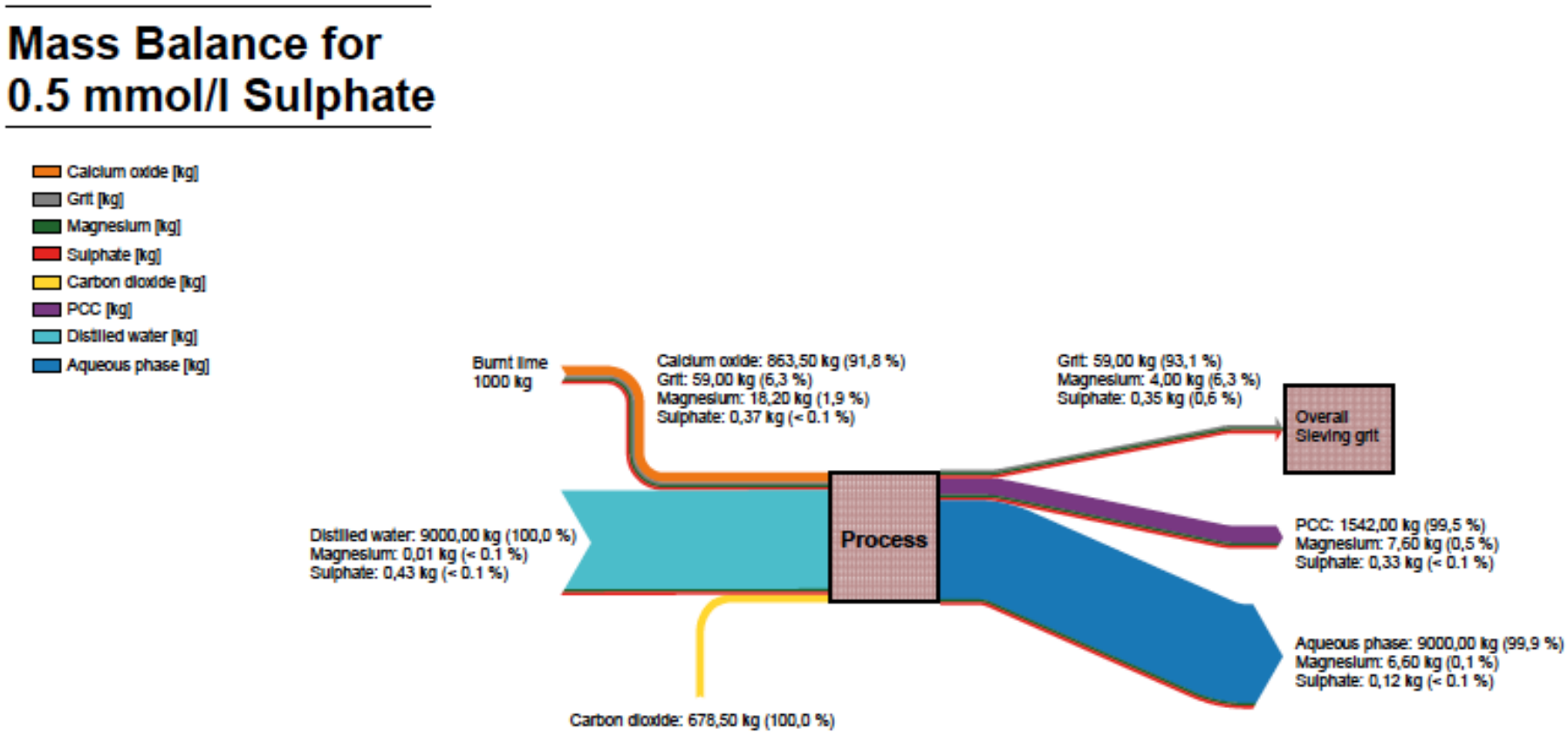

Figure A-4i: Flowchart for mass balance calculation for the experiment with initial 0.5 mM SO_4. Given values represent the percentage according to equations 30 to 35.

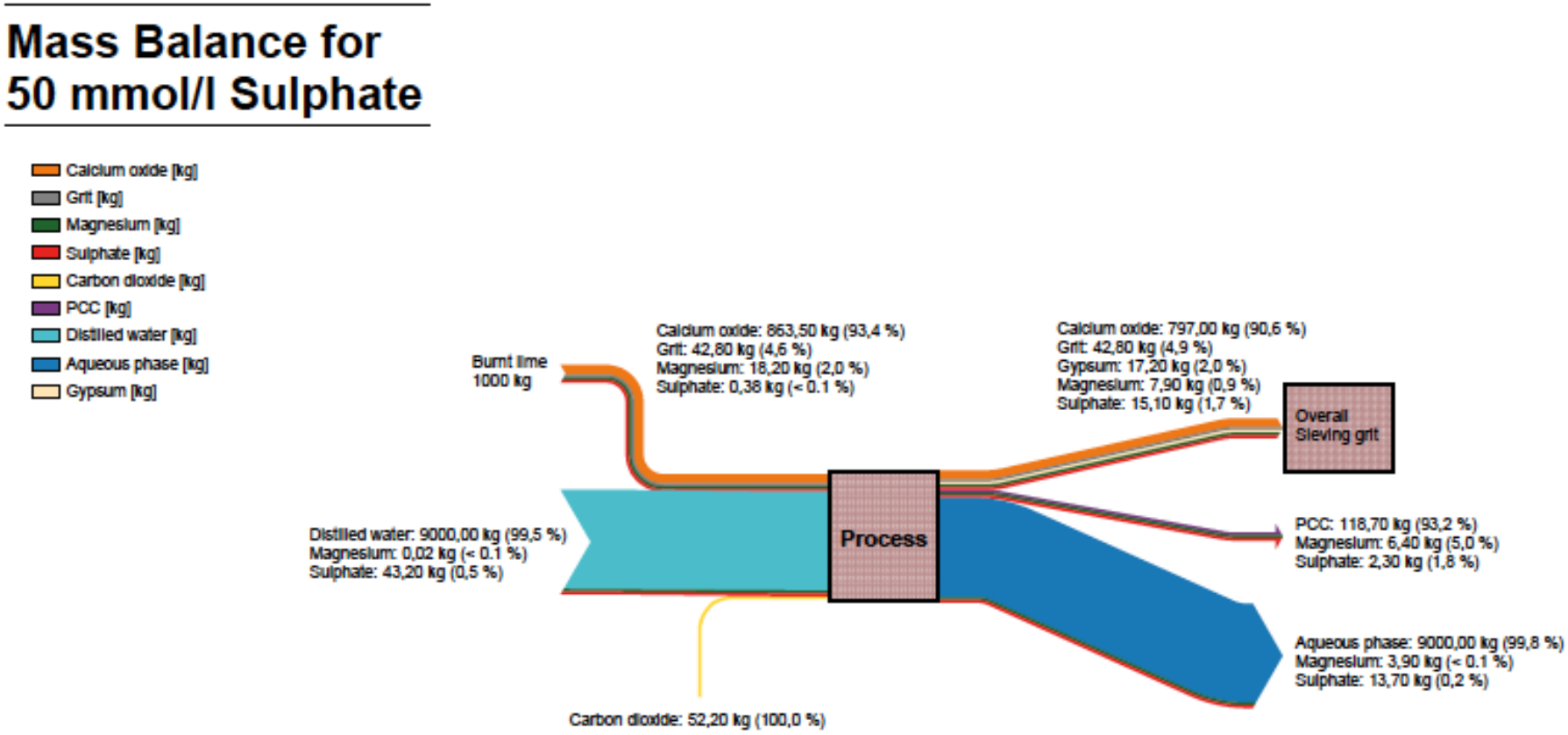

Figure A-4j: Flowchart for mass balance calculation for the experiment with initial 50 mM SO_4. Given values represent the percentage according to equations 30 to 35.

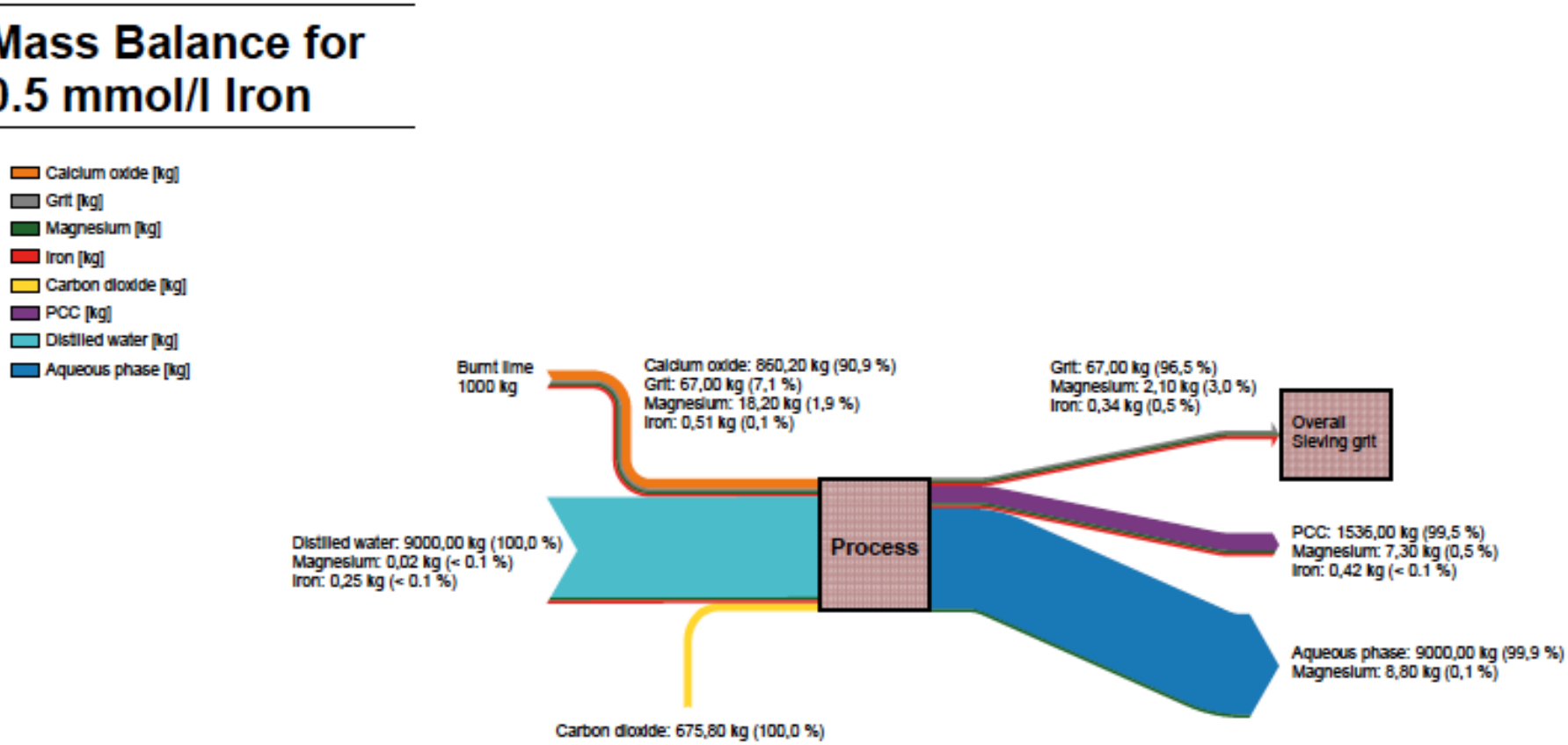

Figure A-4k: Flowchart for mass balance calculation for the experiment with initial 0.5 mM Fe. Given values represent the percentage according to equations 30 to 35.

```
SOLUTION 1
pH 7
Temp 50
units mmol/kgw
#Ca 0.01
#Mg 0.001
#C(4) 0.02 as HCO3
Citrate 0.7 # 50 ppm C gemessen (am Ende nur 6 ppm C)

EQUILIBRIUM_PHASES 1
Calcite 0
portlandite 0 1.805 diss # 1.805 mol portlandite zur verfügung
brucite 0 0.134 diss  # 0.134 mol mg(OH)2
#Nesquehonite  0 0.134 diss
#hydromagnesite   0 0.0268 diss # stoichiometry 1/5
#Mg(OH)2(active)   0 0.134 diss

REACTION 1
CO2 1; KCl 0.00001; 2.45 in 100   # Adds 1.91 mol CO2 in 78 equal steps, verbrauch, dann zusatz!

# SI(CO2) - 0.7 # da ist schluss, da 20% CO2 gas, etwa pH 7.8

SELECTED_OUTPUT
-file H:\1_DIPL_STUD_GUEST\Scheinecker_Stefanie\Ergebnisse\PhreeqC\reference_nesquehonite.xls # file name
-pH
-ionic_strength
-totals Ca Mg C(4) K Na Cl #specific conductance # name from the 1st column of ..._MASTER_SPECIES
-molalities Ca+2 Mg+2 MgOH+ MgCO3 MgHCO3+ CaOH+ CaCO3 CaHCO3+ # name defined in ..._SPECIES
-activities Ca+2 Mg+2
-saturation_indices Calcite Portlandite CO2(g) brucite Mg(OH)2(active) Nesquehonite

USER_GRAPH
 -chart_title "Calcite Equilibrium + Portlandite dissolution + Mg(OH)2 dissolution + co2 addition"
 -axis_titles "K [M]" "pH" "Mg [M]"
 -axis_scale x_axis       0 0.00002 0.000001
 -axis_scale y_axis     4 12 1
 -axis_scale sy_axis       0 1 0.1
 -headings    na pH mg
 -start
 10 graph_x  tot("K")
 20 graph_y  -la("H+")
 30 graph_sy  tot("mg")
 -end
END
```

Figure A-4: Code used for the modelling approach via PhreeqC using modified minteq.v4.dat database regarding the sodium citrate values according to Gautier (2012).

Table A - 1: Origin, water type, physical parameters and chemical composition of the analysed industrial solutions

NH4	NO3	Conductivity	Alkalinity	suspeded	Hardness	DOC	pH	share		
ICP	ICP	SFS - EN27888	SFS 3005	solids	SFS 3018	TOC-V PH + ASI-V				
[mg/l]	[mg/l]	[µS/cm]	[mg/l]	[mg/l]	[°dH]	[mg/l]	[-]	[% of total]	water type	plant
< 0.5	2.5	358	188		8.6	1.11	7.97	20%	PW	A
< 0.5	4.2	423	200		9.2	3.16	8.17	80%	PW	A
1.3	2.5	8020	3061	39963.6	140.5	13.83	12.53	53%	WW	B
3.0	4.8	88	17		0.8	2.20	8.68	46%	PW	B
b.d.l.	b.d.l.	1271	13	3194.8	0.6	38.78	8.52	1%	CFW	B
1.0	0.7	82	1041		47.8	1.48	6.19	50%	COW	C
1.0	0.8	83	17	32.8	0.8	1.98	6.23	50%	COW	C
< 0.5	1.0	88	14	21.4	0.6	4.44	7.75	50%	PW	D
< 0.5	0.5	1729	1442	4993.8	66.2	4.96	8.53	50%	CFW	D
< 0.5	5.3	149	30		1.4	3.13	8.41	99.50%	PW	E
< 0.5	3.8	8970	2788	5560.4	128.0	42.50	12.42	0.50%	CLW	E
< 0.5	3.1	675	135		6.2	1.10	8.10	22%	PW	F
< 0.5	3.8	1751	984	3373.7	45.2	1.92	8.34	56%	CFW	F
< 0.5	3.7	739	174	618.0	8.0	1.22	8.04	22%	WW	F
< 0.5	13.9	2010	224	2118.1	10.3	2.08	7.73	20%	WW	G
< 0.5	12.9	1297	599	273.4	27.5	4.44	9.09	17%	CFW	G
< 0.5	11.2	360	65		3.0	5.12	7.49	63%	PW	G
< 0.5	1.3	947	652		29.9	5.56	7.32	10%	CLW	H
< 0.5	20.3	1441	837	587.4	38.4	1.86	8.55	70%	CFW	H
< 0.5	44.6	254	76		3.5	2.89	7.70	10%	PW	H
< 0.5	13.2	8270	2092	14415.8	96.0	3.73	12.44	10%	WW	H
< 0.5	0.2	439	138		6.3	2.88	8.04	0%	PW	I
< 0.5	0.0	404	133	14.4	6.1	1.09	7.15	50%	COW	I
< 0.5	3.3	1439	312	403.8	14.3	1.84	11.55	10%	WW	I
1.3	3.0	541	104	40.0	4.8	2.65	7.04	10%	CDW	I
< 0.5	b.d.l.	415	137		6.3	2.14	6.25	30%	COW	I
7.0	1.0	1640			b.d.l.	5.22	2.40	95%	COW	J
1.0	0.6	66	160	1.5	7.3	4.00	6.07	5%	PW	J
< 0.5	0.4	213	36	47.2	1.6	6.58	7.41	100%	PW	K
< 0.5	0.6	191	30		1.4	5.65	7.68	0%	PW	K
2.3	1.9	578			b.d.l.	6.88	3.18	64%	COW	L
< 0.5	3.9	2090	1704	378.6	78.2	3.30	8.35	21%	CFW	L
< 0.5	1.2	159	17		0.8	5.60	7.76	15%	CDW	L
b.d.l.	b.d.l.	414	6	0.1	0.3	1.49	7.01	100%	PW	M
< 0.5	0.7	70	9	16.0	0.4	3.29	8.83	100%	PW	N
< 0.5	1.8	228	107		4.9	3.10	6.58	100%	PW	O
237.00	5.7	455	231		10.6	2.28	8.20	4%	PW	P
415.00	3.3	2330	1178	314.4	54.1	75.29	8.75	87%	CFW	P
377.00	2.2	4380	2276	15823.4	104.5	8.50	12.27	9%	WW	P

Fe	Si	Na	K	Mg	Ca	P	F	SO4	Cl		
ICP	ICP	ICP	ICP	ICP	ICP	ICP	ICP	ICP	ICP		
[µg/l]	[mg/l]	[mg/l]	[mg/l]	[mg/l]	[mg/l]	[mg/l]	[mg/l]	[mg/l]	[mg/l]	water type	plant
b.d.l.	2.5	6.1	2.2	12.9	48.5	b.d.l.	< 0,1	27.9	7.1	PW	A
b.d.l.	2.1	13.5	2.8	11.3	58.2	b.d.l.	< 0,1	26.7	21.0	PW	A
0.0	6.1	9.0	6.2	3.1	723.6	b.d.l.	1.1	8.2	7.8	WW	B
917.0	6.7	7.0	3.3	1.3	5.8	b.d.l.	4.0	14.6	7.3	PW	B
93.0	38.9	18.8	14.7	173.6	7.2	6.0	0.7	66.7	10.9	CFW	B
349.0	6.7	8.7	2.1	1.6	3.5	2.0	5.0	13.4	6.9	COW	C
54.0	6.4	8.7	2.1	1.6	4.2	b.d.l.	5.0	13.4	6.9	COW	C
b.d.l.	2.1	5.4	1.2	1.8	7.2	< 0,1	< 0,1	5.6	13.8	PW	D
b.d.l.	12.3	28.6	21.0	310.6	3.6	0.1	0.0	58.7	14.0	CFW	D
b.d.l.	5.5	11.3	1.9	4.0	10.0	0.0	< 0,1	7.3	21.8	PW	E
b.d.l.	1.6	16.6	3.2	0.5	817.3	< 0,1	0.1	35.1	20.8	CLW	E
b.d.l.	1.0	94.0	2.5	4.5	38.5	< 0,1	< 0,1	6.0	140.3	PW	F
b.d.l.	30.5	173.6	12.7	144.2	6.9	0.1	0.0	15.3	168.0	CFW	F
b.d.l.	1.3	95.6	3.0	7.0	49.6	3.5	< 0,1	6.6	139.7	WW	F
b.d.l.	2.0	326.0	5.6	29.6	111.4	0.4	0.2	814.7	39.8	WW	G
b.d.l.	b.d.l.	112.0	16.6	142.8	3.9	< 0,1	< 0,1	252.1	40.6	CFW	G
b.d.l.	1.0	33.9	4.8	5.7	27.3	< 0,1	0.2	51.7	37.0	PW	G
b.d.l.	12.0	52.2	3.2	20.7	134.8	0.3	< 0,1	3.7	20.5	CLW	H
b.d.l.	15.6	286.6	82.1	20.9	4.9	0.5	0.0	71.7	29.7	CFW	H
b.d.l.	8.3	7.9	1.7	4.4	34.1	< 0,1	< 0,1	3.6	1.3	PW	H
b.d.l.	0.0	29.5	24.5	7.0	654.3	< 0,1	0.0	1.6	17.0	WW	H
b.d.l.	10.8	31.8	15.1	11.4	32.2	< 0,1	0.1	27.5	55.0	PW	I
b.d.l.	10.3	32.6	2.9	11.2	32.5	< 0,1	0.1	27.7	46.2	COW	I
b.d.l.	3.4	33.3	3.4	0.2	71.0	0.2	0.1	26.4	54.9	WW	I
b.d.l.	14.1	22.8	2.1	8.1	74.7	0.8	< 0,1	136.3	31.9	CDW	I
b.d.l.	22.1	33.0	3.0	11.4	34.5	< 0,1	0.1	26.4	47.5	COW	I
0.1	4.4	13.8	1.5	2.1	13.0	b.d.l.	b.d.l.	364.2	8.4	COW	J
6.0	2.0	4.8	1.3	1.4	4.2	b.d.l.	3.0	9.5	8.9	PW	J
3.1	5.2	16.2	0.7	3.9	18.9	< 0,1	< 0,1	63.4	3.4	PW	K
b.d.l.	4.8	14.5	0.6	3.7	16.7	< 0,1	< 0,1	57.1	2.3	PW	K
14.2	2.9	8.8	2.0	2.6	18.1	< 0,1	< 0,1	99.8	28.4	COW	L
b.d.l.	34.6	28.9	25.1	379.0	4.0	0.1	< 0,1	83.7	32.4	CFW	L
b.d.l.	3.3	8.8	1.9	2.5	15.3	< 0,1	< 0,1	13.8	27.1	CDW	L
b.d.l.	6.3	21.9	2.4	12.0	47.5	0.0	0.3	62.4	27.6	PW	M
b.d.l.	4.9	4.1	0.8	1.9	5.3	< 0,1	< 0,1	14.0	5.1	PW	N
b.d.l.	6.5	8.5	2.2	6.9	26.9	0.3	0.1	7.9	12.6	PW	O
5.5	1.5	7.0	4.7	16.9	71.7	b.d.l.	0.2	55.3	14.2	PW	P
0.1	0.9	12.8	5.4	1.0	468.6	b.d.l.	< 0.1	52.3	134.2	CFW	P
1.2	8.3	118.0	101.7	366.7	7.2	b.d.l.	b.d.l.	54.1	15.3	WW	P

Zn	Sr	Al	Mn		
ICP	ICP	ICP	ICP		
[µg/l]	[mg/l]	[µg/l]	[µg/l]	water type	plant
6.5	0.15	b.d.l.	b.d.l.	PW	A
b.d.l.	0.11	b.d.l.	b.d.l.	PW	A
b.d.l.	25.3	647.0	b.d.l.	WW	B
297.0	6.0	2696.0	889.00	PW	B
b.d.l.	0.6	24.0	23.00	CFW	B
51.0	5.0	418.0	2.00	COW	C
47.0	6.0	409.0	21.00	COW	C
b.d.l.	7.00	52.4	b.d.l.	PW	D
941.1	b.d.l.	128.7	b.d.l.	CFW	D
b.d.l.	< 5	25.6	117.00	PW	E
2320.7	13.11	418.5	b.d.l.	CLW	E
b.d.l.	9.00	11.6	b.d.l.	PW	F
2318.4	b.d.l.	674.9	126.00	CFW	F
b.d.l.	0.13	2.8	< 1	WW	F
b.d.l.	0.27	45.5	593.00	WW	G
413.6	b.d.l.	90.3	139.00	CFW	G
b.d.l.	0.20	80.7	b.d.l.	PW	G
269.3	1.08	128.4	b.d.l.	CLW	H
1007.8	b.d.l.	172.3	208.00	CFW	H
0.0	0.19	b.d.l.	b.d.l.	PW	H
2291.8	0.63	696.9	b.d.l.	WW	H
5.5	0.46	3.2	b.d.l.	PW	I
b.d.l.	0.39	b.d.l.	< 1	COW	I
956.4	0.44	140.7	< 1	WW	I
b.d.l.	0.29	4.1	285.00	CDW	I
b.d.l.	0.42	b.d.l.	< 1	COW	I
0.4	0.4	74.0	0.17	COW	J
0.4	5.0	171.0	6.00	PW	J
b.d.l.	9.00	78.8	385.00	PW	K
b.d.l.	8.00	69.7	0.91	PW	K
2.6	7.00	226.4	< 1	COW	L
1136.2	b.d.l.	187.2	1.41	CFW	L
b.d.l.	8.00	16.9	b.d.l.	CDW	L
15.0	0.1	37.0	b.d.l.	PW	M
b.d.l.	< 5	b.d.l.	< 1	PW	N
160.3	0.12	b.d.l.	< 1	PW	O
b.d.l.	0.70	10.4	3.90	PW	P
b.d.l.	0.90	30.6	b.d.l.	CFW	P
b.d.l.	b.d.l.	11.2	b.d.l.	WW	P

Table A - 2: Amount and type of additive added for each individual experiment. Sodium citrate is not listed separately since it was added in every experiment.

Experiment	Sample ID	Additive	Amount [mmol/l]
1	8841		
2	8845	Magnesium chloride hexahydrate $MgCl_2.6H_2O$	0.5
3	8825	Magnesium chloride hexahydrate $MgCl_2.6H_2O$	50
4	8826	Strontium chloride hexahydrate $SrCl_2.6H_2O$	0.5
5	8827	Strontium chloride hexahydrate $SrCl_2.6H_2O$	50
6	8828	Zinc chloride $ZnCl_2$	0.5
7	8881	Zinc chloride $ZnCl_2$	50
8	8900	Manganese (II) chloride dioxide $MnCl_2.H_2O$	0.05
9	8899	Manganese (II) chloride dioxide $MnCl_2.H_2O$	0.3
10	8830	Manganese (II) chloride dioxide $MnCl_2.H_2O$	0.5
11	8831	Manganese (II) chloride dioxide $MnCl_2.H_2O$	50
12	8832	Sodium sulphate Na_2SO_4	0.5
13	8833	Sodium sulphate Na_2SO_4	50
14	8905	Iron (II) chloride hydrate $FeCl_2.xH_2O$	0.5

Table A – 3: Chemical composition of the final products via XRF. LOI through loss of ignition at 1050°C

Sample ID	Tagger	8841	8845	8825	8826	8827	8828	8881	8900	8899	8830	8831	8832	8833	8905	8833_1
Oxide	Wt. %	%	Wt. %	Wt. %	Wt. %	Wt. %	Wt. %	%	Wt. %	Wt. %	Wt. %	Wt. %	Wt. %	Wt. %	Wt. %	Wt. %
CaO	88.91	4	54.18	54.08	54.57	52.81	54.21	7	54.74	51.97	54.43	53.06	54.80	49.99	53.76	71.65
MgO	1.81	0.55	1.25	0.70	0.78	0.69	1.35	0.44	0.76	0.80	0.92	0.54	0.75	0.64	0.72	1.36
SiO_2	0.47	0.32	0.32	0.33	0.26	0.17	0.21	0.23	0.20	0.20	0.29	0.46	0.19	0.45	0.48	0.36
Na_2O	0.21	0.17	0.12	0.16	0.06	0.08					0.15	0.38	0.08	0.96	0.35	0.13
Al_2O_3	0.18	0.14	0.14	0.14	0.12	0.09	0.08	0.11	0.09	0.08	0.12	0.20	0.08	0.22	0.14	0.15
SrO	0.03	0.02	0.02	0.02	0.04	2.13	0.02	0.01	0.02	0.02	0.02	0.01	0.02	0.05	0.02	0.01
ZnO	0.01	0.01	0.01	0.01	0.01	0.01	0.03	1.75	0.01	0.01	0.01	0.00	0.01	0.05		0.01
MnO										0.02	0.02	1.64				
SO_3	0.19	0.10	0.10	0.09	0.08	0.11	0.06	0.09	0.08	0.07	0.08	0.11	0.09	1.50	0.10	0.38
BaO	0.06	0.09	0.07	0.15	0.07	0.13		0.18	0.16	0.08	0.05	0.10	0.10	1.04	0.05	0.17
Sb_2O_3	0.12	0.07	0.07	0.06	0.07	0.06	0.06	0.08	0.06	0.06	0.06	0.06	0.06		0.06	0.09
TeO_2	0.11	0.07	0.08	0.06	0.08	0.06	0.08	0.08	0.06	0.06	0.07	0.07	0.07		0.06	0.09
Fe_2O_3	0.09	0.06	0.07	0.06	0.07	0.07	0.06	0.06	0.06	0.06	0.06	0.07	0.05	0.12	0.08	0.08
CdO	0.03	0.02	0.02	0.02	0.01		0.02		0.01	0.02	0.02		0.02	0.19	0.05	0.02
Cl		0.02		0.02		0.21						0.04			0.03	
Pd	0.02	0.01	0.01	0.01	0.01		0.01	0.01	0.01	0.01		0.02	0.01	0.10	0.02	0.02
Ru	0.03	0.01	0.02	0.02	0.02	0.01	0.02	0.01	0.02	0.01	0.01	0.02	0.02	0.10	0.03	0.02
Cr_2O_3		0.01					0.01							0.05		
MoO_3	0.01	0.01	0.01	0.01	0.01		0.01	0.01	0.01	0.01	0.01	0.01	0.01	0.10	0.02	0.01
K_2O	0.04	0.01		0.01							0.01	0.02		0.05		0.01
P_2O_5			0.03	0.03												
WO_3			0.02	0.01	0.02		0.01				0.01	0.01		0.05	0.03	
ZrO_2						0.08										
UO_2						0.01										
NiO										0.01						
LOI	7.7	6	43.49	44	43.72	43.29	43.75	7	43.7	46.51	43.66	43.18	43.65	44.36	44	25.44

Table A - 4: SSA in mg^2/g for the samples after the slaking process (Mxxxx), after carbonation and sieving through 45 µm mesh (Fxxxx) and after carbonation and filtering through 0.45 µm (Pxxxx).

Sample ID	SSA [m^2/g]	Sample ID	SSA [m^2/g]	Sample ID	SSA [m^2/g]
M8841	22.7	**F8841**	5.2	**P8841**	5.2
M8845	25.6	**F8845**	6.7	**P8845**	5.7
M8825	15.0	**F8825**	5.3	**P8825**	5.9
M8826	24.7	**F8826**	5.7	**P8826**	5.4
M8827	16.5	**F8827**	20.9	**P8827**	20.0
M8828	26.4	**F8828**	6.4	**P8828**	5.8
M8881	12.2	**F8881**	8.0	**P8881**	8.5
M8900	22.4	**F8900**	5.3	**P8900**	4.9
M8899	25.0	**F8899**	6.2	**P8899**	6.0
M8830	26.0	**F8830**	4.9	**P8830**	5.0
M8831	24.3	**F8831**	8.5	**P8831**	8.8
M8832	25.2	**F8832**	4.9	**P8832**	4.7
M8833	18.2	**F8833**	13.9	**P8833**	11.6
M8905	24.2	**F8905**	5.3	**P8905**	5.4

Table A – 5: Brightness according to R457 in percentage and brightness index. Mxxxx..sample after slaking; Fxxxx...sample after carbonation and sieving through 45 µm mesh; Pxxxx sample after carbonation and filtering through 0.45 µm.

Sample ID	Brightness Tappi (=R457) [%]	Brightness Index (=Gw)
M8841	95.5	1.78
F8841	97.3	0.94
P8841	97.2	1.00
M8845	94.4	2.18
F8845	96.8	1.10
P8845	96.4	1.37
M8825	94.7	1.88
F8825	96.3	1.55
P8825	96.4	1.49
M8826	94.6	2.23
F8826	97.0	1.15
P8826	96.4	1.56
M8827	94.5	2.16
F8827	96.5	0.98
P8827	96.7	0.99
M8828	94.9	1.99
F8828	96.8	1.12
P8828	96.8	1.11
M8881	94.1	2.20
F8881	96.2	1.78
P8881	96.2	1.72
M8830	86.2	6.11
F8830	86.1	7.78
P8830	86.4	7.49
M8831	24.5	45.68
F8831	25.4	49.72
P8831	26.7	44.64
M8899	87.1	4.76
F8899	86.7	7.40
P8899	86.4	7.53
M8900	92.4	3.37
F8900	93.6	3.13
P8900	92.9	3.65
M8832	95.8	1.48
F8832	96.9	1.19
P8832	96.8	1.24
M8833	92.6	1.98
F8833	90.5	3.85
P8833	90.7	3.74
M8905	95.4	1.67
F8905	96.2	1.44
P8905	96.1	1.46

Table A-6a: Solution chemistry of the initial solutions of the precipitation experiments. *the manganese values for these samples may be unreliable due to precipitation of $Mn(OH)_2$ before the measurement took place.

Sample ID	Cond [µS/cm]	Temp [°C]	pH [-]	HCO_3 [mmol/L]	Ag [µg/L]	Al [µg/L]	B [µg/L]	Bi [µg/L]	Cd [µg/L]	Co [µg/L]
8841	246	24	8		0.2	9	b.d.l.	2	b.d.l.	0.2
8824	320	22	10		b.d.l.	8	b.d.l.	b.d.l.	b.d.l.	0.2
8825	15990	32	9		b.d.l.	160	b.d.l.	b.d.l.	4	b.d.l.
8826	337	21	9		0.1	72	b.d.l.	b.d.l.	b.d.l.	0.3
8827	17200	23	9		22	55	b.d.l.	b.d.l.	1	14
8828	310	22	7		0.1	12	b.d.l.	2	0.3	b.d.l.
8881	303	25	9		b.d.l.	99	b.d.l.	b.d.l.	1	b.d.l.
8900	15370	27	7		2	7	b.d.l.	2	0.4	0.2
8899	430	21	9		10	29	b.d.l.	10	0.3	1
8830	14390	22	9		7	8	b.d.l.	9	0.2	0.4
8831	15520	22	8		721	60	b.d.l.	713	10	b.d.l.
8832	371	20	7		0	17	b.d.l.	3	b.d.l.	0.4
8833	235	22	8		b.d.l.	18	b.d.l.	b.d.l.	b.d.l.	b.d.l.
8905	286	21	7		b.d.l.	13	b.d.l.	b.d.l.	1	2

Si [mg/L]	P [mg/L]	Zn [µg/L]	Tl [µg/L]	Pb [µg/L]	Ni [µg/L]	Mn [µg/L]	In [µg/L]	Fe [µg/L]	Cu [µg/L]	Cr [µg/L]	Sample ID
1	b.d.l.	17	1	b.d.l.	9	1	b.d.l.	30	b.d.l.	0.2	**8841**
1	0.0	18	1	b.d.l.	7	1	b.d.l.	15	b.d.l.	b.d.l.	**8824**
8	0.2	95	b.d.l.	14	36	2	b.d.l.	43	b.d.l.	b.d.l.	**8825**
1	0.1	133	b.d.l.	b.d.l.	94	2	b.d.l.	45	10	2	**8826**
12	0.3	37	70	b.d.l.	60	4	b.d.l.	45	b.d.l.	2	**8827**
1	0.1	53192	b.d.l.	b.d.l.	16	2	b.d.l.	49	1	0.4	**8828**
10	2	4741198	b.d.l.	57	224	61	b.d.l.	42	b.d.l.	b.d.l.	**8881**
2	0.1	75	b.d.l.	0.3	25	10946	0.3	15	5	2	**8900**
1	0.1	400	b.d.l.	7	240	48609	b.d.l.	40	8	12	**8899**
1	b.d.l.	1409	b.d.l.	2	250	36355	b.d.l.	43	2	8	**8830**
17	1	380	b.d.l.	547	23	2199785	b.d.l.	11	21	656	**8831**
1	b.d.l.	205	b.d.l.	1	323	728	b.d.l.	31	13	2	**8832**
15	b.d.l.	104	b.d.l.	31	77	435	b.d.l.	34	b.d.l.	b.d.l.	**8833**
1	b.d.l.	70	b.d.l.	b.d.l.	25	630	7	35266	0.4	b.d.l.	**8905**

NO_3 [mg/L]	Br [mg/L]	Cl [mg/L]	F [mg/L]	Ba [mg/L]	Sr [mg/L]	Ca [mg/L]	Mg [mg/L]	K [mg/L]	Na [mg/L]	Li [mg/L]	Sample ID
b.d.l.	b.d.l.	0.2	b.d.l.	b.d.l.	b.d.l.	5	0.2	0.1	59	b.d.l.	**8841**
b.d.l.	b.d.l.	68	b.d.l.	0.1	b.d.l.	6	26	0.4	59	b.d.l.	**8824**
b.d.l.	b.d.l.	6265	b.d.l.	b.d.l.	b.d.l.	3	2177	1	53	b.d.l.	**8825**
b.d.l.	b.d.l.	98	b.d.l.	b.d.l.	78	6	16	1	57	b.d.l.	**8826**
b.d.l.	b.d.l.	5961	b.d.l.	b.d.l.	7420	36	8	61	56	b.d.l.	**8827**
b.d.l.	0.1	70	b.d.l.	b.d.l.	6	7	1	0.5	54	b.d.l.	**8828**
b.d.l.	b.d.l.	6389	b.d.l.	b.d.l.	b.d.l.	8	0.5	3	56	b.d.l.	**8881**
b.d.l.	b.d.l.	19	b.d.l.	b.d.l.	0.1	3	1	0.3	55	b.d.l.	**8900**
b.d.l.	b.d.l.	86	b.d.l.	b.d.l.	b.d.l.	8	1	0.3	61	b.d.l.	**8899**
b.d.l.	b.d.l.	66	b.d.l.	b.d.l.	0.4	6	0.4	0.4	57	b.d.l.	**8830**
b.d.l.	b.d.l.	6334	0.1	b.d.l.	1	14	2	0.3	55	b.d.l.	**8831**
b.d.l.	b.d.l.	2	b.d.l.	b.d.l.	0.1	5	0.4	1	101	b.d.l.	**8832**
b.d.l.	b.d.l.	0.5	b.d.l.	b.d.l.	b.d.l.	7	1	0.5	4232	b.d.l.	**8833**
b.d.l.	0.3	57	b.d.l.	b.d.l.	0.1	6	1	0.4	54	b.d.l.	**8905**

Sample ID	SO_4 [mg/L]	PO_4 [mg/L]
8841	0.1	b.d.l.
8824	0.2	b.d.l.
8825	b.d.l.	b.d.l.
8826	0.3	b.d.l.
8827	b.d.l.	b.d.l.
8828	0.2	b.d.l.
8881	1	b.d.l.
8900	0.1	0.1
8899	0.3	b.d.l.
8830	0.1	0.0
8831	3	b.d.l.
8832	96	0.4
8833	9242	b.d.l.
8905	0.1	0.0

Table A-6b: Solution chemistry of the MoL of the precipitation experiments. *the manganese values for these samples may be unreliable due to precipitation of $Mn(OH)_2$ before the measurement took place.

Sample ID	Cond [µS/cm]	Temp [°C]	pH [-]	HCO_3 [mmol/L]	Ag [µg/L]	Al [µg/L]
M8841	4520	19	13		b.d.l.	10
M8845	8170	22	13		b.d.l.	115
M8825	16200	18	13		b.d.l.	144
M8826	8890	23	13		b.d.l.	98
M8827	19670	21	13		6	102
M8828	8570	22	13		b.d.l.	121
M8881	8000	21	13		b.d.l.	164
M8900	10000	21	13		b.d.l.	57
M8899	8320	21	12		b.d.l.	54
M8830	18430	21	12		b.d.l.	786
M8831	14780	23	12		b.d.l.	209
M8832	7970	20	13		1	65
M8833	8200	21	13		b.d.l.	76
M8905	8240	22	13		1	146

Pb [µg/L]	Ni [µg/L]	Mn [µg/L]	In [µg/L]	Fe [µg/L]	Cu [µg/L]	Cr [µg/L]	Co [µg/L]	Cd [µg/L]	Bi [µg/L]	B [µg/L]	Sample ID
b.d.l.	21	b.d.l.	b.d.l.	15	b.d.l.	286	b.d.l.	b.d.l.	b.d.l.	118	**M8841**
b.d.l.	30	b.d.l.	33	b.d.l.	b.d.l.	22	3	b.d.l.	b.d.l.	159	**M8845**
b.d.l.	8	87	b.d.l.	12	b.d.l.	67	7	b.d.l.	b.d.l.	b.d.l.	**M8825**
b.d.l.	8	21	b.d.l.	22	b.d.l.	25	b.d.l.	2	b.d.l.	b.d.l.	**M8826**
b.d.l.	32	37	b.d.l.	19	b.d.l.	58	b.d.l.	1	b.d.l.	b.d.l.	**M8827**
b.d.l.	5	15	b.d.l.	10	b.d.l.	25	1	3	b.d.l.	b.d.l.	**M8828**
b.d.l.	26	24	b.d.l.	20	b.d.l.	68	b.d.l.	10	b.d.l.	b.d.l.	**M8881**
b.d.l.	18	b.d.l.	32	b.d.l.	b.d.l.	31	1	b.d.l.	12	b.d.l.	**M8900**
b.d.l.	10	b.d.l.	17	3	b.d.l.	32	8	3	b.d.l.	b.d.l.	**M8899**
b.d.l.	14	b.d.l.	12	35	b.d.l.	41	0.2	b.d.l.	31	b.d.l.	**M8830**
b.d.l.	50	71	39	7	b.d.l.	7	b.d.l.	10	b.d.l.	b.d.l.	**M8831**
b.d.l.	15	19	1	20	b.d.l.	34	b.d.l.	b.d.l.	b.d.l.	b.d.l.	**M8832**
b.d.l.	28	105	35	63	b.d.l.	105	b.d.l.	b.d.l.	b.d.l.	b.d.l.	**M8833**
b.d.l.	17	0	27	4	b.d.l.	18	6	b.d.l.	3	b.d.l.	**M8905**

Ba [mg/L]	Sr [mg/L]	Ca [mg/L]	Mg [mg/L]	K [mg/L]	Na [mg/L]	Li [mg/L]	Si [mg/L]	P [mg/L]	Zn [µg/L]	Tl [µg/L]	Sample ID
1	47	900	0.4	34	50	b.d.l.	4	b.d.l.	b.d.l.	3	**M8841**
1	25	942	1	44	57	0.1	5	b.d.l.	b.d.l.	15	**M8845**
b.d.l.	28	3030	0.4	38	51	0.1	22	b.d.l.	b.d.l.	b.d.l.	**M8825**
0.4	58	885	0.1	40	51	0.1	12	b.d.l.	51	28	**M8826**
b.d.l.	3999	1271	1	50	52	0.1	31	b.d.l.	82	b.d.l.	**M8827**
0.4	24	864	0.1	38	49	b.d.l.	13	b.d.l.	1491	b.d.l.	**M8828**
b.d.l.	39	2724	0.4	38	50	b.d.l.	22	b.d.l.	28449	b.d.l.	**M8881**
1	31	980	0.1	36	51	0.2	8	b.d.l.	b.d.l.	b.d.l.	**M8900**
1	30	950	0.1	37	52	0.2	7	b.d.l.	17	b.d.l.	**M8899**
1	29	979	0.2	43	50	0.2	7	b.d.l.	946	b.d.l.	**M8830**
b.d.l.	33	3494	0.1	36	49	0.1	23	b.d.l.	47	179	**M8831**
0.4	22	800	0.1	37	75	b.d.l.	16	b.d.l.	238	15	**M8832**
b.d.l.	15	866	0.1	35	2492	b.d.l.	11	0.2	150	75	**M8833**
b.d.l.	21	838	0.2	34	49	b.d.l.	5	b.d.l.	30	26	**M8905**

Sample ID	F [mg/L]	Cl [mg/L]	Br [mg/L]	NO_3 [mg/L]	SO_4 [mg/L]	PO_4 [mg/L]
M8841	b.d.l.	3	b.d.l.	0.4	144	b.d.l.
M8845	b.d.l.	37	b.d.l.	b.d.l.	100	1
M8825	b.d.l.	3712	b.d.l.	b.d.l.	89	b.d.l.
M8826	0.1	33	b.d.l.	7	54	b.d.l.
M8827	b.d.l.	3749	b.d.l.	b.d.l.	58	b.d.l.
M8828	0.1	36	b.d.l.	0.3	85	b.d.l.
M8881	b.d.l.	3549	b.d.l.	2	107	b.d.l.
M8900	0.3	12	b.d.l.	1	92	b.d.l.
M8899	1	69	b.d.l.	5	89	b.d.l.
M8830	0.1	33	b.d.l.	0.2	87	b.d.l.
M8831	b.d.l.	3161	b.d.l.	b.d.l.	24	b.d.l.
M8832	0.1	1	b.d.l.	0.4	102	b.d.l.
M8833	0.1	1	b.d.l.	0.3	4540	b.d.l.
M8905	b.d.l.	30	0.2	0.2	81	b.d.l.

Table A-6c: Solution chemistry of the final solution of the precipitation experiments. *the manganese values for these samples may be unreliable due to precipitation of $Mn(OH)_2$ before the measurement took place.

Sample ID	Cond [µS/cm]	Temp [°C]	pH [-]
P8841	1567	21	9
P8845	1988	24	10
P8825	12270	21	8
P8826	2870	21	10
P8827	5080	22	8
P8828	1235	23	10
P8881	782	21	12
P8900	5400	21	12
P8899	2240	22	9
P8830	6190	22	9
P8831	9340	25	9
P8832	2470	21	9
P8833	2970	22	9
P8905	3000	25	9

Fe [µg/L]	Cu [µg/L]	Cr [µg/L]	Co [µg/L]	Cd [µg/L]	Bi [µg/L]	B [µg/L]	Al [µg/L]	Ag [µg/L]	HCO_3 [mmol/L]	Sample ID
15	b.d.l.	286	b.d.l.	b.d.l.	b.d.l.	118	10	b.d.l.	2816	**P8841**
0.5	b.d.l.	298	b.d.l.	b.d.l.	b.d.l.	51	5	1	2329	**P8845**
30	b.d.l.	213	5	b.d.l.	b.d.l.	b.d.l.	101	2	3048	**P8825**
1	b.d.l.	339	1	b.d.l.	b.d.l.	b.d.l.	6	b.d.l.	3951	**P8826**
18	b.d.l.	96	1	b.d.l.	5	b.d.l.	40	3	95	**P8827**
3	b.d.l.	259	0.1	b.d.l.	b.d.l.	b.d.l.	37	b.d.l.	1178	**P8828**
12	b.d.l.	47	b.d.l.	1	b.d.l.	b.d.l.	52	1	748	**P8881**
6	b.d.l.	221	b.d.l.	b.d.l.	b.d.l.	b.d.l.	7	b.d.l.	610	**P8900**
5	b.d.l.	256	1	b.d.l.	0.4	b.d.l.	7	0.4	2502	**P8899**
1	b.d.l.	270	0.2	0.2	1	b.d.l.	81	b.d.l.	1725	**P8830**
4	b.d.l.	119	12	b.d.l.	b.d.l.	b.d.l.	97	b.d.l.	101	**P8831**
2	b.d.l.	280	1	b.d.l.	b.d.l.	b.d.l.	11	1	2278	**P8832**
9	b.d.l.	188	b.d.l.	b.d.l.	b.d.l.	b.d.l.	237	b.d.l.	3169	**P8833**
76	b.d.l.	225	b.d.l.	0.1	b.d.l.	b.d.l.	20	b.d.l.	3192	**P8905**

K [mg/L]	Na [mg/L]	Li [mg/L]	Si [mg/L]	P [mg/L]	Zn [µg/L]	Tl [µg/L]	Pb [µg/L]	Ni [µg/L]	Mn [µg/L]	In [µg/L]	Sample ID
34	50	0.2	26	0.5	65	b.d.l.	b.d.l.	21	b.d.l.	b.d.l.	**P8841**
44	56	0.1	7	b.d.l.	b.d.l.	1	b.d.l.	19	b.d.l.	b.d.l.	**P8845**
41	60	0.2	12	0.3	102	b.d.l.	b.d.l.	32	b.d.l.	39	**P8825**
43	50	0.2	13	0.2	b.d.l.	35	b.d.l.	13	b.d.l.	4	**P8826**
34	44	0.2	82	b.d.l.	b.d.l.	b.d.l.	b.d.l.	139	15	18	**P8827**
39	50	0.1	3	0.2	b.d.l.	4	b.d.l.	13	b.d.l.	b.d.l.	**P8828**
38	55	0.2	4	0.1	3283	b.d.l.	b.d.l.	14	9	32	**P8881**
29	43	0.2	22	0.1	b.d.l.	b.d.l.	24	23	21	b.d.l.	**P8900**
37	51	0.1	10	0.1	b.d.l.	b.d.l.	b.d.l.	9	39	4	**P8899**
38	46	0.2	1	b.d.l.	b.d.l.	b.d.l.	b.d.l.	2	b.d.l.	5	**P8830**
34	46	b.d.l.	11	b.d.l.	b.d.l.	52	b.d.l.	31	b.d.l.	43	**P8831**
37	69	0.2	12	0.1	9	b.d.l.	b.d.l.	11	17	b.d.l.	**P8832**
37	2402	0.1	47	0.3	43	8	b.d.l.	49	39	93	**P8833**
35	47	0.2	26	b.d.l.	135	b.d.l.	b.d.l.	20	70	14	**P8905**

PO_4 [mg/L]	SO_4 [mg/L]	NO_3 [mg/L]	Br [mg/L]	Cl [mg/L]	F [mg/L]	Ba [mg/L]	Sr [mg/L]	Ca [mg/L]	Mg [mg/L]	Sample ID
1	20	b.d.l.	b.d.l.	2	b.d.l.	b.d.l.	b.d.l.	6	611	**P8841**
0.5	33	b.d.l.	b.d.l.	40	b.d.l.	b.d.l.	b.d.l.	6	490	**P8845**
0.4	12	b.d.l.	b.d.l.	3881	b.d.l.	b.d.l.	b.d.l.	19	1956	**P8825**
1	24	b.d.l.	b.d.l.	49	0.1	b.d.l.	4	3	531	**P8826**
b.d.l.	34	b.d.l.	b.d.l.	3526	b.d.l.	b.d.l.	47	266	973	**P8827**
0.4	28	0.4	b.d.l.	43	0.0	b.d.l.	b.d.l.	4	232	**P8828**
b.d.l.	22	b.d.l.	b.d.l.	3494	b.d.l.	b.d.l.	12	712	732	**P8881**
0.4	27	b.d.l.	b.d.l.	19	b.d.l.	b.d.l.	b.d.l.	2	520	**P8900**
0.4	39	b.d.l.	b.d.l.	59	b.d.l.	b.d.l.	b.d.l.	4	479	**P8899**
0.5	33	0.2	b.d.l.	37	b.d.l.	b.d.l.	b.d.l.	2	137	**P8830**
b.d.l.	34	b.d.l.	b.d.l.	3526	b.d.l.	b.d.l.	47	2192	0.4	**P8831**
0.5	26	b.d.l.	b.d.l.	5	0.1	b.d.l.	b.d.l.	3	441	**P8832**
0.3	4051	b.d.l.	b.d.l.	7	b.d.l.	b.d.l.	1	55	258	**P8833**
0.3	35	b.d.l.	0.1	38	0.1	b.d.l.	b.d.l.	6	583	**P8905**

Table A - 7: Ion balance for the different process stages for calcium, magnesium and the additives in %.

Ca	Initial Solution	Tagger	MoL	Final Solution	End product
reference	0.01	99.99	1.27	0.01	61.23
0.5 Mg	0.01	99.99	1.33	0.01	60.93
50 Mg	0.00	100.00	4.29	0.03	60.82
0.5 Sr	0.01	99.99	1.25	0.00	61.37
50 Sr	0.05	99.95	1.80	0.38	59.36
0.5 Zn	0.01	99.99	1.22	0.01	60.97
50 Zn	0.01	99.99	3.86	1.01	59.90
0.05 Mn	0.00	100.00	1.39	0.00	58.45
0.3 Mn	0.01	99.99	1.34	0.01	58.45
0.5 Mn	0.01	99.99	1.39	0.00	61.22
50 Mn	0.02	99.98	4.95	3.10	59.66
0.5 SO_4	0.01	99.99	1.13	0.00	61.63
50 SO_4	0.01	99.99	1.23	0.08	56.22
0.5 Fe	0.01	99.99	1.19	0.01	60.46

Mg	Initial Solution	Tagger	MoL	Final Solution	End product
reference	0.02	99.98	0.03	50.51	30.63
0.5 Mg	2.10	97.90	0.07	39.68	67.95
50 Mg	64.28	35.72	0.01	57.75	13.76
0.5 Sr	1.34	98.66	0.01	43.30	42.87
50 Sr	0.65	99.35	0.04	79.88	37.79
0.5 Zn	0.06	99.94	0.01	19.18	74.81
50 Zn	0.04	99.96	0.03	60.48	24.38
0.05 Mn	0.06	99.94	0.01	42.97	44.21
0.3 Mn	0.05	99.95	0.00	39.58	44.22
0.5 Mn	0.03	99.97	0.01	11.34	50.91
50 Mn	0.13	99.87	0.01	0.03	29.94
0.5 SO_4	0.03	99.97	0.01	36.45	41.65
50 SO_4	0.12	99.88	0.01	21.27	35.34
0.5 Fe	0.11	99.89	0.02	48.10	39.93

Table A - 7: Ion balance for the different process stages for calcium, magnesium and the additives in %.

Additive	Initial Solution	Tagger	MoL	Final Solution	End product
reference	0.00	0.00	0.00	0.00	0.00
0.5 Mg	2.10	97.90	0.07	39.68	67.95
50 Mg	64.28	35.72	0.01	57.75	13.76
0.5 Sr	75.50	24.50	0.14	3.52	36.97
50 Sr	99.66	0.34	0.01	0.63	26.83
0.5 Zn	90.27	9.73	0.12	0.00	37.89
50 Zn	99.88	0.12	0.01	0.07	32.91
0.05 Mn	100.00	0.00	0.00	0.20	156.21
0.3 Mn	100.00	0.00	0.00	0.08	13.06
0.5 Mn	100.00	0.00	0.00	0.00	13.84
50 Mn	100.00	0.00	0.00	0.00	60.86
0.5 SO_4	53.71	46.29	57.38	14.70	41.03
50 SO_4	99.12	0.88	48.69	43.45	7.17
0.5 Fe	32.75	67.25	0.00	0.07	55.48